

IntechOpen

Sintering Technology
Method and Application

Edited by Malin Liu



SINTERING TECHNOLOGY - METHOD AND APPLICATION

Edited by **Malin Liu**

Sintering Technology - Method and Application

<http://dx.doi.org/10.5772/intechopen.75146>

Edited by Malin Liu

Contributors

Ismayadi Ismail, Zhi Huang Low, Kim Song Tan, Amparo Borrell, Maria Salvador, Mohd Sabri Mohd Ghazali, Muhamad Syaizwadi Shaifudin, Wan Rafizah Wan Abdullah, Muhamad Azman Zulkifli, Wan Mohamad Ikhmal Wan Mohamad Kamaruzzaman, Maria Fazira Mohd Fekeri, Miguel H Bocanegra-Bernal, Armando Reyes-Rojas, Alfredo Aguilar-Elguezabal, Carlos Dominguez-Rios, Armando Garcia-Reyes, Rabaah Syahidah Azis, Muhd Syazwan Mustafa, Nuraine Mariana Mohd Shahrani, Alain Largeteau, Mohammed Taha, Mahmoud Zawrah, Rasha A. Youness

© The Editor(s) and the Author(s) 2018

The rights of the editor(s) and the author(s) have been asserted in accordance with the Copyright, Designs and Patents Act 1988. All rights to the book as a whole are reserved by INTECHOPEN LIMITED. The book as a whole (compilation) cannot be reproduced, distributed or used for commercial or non-commercial purposes without INTECHOPEN LIMITED's written permission. Enquiries concerning the use of the book should be directed to INTECHOPEN LIMITED rights and permissions department (permissions@intechopen.com).

Violations are liable to prosecution under the governing Copyright Law.



Individual chapters of this publication are distributed under the terms of the Creative Commons Attribution 3.0 Unported License which permits commercial use, distribution and reproduction of the individual chapters, provided the original author(s) and source publication are appropriately acknowledged. If so indicated, certain images may not be included under the Creative Commons license. In such cases users will need to obtain permission from the license holder to reproduce the material. More details and guidelines concerning content reuse and adaptation can be found at <http://www.intechopen.com/copyright-policy.html>.

Notice

Statements and opinions expressed in the chapters are those of the individual contributors and not necessarily those of the editors or publisher. No responsibility is accepted for the accuracy of information contained in the published chapters. The publisher assumes no responsibility for any damage or injury to persons or property arising out of the use of any materials, instructions, methods or ideas contained in the book.

First published in London, United Kingdom, 2018 by IntechOpen

eBook (PDF) Published by IntechOpen, 2019

IntechOpen is the global imprint of INTECHOPEN LIMITED, registered in England and Wales, registration number:

11086078, The Shard, 25th floor, 32 London Bridge Street

London, SE19SG – United Kingdom

Printed in Croatia

British Library Cataloguing-in-Publication Data

A catalogue record for this book is available from the British Library

Additional hard and PDF copies can be obtained from orders@intechopen.com

Sintering Technology - Method and Application

Edited by Malin Liu

p. cm.

Print ISBN 978-1-78984-281-4

Online ISBN 978-1-78984-282-1

eBook (PDF) ISBN 978-1-83881-814-2

We are IntechOpen, the world's leading publisher of Open Access books Built by scientists, for scientists

3,800+

Open access books available

116,000+

International authors and editors

120M+

Downloads

151

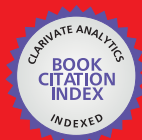
Countries delivered to

Our authors are among the
Top 1%

most cited scientists

12.2%

Contributors from top 500 universities



WEB OF SCIENCE™

Selection of our books indexed in the Book Citation Index
in Web of Science™ Core Collection (BKCI)

Interested in publishing with us?
Contact book.department@intechopen.com

Numbers displayed above are based on latest data collected.
For more information visit www.intechopen.com



Meet the editor



Malin Liu is Associate Professor and Associate Director of the New Materials Division, Institute of Nuclear and New Energy Technology (INET), Tsinghua University, Beijing, PRC. Dr. Liu obtained his Ph.D. degree in the Department of Chemical Engineering, Tsinghua University, Beijing, PRC, in July 2009, before beginning his research and teaching career at INET. He also served as a visiting scholar at the Ohio State University, Columbus, OH, USA, from 2008 to 2009. Dr. Liu has published more than 80 peer-reviewed papers, 30 China and PCT patents, and has also been elected to be responsible for 13 research projects. His research interests include design, fabrication, and evaluation of advanced nuclear fuels, including the FB-CVD method, (nano)particle fabrication/coating and process simulation, CFD/DEM/PBM simulation methods, and SiC sintering technology.

Contents

Preface XI

Section 1 Method 1

Chapter 1 **Advanced Ceramic Materials Sintered by Microwave Technology 3**

Amparo Borrell and Maria Dolores Salvador

Chapter 2 **Sintering Processing of Complex Magnetic Ceramic Oxides: A Comparison Between Sintering of Bottom-Up Approach Synthesis and Mechanochemical Process of Top-Down Approach Synthesis 25**

Zhi Huang Low, Ismayadi Ismail and Kim Song Tan

Chapter 3 **Sintering Temperature Effect on Microstructure and Magnetic Evolution Properties with Nano- and Micrometer Grain Size in Ferrite Polycrystals 45**

Raba'ah Syahidah Azis, Muhammad Syazwan Mustaffa and Nuraine Mariana Mohd Shahrani

Section 2 Application 63

Chapter 4 **Conventional Sintering Effects on the Microstructure and Electrical Characteristics of Low-Voltage Ceramic Varistor 65**

Mohd Sabri Mohd Ghazali, Muhamad Syaizwadi Shaifudin, Wan Rafizah Wan Abdullah, Wan Mohamad Ikhmal Wan Mohamad Kamaruzzaman, Maria Fazira Mohd Fekeri and Muhamad Azman Zulkifli

Chapter 5 **Nanostructured Pure and Doped Zirconia: Synthesis and Sintering for SOFC and Optical Applications 85**

Mythili Prakasam, Sorina Valsan, Yiyang Lu, Felix Balima, Wenzhong Lu, Radu Piticescu and Alain Largeteau

Chapter 6 **On the Performance of Carbon Nanotubes on Sintered Alumina-Zirconia Ceramics 107**

Miguel Humberto Bocanegra-Bernal, Alfredo Aguilar-Elguezabal, Armando Reyes-Rojas, Carlos Dominguez-Rios and Armando Garcia-Reyes

Preface

Sintering Technology - Method and Application is a collection of several chapters proposed by many authors. Sintering technology is an old and extensive technology in many areas, and it has been used especially in ceramic fabrication. This book covers many fields, such as traditional sintering techniques, including hot isostatic pressing, mold casting and sintering in conventional ovens, and also development of different sintering technologies in recent years, including spark plasma sintering, flash sintering, microwave sintering, reaction and laser sintering, and so on. However, the focus is mainly on microwave sintering technology. The effects of temperature on sintering behavior are given. A top-down approach called the mechanochemical method is compared with the sintering technique. Also described in this book are the applications of sintering technology, such as carbon nanotubes mixed with alumina and zirconia ceramics, pure and doped zirconia, and ZnO ceramic varistors.

The editor thanks all the authors and staff who assisted in the project. This book will be helpful for those researchers who are engaged in sintering technology and related fields.

Malin Liu

Institute of Nuclear and New Energy Technology

Tsinghua University

Beijing, China

Method

Advanced Ceramic Materials Sintered by Microwave Technology

Amparo Borrell and Maria Dolores Salvador

Additional information is available at the end of the chapter

<http://dx.doi.org/10.5772/intechopen.78831>

Abstract

Processing of ceramic materials has also a strong impact in the quality of the consolidated body, as it plays a key role in the resulting microstructure and, as a consequence, in its final properties. Advanced ceramic materials are commonly processed as powders and densified via a high-temperature process. Traditional processing techniques include hot isostatic pressing, mold casting, and sintering in conventional ovens. As ceramics require very high processing temperatures compared to metals and polymers, these processes tend to be very energy intensive and result in higher production costs to the manufacturers. Therefore, new technologies known as nonconventional sintering techniques, such as microwave technology, are being developed in order to reduce energy consumption, while maintaining or even improving the characteristics of the resulting ceramic material. This novel and innovative technology aims at helping industrial sectors lower their production costs and, at the same time, lessen their environmental impact. On the other hand, it is interesting and necessary to know and explore the basic principles of microwaves to advance in the development of materials that demand, every day more, the different industrial sectors. This chapter presents the most recent advances of two materials with a great industrial future: zirconia and lithium aluminosilicate.

Keywords: ceramic materials, microwave technology, microstructure, mechanical properties, advanced applications

1. Introduction

High-temperature processes are required to consolidate ceramic powders, such as zirconia (Y-TZP), alumina, silicon carbide, and so on, in order to obtain full densification of the material. Sintering is a common material processing technique aimed at fulfilling this task.

The fundamental principle behind sintering consists in the thermal activation of mass transfer mechanisms when exposing a powder compact, known as a “green” body, to a high-temperature process, at a dwell temperature below the melting point of the material. The main purpose of sintering is to obtain a dense and resistant body with properties as close as possible to those of a theoretical, fully dense solid. However, in some cases, sintering can also be employed to adjust some of the properties based on the performance requirements of the material by not reaching full consolidation, such as in porous materials.

Two main types of sintering can be identified based on the nature of the process: liquid phase and solid phase. Even though the term liquid phase may suggest exceeding the melting point of the material, it is used to describe the addition of compounds with significantly lower melting points that aid in the consolidation of the main powder, which is regarded as the matrix phase and provides the main properties of the consolidated body. In this chapter, however, only solid phase sintering is considered.

Currently, innovative sintering methods are being explored and studied in order to modify densification mechanisms that may improve the microstructure and mechanical properties of sintered materials and also is very important to reduce time fabrication of these materials. Two main stages have been recognized during the sintering process: densification and grain growth [1]. The main purpose for modifying sintering mechanisms is to obtain relative densities close to theoretical values, while maintaining a controlled, but limited, grain growth [2]. Also, the optimization of the process by reducing the sintering time to decrease energy consumption and/or increasing heating rates is an important aspect that is being considered [3]. As a consequence, in order to improve the sintering process, novel non-conventional sintering methods have been investigated and developed.

Particularly, microwave sintering represents an interesting opportunity at consolidating advanced ceramic materials with a reduced processing time and energy consumption by utilizing electromagnetic radiation to provide high-enough temperatures that allow full densification of the material. The most important advantages of microwave sintering against conventional sintering methods are listed as follows [4, 5]:

- shorter sintering time and lower energy consumption;
- higher heating rates can be used;
- materials with a finer (nanometric) microstructure with a high degree of densification and enhanced mechanical properties may be obtained due to the densification mechanisms involved;
- flexible due to the possibility of processing *near-net-shape* materials.

This chapter reports on microwave material interaction, the basics of microwave processing, heating mechanisms, theoretical aspects in dielectric heating, and microwave systems for heating. The challenges in the field of microwave processing of advanced materials, such as zirconia and lithium aluminosilicate, have been discussed and studied from the point of view of different authors.

2. Microwave sintering technology

2.1. Microwave sintering

Microwaves have been used since the 1960s for heating purposes, particularly for food- and water-based products. Industrially, the use of microwave energy has become increasingly important because it represents an alternative to traditional with high-temperature processes. For example, so far, it has been employed in wood drying, resin curing, and polymer synthesis. The growing interest in industrial microwave heating is due mostly to the reduction of production costs resulting from lower energy consumption and shorter processing times [6–8]. However, several aspects need to still be investigated as each material behaves differently in the presence of microwaves.

The application of microwave heating has now expanded to material science and technology, beginning with process control and moving onto ceramic drying, powder calcination, and decomposition of gases with microwave plasma, in addition to powder synthesis [5]. Scientific interest on this powerful tool has been recorded in the study as there has been an increase of bibliographical entries for the term “microwaves” in the last decades because the applications of this technology have diversified enormously. In the last 25 years, research and development on the dielectric heating attributed to microwaves began with topics in chemical synthesis and material processing, such as reactive sintering of superconductors, magnetoresistors, nanomaterials production, vitreous phase formation, hydrothermal generation of zeolites, among others [9]. In this sense, one of the major areas for research and development of microwave heating involves sintering of ceramic powders [10, 11].

Microwave sintering is considered a relatively new ceramic material processing technique that differs significantly from conventional sintering methods due to the nature of the heat transfer mechanisms involved. Hence, microwave sintering is classified as a non-conventional sintering technique. This method presents itself as a fast, economical, and flexible processing tool. Some of the most important advantages against conventional sintering systems include lower energy consumption and production costs, reduction of processing times, higher heating rates, and, in some cases, even an improvement in the physical properties of the consolidated material [6, 12]. As a consequence, scientific interest in this novel technique has been developed progressively.

In a general sense, microwave sintering increases the densification of the material at lower dwell temperatures when compared to conventional sintering [13, 14], employing shorter times and less energy [15, 16], and resulting in an improvement of the microstructure and mechanical properties [17, 18].

The first sinterability studies of ceramics by exposure to microwave energy were carried out on the so-called black ceramics, which are the compounds based on tungsten carbide (WC). Two of the main issues regarding sintering of these materials by conventional means are the high temperatures (>1500°C) and long dwell times that result in grain coarsening. For the first time, in 1991, J. P. Cheng showed that the WC/Co system could be sintered by microwave heating technology [19]. In his work, a commercial WC powder with a 6–12 mol% Co content was investigated, and an improvement in the mechanical properties was achieved when

compared to conventional methods by utilizing sintering temperature between 1250 and 1320°C and dwell times of only 10–30 min. The relative density values were close to theoretical and a fine and homogeneous microstructure was observed, without the use of grain growth inhibitors. Also, the materials exhibited a higher resistance to corrosion and erosion [20].

The next step involved the processing of more traditional ceramic materials such as alumina and zirconia. Even though alumina behaves as a transparent material in the presence of microwaves, susceptors, which are materials with a high microwave absorbance, or dopants can be employed. Tian et al. were able to obtain 99.9% relative density values with an average grain size of 1.9 μm for MgO-doped Al_2O_3 sintered at 1700°C in a microwave oven [21]. Additionally, Katz and Blake were able to reach a densification of 99% for α -alumina with grain sizes between 5 and 50 μm after microwave sintering, where the total processing time was 100 min at a dwell temperature of 1400°C [22]. Transparent alumina materials have also been obtained via microwave processing at lower sintering temperature and shorter times [23].

In the case of nanometric yttria-stabilized zirconia (YSZ), microstructure and mechanical properties can be enhanced when processed via microwave sintering [24]. By application of hybrid heating with the aid of a susceptor, sintered materials with densities close to theoretical values can be obtained at temperatures 200°C below those employed in conventional sintering [25, 26]. Moreover, the grain size decreases considerably and hardness values are almost 2 GPa higher [18].

In the last 5 years, research on microwave sintering has also focused in the processing of ceramic composites to improve their functional as well as structural properties and extend its applications to several industrial sectors. Also, the design and optimization of current microwave ovens has also been an important research topic. These systems need to be adjusted to the characteristics of the material that is to be processed, since the behavior under a microwave field varies from one to another. Therefore, studying the fundamental principles and involved mechanisms in microwave energy conversion may allow the production of more energy-efficient ovens.

2.2. Microwave heating fundamentals

Microwaves are a form of electromagnetic radiation that correspond to frequencies between 300 MHz ($\lambda = 1$ m) and 300 GHz ($\lambda = 1$ mm), as shown in **Figure 1**. Among their most important industrial applications are telecommunications and heating. The possibility to use microwave energy for heat generation was first discovered in the late 1940s, while tests were being carried out with magnetrons [8]. Consequently, the first microwave systems for food heating were developed. As research in microwave energy and its applications continued, uses expanded to industrial processes such as drying and curing. In the last few decades, sintering of materials with microwave radiation has also become an active field of investigation.

2.2.1. Interaction of microwaves with matter

Microwaves, as any other type of electromagnetic radiation, have electrical and magnetic field components, amplitude, phase angle, and the ability to propagate, that is, to transfer

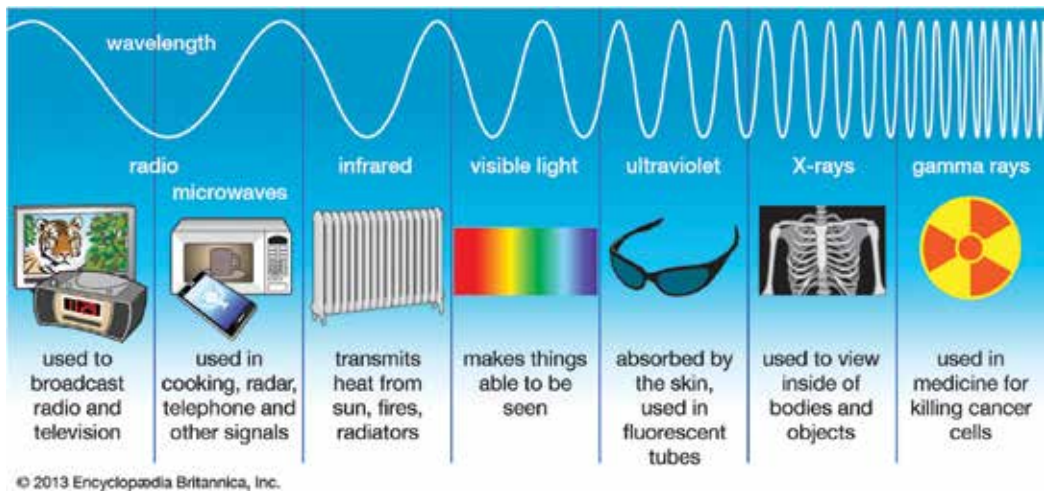


Figure 1. Electromagnetic spectrum diagram.

energy from one point to another. These properties govern the interaction of microwaves with materials and produce heating in some of them. Depending on the electrical and magnetic properties of the material, their interaction with microwaves can be classified as one of three types [5]:

- **Transparent:** Microwaves penetrate and are transmitted through the material completely with no energy transfer occurring (**Figure 2a**). These materials are known as low-loss insulators.
- **Opaque:** Microwaves are reflected with no penetration into the material and no energy transfer. These are known as conductors (**Figure 2b**). Metals are mostly considered to be opaque to microwave energy.
- **Absorbent:** Microwaves are absorbed by the material, and an exchange of electromagnetic energy occurs (**Figure 2c**). The amount of absorption depends on the dielectric properties of the material.

A fourth type of interaction known as mixed absorption has also been proposed. In this particular case, mixed or multi-phase materials with different degrees of microwave absorption are sought after. Most electrically insulating ceramics such as alumina, MgO, silica, and glasses are transparent to microwaves at room temperature, but, when heated above a certain critical temperature T_c , they begin to absorb and couple more effectively with microwave radiation. Other ceramics, such as SiC, are able to absorb microwave energy more efficiently at room temperature. Therefore, the addition of a microwave-absorbing second phase to ceramics that behave transparent at room temperature can greatly enhance the interaction of the system with microwaves allowing a hybrid heating of the material. In Section 5, a more in-depth description of hybrid heating is given.

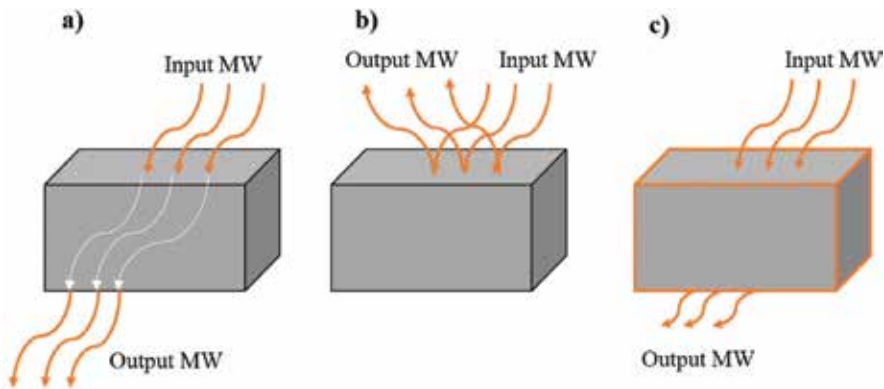


Figure 2. Material/microwave interaction representation classified according to their behavior: (a) transparent, (b) opaque, and (c) absorber.

2.2.2. Microwave heating mechanisms

In order to explain the interaction of absorbing materials with microwave radiation and the energy transfer that occurs during this interaction, several physical mechanisms have been proposed. These mechanisms include bipolar rotation, resistive heating, electromagnetic heating, and dielectric heating. Depending on the material, the response to incoming radiation can be attributed to one mechanism or a combination of several of them:

- **Bipolar rotation** occurs when electrically neutral polar molecules with positive and negative charges are separated. Within a microwave field, these dipoles rotate in the direction of increasing amplitude. As a consequence of this rotation, friction among the molecules arises generating heat uniformly throughout the material.
- **Resistive heating** occurs in conductors or semiconductors with relatively high electrical resistivity. These materials possess free electrons or a high ionic content where the ions receive enough freedom so current can be generated.
- **Electromagnetic heating** takes place in materials with magnetic properties that are highly susceptible to external electromagnetic fields, such as those induced by microwave radiation. This type of heating can be described as magnetic pole rotation of the material analogous to the rotation of polar molecules in oscillating electrical fields.
- Finally, the fourth mechanism, **dielectric heating**, is a mix of bipolar rotations and resistive heating. In microwave sintering of ceramics, this is the predominant mechanism. In the next section, the principles of dielectric heating in microwave-absorbent materials are described.

2.3. Theoretical aspects in dielectric heating

The degree of interaction between the microwave electric and magnetic field components with the dielectric or magnetic material determines the rate at which energy is dissipated in the

material by the various mechanisms. The properties of the material that are most important for the interaction are the permittivity ϵ for a dielectric material and the permeability μ for a magnetic material [27]. Considering that dielectric heating is the most relevant mechanism for ceramics, this description will only focus in aspects related to permittivity and properties that arise from it.

When microwaves penetrate the material, the electromagnetic field induces motion in the free and bound charges (electrons and ions) and in dipoles. The induced motion is resisted because it causes a departure from the natural equilibrium of the system, and this resistance due to frictional, elastic, and inertial forces leads to the dissipation of energy. As a result, the electric field associated with microwave radiation is attenuated, and heating of the material occurs.

The dielectric interaction between materials and microwave radiation can be described by two main parameters [6, 28–30]:

- absorbed power, P
- depth of microwave penetration, D

Both parameters play a critical role in the uniform heating of the material. The absorbed power is the volumetric absorption of microwave energy (in W/m^3) and is expressed according to the following equation:

$$P = \sigma |E|^2 = 2\pi f \epsilon_0 \epsilon'' |E|^2 = 2\pi f \epsilon_0 \epsilon' \tan\theta |E|^2 \quad (1)$$

where f = frequency of the electric field and E = amplitude of the electric field.

The loss tangent, $\tan\theta$, is a term associated with the capacity of the material to be polarized and heat itself. In other words, these terms describe the microwave energy conversion into heat. The relationship describing the loss tangent is given by

$$\tan\theta = \epsilon''/\epsilon' \quad (2)$$

where ϵ'' = loss factor; ϵ' = dielectric constant, inherent to the material.

The loss factor, ϵ'' , measures the ability of the material to convert the incoming microwave energy into heat, and the dielectric constant, ϵ' , measures the polarizability of the material. In microwave material processing, maximum values for ϵ'' in combination with mild values of ϵ' are desired (**Figure 3**).

Both, ϵ' and ϵ'' , depend on temperature and the frequency of the field. At low frequencies, all microwave energy is absorbed by the rotating movement of the dipoles and ϵ' reaches a maximum; however, there are no collisions because the displacement is very slow. At high frequencies, the material does not have enough time to respond to the oscillating electric field, and therefore, ϵ' reaches a minimum. The loss of energy caused by the collisions is represented by ϵ'' . The key relies on finding a frequency for each material at which the absorption of energy (ϵ') as well as the loss of energy (ϵ'') is high.

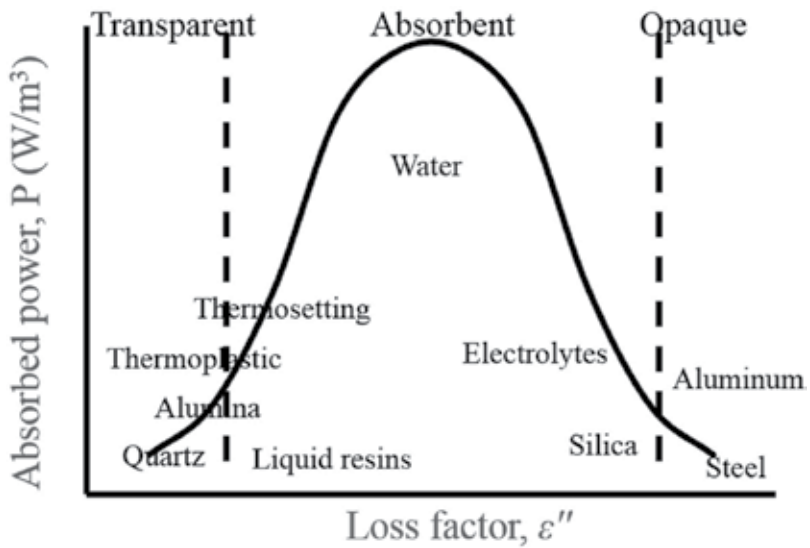


Figure 3. Relationship between factor loss and absorbed power at a frequency of 2.45 GHz and room temperature for some common materials.

A general explanation is based on a fundamental body, such as a grain particle, in its neutral state containing polarized molecules distributed in random positions. These molecules can easily be reoriented by the effect of an external electric field, as shown in **Figure 4**.

If the polarity of the electric field is changing constantly, molecules will modify their orientation accordingly in a very fast manner so as to align with the field (**Figure 5**) and, as a consequence, heat will be generated due to the friction among them and electrical resistive effects from unbound charges. The material heats up as a function of the absorbed energy during this process.

The main difference with respect to conventional sintering is the direction of heat flow [31], because in conventional sintering, heat is transferred from the surface of the material toward the inside due to the heating mechanisms involved. In contrast, in microwave sintering, in the presence of a strong electric field, molecules vibrate with the same intensity and at the same

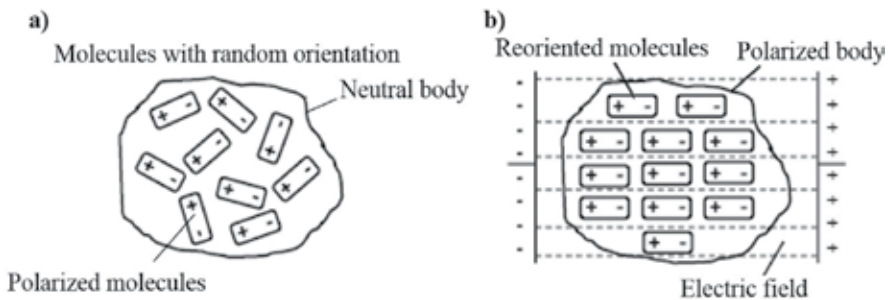


Figure 4. Position of the molecules (a) in its natural state, and (b) with the application of an external electric field.

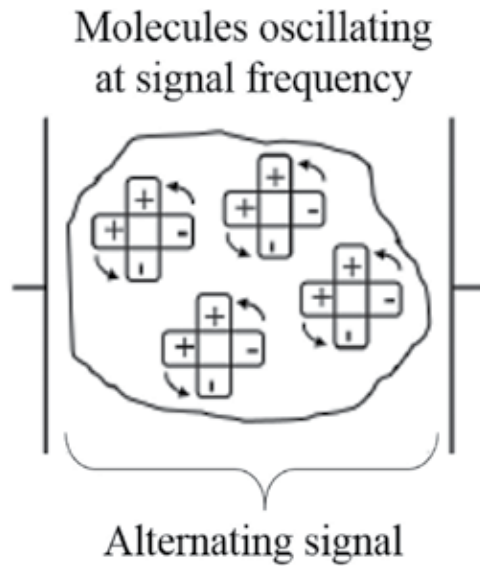


Figure 5. Representation of the reorientation of the molecules in the presence of an alternating electric field, such as that induced by microwaves.

time generate heat throughout the whole material as a consequence of the characteristics of dielectric heating.

The second main parameter in microwave/material interaction is microwave penetration depth, D . This parameter determines the penetration depth at which the power is reduced by half and is expressed in the following manner:

$$D = \frac{3 \pi_0}{8.686 \pi \tan \theta \left(\frac{\epsilon'}{\epsilon_0} \right)^{\frac{1}{2}}} = \frac{C}{2 \pi f \sqrt{2} \epsilon' (\sqrt{1 + \tan^2 \theta} - 1)^{\frac{1}{2}}} \quad (3)$$

High frequencies in combination with high dielectric property values translate into superficial heating of the material, while low frequencies with small dielectric property values give place to volumetric heating.

Based on the properties of materials, it is well known that those with a high conductivity and permeability present a lower penetration depth for a given frequency. The penetration depth of many materials oscillates around $1 \mu\text{m}$, which means that heating tends to stay at the surface. If powders with a particle size of approximately that of D are employed, there is the possibility to heat the whole surface directly and homogeneously.

2.4. Microwave systems for heating

A microwave oven is composed of three main elements: (1) microwave source, which is in charge of generating the electromagnetic radiation, (2) transmission lines, which transmit the microwaves, and (3) a resonant cavity, which is where the interaction with matter takes place [28].

The theoretical principle that governs each of the components is based on Maxwell Equations [30, 32]:

$$\nabla \times \mathbf{E} = \frac{\partial \mathbf{B}}{\partial t}, \quad \nabla \cdot \mathbf{B} = 0. \quad (4)$$

$$\nabla \times \mathbf{H} = \frac{\partial \mathbf{D}}{\partial t} + \mathbf{J}, \quad \nabla \cdot \mathbf{D} = \rho \quad (5)$$

where \mathbf{E} = electric field vector; \mathbf{B} = magnetic flux density vector; \mathbf{H} = magnetic field vector; \mathbf{J} = current density vector; \mathbf{D} = electric flux density vector; ρ = charge density.

Maxwell equations are the physical laws that describe an electromagnetic field and its variations with time. The design of an efficient microwave system to process materials requires understanding of electromagnetic theory.

In the following paragraphs, a description of the different components that are part of a microwave system is given.

Magnetron: This is the most important part of a microwave source. This device transforms the electrical energy from the low-frequency electric grid into a high-frequency electromagnetic energy (microwaves). It consists of a metallic cylinder where a series of resonant cavities are disposed radially and communicated to a major central cavity, which has a titanium filament in its axis (**Figure 6**). The cylinder acts as an anode and the central filament as a cathode. The filament, which is connected to the negative pole of a continuous current source, becomes

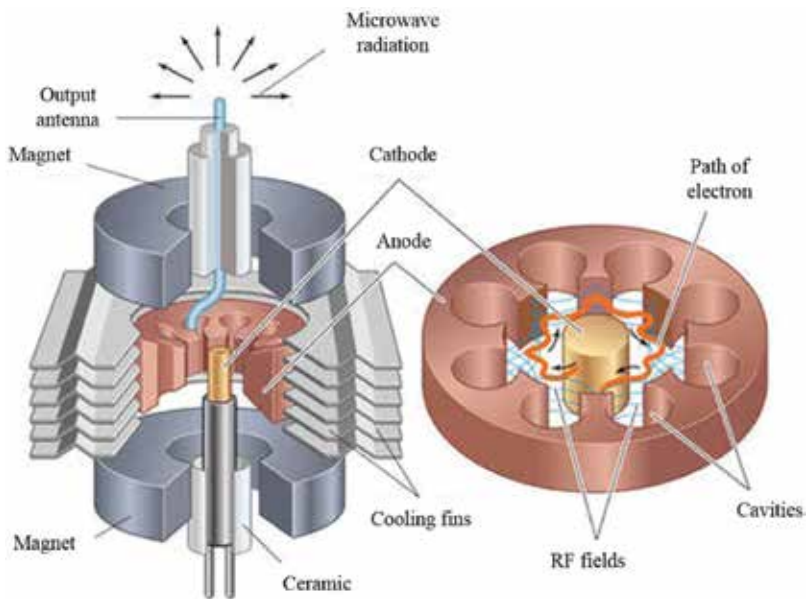


Figure 6. Magnetron schematic showing all the elements required for generation of microwave radiation.

incandescent and emits electrons by thermionic effect. The cylinder, connected to the positive pole, attracts the electrons. The whole setup is located between the poles of a powerful electromagnet.

The open space between the plate and the cathode is referred to as interaction space. In this space, electric and magnetic fields interact to exert a force on the electrons. Given that an electric charge creates an electromagnetic field around it, all the electrons, moving in circles in the cavities, produce electromagnetic waves, in this case microwaves, perpendicular to their own displacement and with a frequency that depends on the size of the cavities.

Usually, for microwave heating applications, the frequency of the generated electromagnetic radiation is 2.45 GHz. This frequency corresponds to one of the so-called Industrial, Scientific and Medical (ISM) frequencies, which are free of utilization for these types of applications. The insertion of magnetrons in commercial microwave ovens for home use has translated in more economical sources of this frequency by allowing the fabrication of magnetrons in a large scale. Moreover, other ISM frequencies are also employed for heating applications, such as Bluetooth and WiFi [33]. The power generated by the magnetron can be controlled by changing the amplitude of the cathode's current or the intensity of the magnetic field.

Transmission lines: This element is responsible for transmitting the generated microwave radiation by the source to the main cavity. In low-power systems, transmission lines are usually coaxial cables. However, for high-frequency systems, the loss occurring in the coaxial cables is quite substantial. Therefore, circular or rectangular waveguides are necessary for proper wave transmission.

Circulator: This component provides protection to the source against possible unwanted load reflections. The circulator is capable of redirecting the microwave power that was not consumed by the material to be sintered toward a water load. This water load heats up avoiding that the reflected power gets back causing damages to the source.

Reflectometer: This element measures the effective consumed power by the material sample to be heated. This information provides reliable information about the power consumed during the sintering of the sample.

Tuning system: This element is fixed to the microwave oven and is employed to couple the microwave incident radiation to the cavity. Different types of tuners can be utilized. For example, the simplest one consists of an iris that couples the incident power directly to the cavity. More complex tuners are the three-stub adapter that allows a dynamic adaptation of the coupling process to the cavity.

Resonant cavity: This is the microwave system nucleus, where the incident electromagnetic radiation heats and sinters the material. Cavity design is one of the most critical parts of microwave equipment for material processing. The temperature distribution within the material, which is heated by microwave radiation, is inherently linked to the distribution of the electric field inside the cavity. In material processing, resonant cavities with different mode configurations, including single-mode, multi-mode, and multi-mode with variable frequency, are employed [32, 34].

The size of a single-mode resonant cavity must be in the order of one wavelength. Additionally, in order to maintain a resonant mode, these systems require a microwave source that allows frequency variations or that the cavity dynamically changes its size to couple the frequency of the microwaves. Generally, the distribution of the electromagnetic field in this type of cavity is well known. With an adequate cavity design, the microwave field may be focalized to a particular zone where the material sample can be sintered. An additional advantage for this type of cavity is the fact that the dielectric properties of the material can be monitored during sintering.

Multi-mode cavities are able to maintain several modes simultaneously. The design of home microwave ovens is based on this type of cavity. The greater the size of the cavity, the higher the number of possible resonant modes. Hence, multi-mode cavities are larger than a wavelength, which contrast with the size of single-mode systems.

The presence of different resonant modes results in the existence of multiple hotspots inside the cavity. Local fluctuations in the electromagnetic field can result in overheating of certain areas. In order to minimize these hotspots, the electromagnetic field must be uniform. Field uniformity can be achieved by increasing the size of the cavity and varying the sample position dynamically, for example, with a rotating plate or stirrers. By increasing cavity size, the number of modes increases and, as a consequence, the heating patterns of each mode begin to superimpose and the stirrers or the plates change the distribution of the field inside the cavity.

2.5. Microwave hybrid heating: bidirectional heating

One of the main issues associated with microwave sintering of materials is their initial microwave radiation absorption and heating. Most of the processing is carried out at a relatively low frequency of 2.45 GHz, which makes the initial heating of the material very difficult to control. Another important problem that may arise consists in the thermal instability that materials are prone to due to the changes in their properties, such as their dielectric constant, ϵ' . Variations in dielectric properties as a function of temperature may translate into poor temperature control and overheating of the specimen. Such behavior is present in several materials such as alumina and zirconia.

Temperature gradients that arise during heating can produce microcracking and an unequal distribution of resulting physical properties, such as density and hardness. Therefore, thermal insulators or coatings may be necessary to avoid the presence of these gradients. Nonetheless, these insulators can provoke the control loss of the temperature.

Ceramics tend to exhibit an abrupt increase in ϵ'' as a function of increasing temperature. The temperature at which dielectric properties change is known as the critical temperature, T_c . Below T_c , at a given frequency, most ceramics are poor absorbers behaving as transparent materials and need to be heated by an external source. No mathematical relationship has been found that relates temperature to fundamental material properties, hence T_c values must be measured experimentally [35, 36]. This T_c can pose some problems when processing complex and large samples. Unless heated uniformly by an external source, localized hotspots can develop in the material. These spots begin to absorb microwave radiation before the rest of the material in phenomenon known as thermal runaway. As a consequence, this can lead to the fracture and/or warping of specimens. Thermal runaway can be limited by using uniform external heating and a homogeneous microwave field.

A plausible solution that materials scientists and engineers have developed consists on a hybrid method that combines direct microwave heating coupled with heat transfer coming from another material that surrounds the specimen to be sintered [37]. This system is an example of mixed absorption heating, with a high dielectric loss at both low and high temperatures.

In this scenario, microwaves are absorbed by the material with highest dielectric losses at room temperature while microwaves propagate through the material with lower losses at room temperature. Heat and energy are transferred from the absorbing material to the transparent material. This type of heating makes use of a specific component known as a susceptor. This heating-aid element is the absorbent material and possesses a very high dielectric loss at room temperature, transmitting heat to the material to be sintered via conventional heat transfer mechanisms. Once the material has heated sufficiently surpassing its T_c , changing its dielectric properties, and inducing high dielectric losses, it is able to absorb microwave energy and heat itself.

This combined action, known as microwave hybrid heating, can be employed for fast sintering of compacted powders. In this particular case, the direction of heat flow in the specimen to be sintered occurs in two directions: from the surface to the nucleus due to the effect of the susceptor and from the nucleus to the surface once it is able to absorb microwave radiation [37]. A representation of a bidirectional hybrid heating can be seen in **Figure 7**.

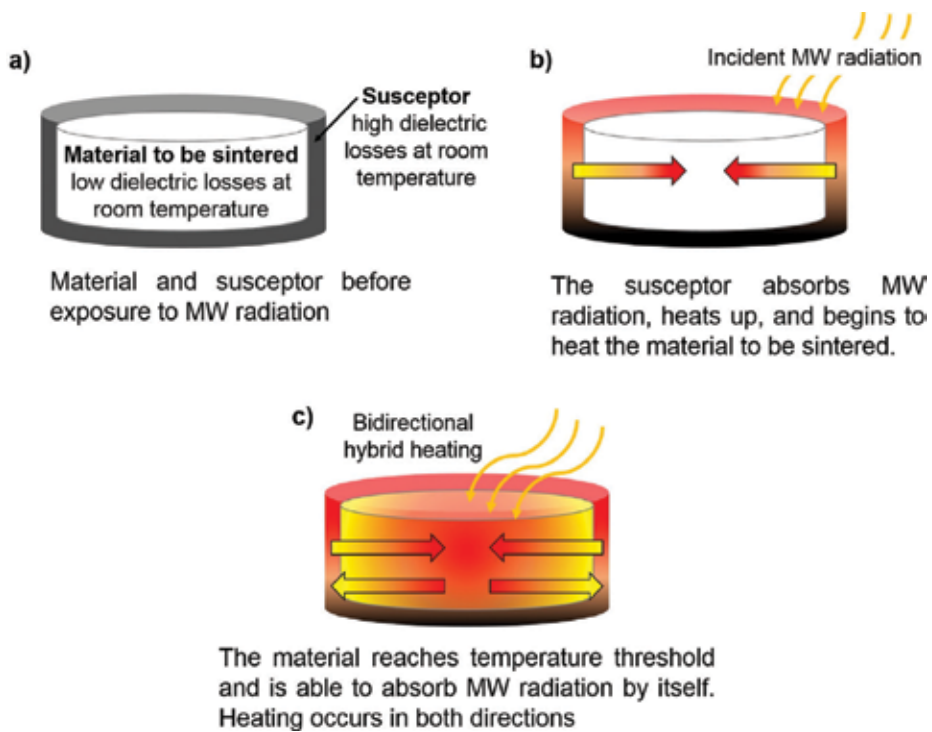


Figure 7. Sequence diagram of microwave hybrid heating for material sintering: (a) before exposure to microwave radiation, (b) susceptor heating under MW radiation, and (c) specimen to be sintered able to absorb MW energy giving place to bidirectional hybrid heating.

2.6. Microwave sintering of zirconia

Mechanical properties and microstructure of Y-TZP-sintered materials are strongly influenced by the degree of densification and grain nucleation that result due to the sintering process. This is, in turn, determined by the heating mechanisms that take place within the material. Current commercial sintering of ceramic materials is based on conventional heat transfer mechanisms: conduction, convection, and radiation. In this case, heat is generated from heating elements and a temperature gradient arises, as heat is transferred from the surface to the material's core. This method, however, requires long processing times. As a consequence, grain broadening occurs [38], which leads to a decrease in the final mechanical properties of the material [39]. It also requires a high-energy consumption to reach such high temperatures, which must also be maintained for long periods of time (around 2–4 h or more) if fully dense materials are desired.

One advantageous and useful non-conventional method that can modify the densification mechanisms and results in faster processing of Y-TZP ceramics is microwave sintering [40]. The energy conversion of electromagnetic radiation into heat by the material itself due to the material's dielectric properties is the driving force for densification [41]. The rise in temperature is determined by the amount of energy absorbed in the process. The acceleration of diffusion mechanisms during sintering by the oscillating electric field has also been proposed by some authors to explain enhancement of the sintering process, in what is called a "microwave effect" [42]. Because it is a non-contact technique, the effects of differential sintering are minimized [43], which is another advantage over conventional sintering methods, where differential densification is an important problem that arises from the slow heating rates.

The dielectric loss factor of zirconia is quite different from those of other oxide and non-oxide ceramics. At a frequency of 2.45 GHz, zirconia does not couple adequately with microwaves at room temperature. The loss factor, ϵ'' , of Y-TZP at room temperature is similar to microwave-transparent materials, with a value of approximately 0.04 [25]. However, the dielectric loss increases tremendously with temperature, reaching a value of almost 100 at 1000°C. Therefore, zirconia can become a very absorptive material by raising its temperature. In order to achieve this, two different approaches can be found:

- With the aid of a susceptor, generally (SiC), as it has been described in the previous section. This method is the most commonly found in the study [25, 44, 45].
- Employing conventional resistive elements to initially heat the zirconia until its T_c is reached, and zirconia is able to interact with the microwave field by itself [46].

Previous reports [4, 18, 47] have demonstrated that with microwave sintering, highly dense materials can be obtained without a substantial grain coarsening because dwell time is considerably shorter and heating rates are quite high in comparison with conventional sintering [48]. Energy consumption is also significantly reduced as a consequence of the mechanisms involved in microwave heating and the abovementioned shortening of processing times. As a result, several advantages arise including improved mechanical properties and reduced environmental impact [5, 49]. This method may provide lower costs for professionals and customers maintaining or even improving the quality of the final product.

In general, the study suggests that microwave sintering of zirconia can result in comparable mechanical properties and high degrees of densification comparable to those achieved with conventional sintering systems at lower dwell temperatures and significantly shorter sintering times [50–54]. Moreover, some studies have demonstrated that microwave-sintered specimens exhibit enhanced crystallinity [55] and improved mechanical properties [18, 49, 56].

2.7. Microwave sintering of lithium aluminosilicate

Over the past few decades, the lithium aluminosilicate (LAS) compositions have been extensively studied because it is very low or even negative thermal expansion compounds have found a wide application field including cookware, bakeware, electronic devices, telescope mirror blanks, ring-laser gyroscopes, and optically stable platforms [57]. Sintered negative thermal expansion materials have usually low mechanical strength because the expansion anisotropy causes microcracking. This is due to different extents of thermal expansion in different crystallographic orientations, which induces internal stress with temperature change. On the other hand, it has been reported by Pelletant et al. [58] that the microcracking depends on the grain size; therefore, an increase in the β -eucryptite grain size causes a progressive microcracking and consequently a more negative bulk of thermal expansion coefficient. Nevertheless, the usefulness of these thermal properties in the production of materials with null expansion has a wide range of potential engineering, photonic, electronic, and structural applications [59].

β -Eucryptite is the most negative thermal expansion phase in the lithium aluminosilicate system, and therefore β -eucryptite has been thoroughly studied [60]. Compared with the number of studies of glass–ceramic materials, there are few studies in the literature, which deal with this system as a ceramic material in the solid state [61]. This is important because as far as possible, obtaining 100% theoretically dense materials in this system in solid state would improve the mechanical properties as such modulus of elasticity compared with glass-ceramic materials with similar thermal shock characteristics. In LAS system, the high temperatures required to fully densify ceramic powders result in large grain sizes due to Ostwald ripening when traditional sintering techniques are used [38]. This makes obtaining dense materials with nanometric and submicrometric grain sizes extremely difficult, and, as a consequence, the sintered materials do not achieve high mechanical properties. To overcome the problem of grain growth, non-conventional sintering methods have emerged as promising techniques [62–65].

Spark plasma sintering (SPS) was reported in [62] as a non-conventional sintering technique for LAS materials that can lead to high relative dense ceramics with no or with very low amounts of a glassy phase. This technique is restricted to materials with disk forms of different diameters, whereas materials with a near-net-shape approach have still not been possible to obtain. Moreover, Vanmeensel et al. [66] reported that the temperature distribution inside the tool and specimen is not homogeneous during the spark plasma sintering technique, especially, for electrical insulating samples (such as LAS ceramics), due to temperature gradient existing between the border and the center of the sample in the intermediate and final stage of sintering. Other important factor to consider is the high-energy consumption of SPS technique.

Microwave heating is a non-conventional sintering technique to solve the difficulties found with previous techniques such as SPS. The microwave technique was specially designed to fabricate ceramic LAS bodies with a high density, a very low glass proportion, and high mechanical properties (hardness and Young's modulus) [63]. An important characteristic associated to microwave process, it is possible to directly obtain materials with complex parts (*near-net-shape* components) directly in the microwave furnace without the application of pressure and without any carbon contamination. This supposes other significant advantage compared with the spark plasma sintering [64]. This point is essential in order to use this sintering technology where the final dimension of the sintered component has to be almost constant in order to reduce the final machining cost of nanocomposites.

Previous reports [63–65] confirmed the possibility of successfully obtaining well-densified β -eucryptite ceramics by using microwave sintering technology with glass-free at relatively low temperatures (1200°C) and very low energy consumed (<80 W). **Figure 8** shows the temperature profile and microwave-absorbed power during the sintering process of an LAS specimen [63]. The figure shows a microwave experiment with a resident time of the ceramic sample of 10 min around 1200°C. The LAS material is a good absorber of microwave radiation at 2.45 GHz, and this implies that the heating is homogeneously distributed throughout the material. The dilatometric data presented for the cryogenic temperature interval are essential in order to design these kinds of materials for space applications in which controlled and very low thermal expansion behavior are needed at very low temperatures. This is the case of mirror blanks in satellites, where exceptional thermal properties are demanded together with exceptional mechanical properties, that is, the β -eucryptite sample sintered at 1200°C shows Young's modulus of 110 MPa and a hardness of 7.1 GPa values [63]. Compared with other heating modes, conventional, and spark plasma sintering [64], the most important characteristics associated to microwave process are the rapid and volumetric heating, which improves the final properties of the materials.

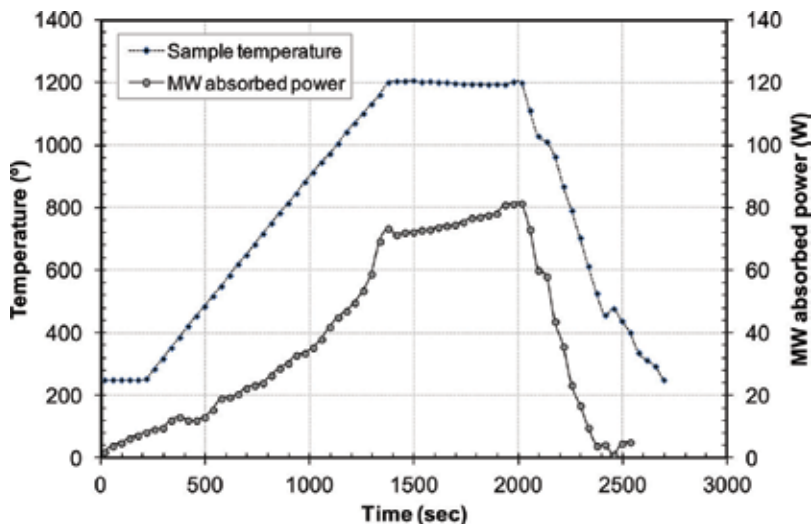


Figure 8. Temperature profile and microwave absorbed power during the sintering process of the LAS specimen.

2.8. Advantages and disadvantages of microwave sintering technology

During sintering process, the heating occurs by the three conventional heat transfer mechanisms: conduction, convection, and radiation. Conduction results by heat diffusion between surfaces in contact, for example, in walls inside the furnace that are in contact with the compact. Convective heat transfer occurs from the bulk flow of the gas in the furnace to the compact surface. Thermal radiation is emitted by high-temperature furnace elements and converted into electromagnetic energy that is transferred to the surroundings. The compact receives this electromagnetic energy causing it to heat up. Heat from radiation is, however, quite low, and most of the heating of the compact occurs by means of conduction and convection. Due to the nature of heat transfer mechanisms involved in this method, the surface of the material always heats first, and a temperature gradient between the compact surface and the interior of the material arises, resulting in heat flow from the surface to the bulk. As a consequence, considerably long dwell times (>2 h) are required in order to obtain a complete temperature homogenization and uniform heat distribution.

Another important sintering approach is pressure-assisted sintering, which consists in the external application of pressure during the heating process. Four main ways can be employed to apply pressure. The first one is hot pressing (HP), resulting from uniaxially applying pressure to the powder in a die. The second one is sinter forging, which is similar to hot pressing but without confining the sample in a die. The third one is called hot isostatic pressing (HIP), which consists in the isostatic application of pressure by means of a gas. The fourth one is spark plasma sintering (SPS) and flash sintering which is similar to HP but using a high heating rate. Pressure-assisted sintering enhances the rate of densification significantly relative to the coarsening rate [27]. However, an important disadvantage of pressure-assisted sintering is the high cost of production being only available for specific industrial applications that require specialized, high-cost components. Another limitation is that only simple shapes can be processed due to the use of dies.

Currently, most commercial materials are processed by conventional sintering and SPS. One of the major drawbacks of these systems, particularly for ceramics, is the high-energy consumption required to reach such high temperatures and dwell times in order to obtain an adequate densification and mechanical properties. Therefore, new approaches on sintering of these materials need to be explored. For example, employing furnaces for heating components with small dimensions would not be energetically efficient. Hence, sintering systems with a focalized energy delivery to the material, such as microwave sintering, can decrease energy use significantly. Moreover, techniques must be flexible and allow for the processing of near-net-shape materials because complex and unique pieces are needed since shapes vary completely from one application to the next. Therefore, microwave sintering confirms as an interesting alternative for the processing of advance ceramics.

3. Conclusions

Currently, innovative sintering methods are being explored and studied in order to reduce energy consumption and production costs, as well as processing tools that allow modification of the densification mechanisms that may improve the microstructure and mechanical

properties of sintered materials. The main purpose for modifying sintering mechanisms is to obtain relative densities close to theoretical values, while maintaining a controlled, but limited, grain growth. Potential of microwaves in material processing has been identified several decades ago. However, owing to limited understanding of the phenomena, their use remained largely confined to only a few materials. Moreover, the overwhelming success of microwave in communication overshadowed its application in other areas. However, discrete attempts in material processing yielded many breakthroughs. In the last 65 years, the microwave processing of materials has become popular due to its potential advantages over the conventional techniques. Overall, microwave sintering is a very good alternative for sintering and consolidating commercial materials for structural applications due to the resulting finer microstructure, enhanced mechanical properties, and reduction in processing times and energy consumption.

Acknowledgements

The authors gratefully acknowledge the funding support of the Spanish Ministry of Economy and Competitiveness (JCI-2011-10498, IJCI-2014-19839, and RYC-2016-20915), the Generalitat Valenciana (GV/2014/009, GRISOLIA/2013/035, and GRISOLIAP/2018/168), Universitat Politècnica de València, and Dr. A. Presenda and Dr. R. Benavente for contributing to the research work described in this chapter.

Author details

Amparo Borrell* and Maria Dolores Salvador

*Address all correspondence to: aborrell@upv.es

Institute of Materials Technology, Polytechnic University of Valencia, Valencia, Spain

References

- [1] Barba A, Clausell C, Felú C, Monzó M. Sintering of $(\text{Cu}_{0.25}\text{Ni}_{0.25}\text{Zn}_{0.50})\text{Fe}_2\text{O}_4$ ferrite. *Journal of the American Ceramic Society*. 2004;**87**:571-577
- [2] Nightingale SS, Dunne DP, Worner HK. Sintering and grain growth of 3 mol% yttria zirconia in a microwave field. *Journal of Materials Science*. 1996;**31**:5039-5043
- [3] Carter CB, Norton MG. *Ceramic Materials Science and Engineering*. 1st ed. New York: Springer; 2007
- [4] Oghbaei M, Mirzaee O. Microwave versus conventional sintering: A review of fundamentals, advantages and applications. *Journal of Alloys and Compounds*. 2010;**494**:175-189
- [5] Clark DE, Sutton WH. Microwave processing of materials. *Annual Review of Materials Science*. 1996;**26**:299-331

- [6] Presenda A, Salvador MD, Penaranda-Foix FL, Moreno R, Borrell A. Effect of microwave sintering on microstructure and mechanical properties in Y-TZP materials used for dental applications. *Ceramics International*. 2015;**41**:7125-7132
- [7] Rybakov KI, Olevsky EA, Krikun EV. Microwave sintering: Fundamentals and modeling. *Journal of the American Ceramic Society*. 2013;**96**:1003-1020
- [8] Osepchuk JM. History of microwave heating applications. *IEEE Transactions on Microwave Theory and Techniques*. 1984;**32**:1200-1224
- [9] Whittaker AG. Diffusion in microwave-heated ceramics. *Chemistry of Materials*. 2005; **17**:3426-3432
- [10] Boch P, Lequeux N. Do microwaves increase the sinterability of ceramics? *Solid State Ionics*. 1997;**101-103**:1229-1233
- [11] Agrawal DK. Microwave processing of ceramics. *Current Opinion in Solid State & Materials Science*. 1998;**3**:480-485
- [12] Gupta M, Wong WLE. Enhancing overall mechanical performance of metallic materials using two-directional microwave assisted rapid sintering. *Scripta Materialia*. 2005; **52**:479-483
- [13] Wang J, Binner J, Vaidhyanathan B, Joomun N, Kilner J, Dimitrakis G, et al. Evidence for the microwave effect during hybrid sintering. *Journal of the American Ceramic Society*. 2006;**89**:1977-1984
- [14] Charmond S, Carry CP, Bouvard D. Densification and microstructure evolution of Y-tetragonal zirconia polycrystal powder during direct and hybrid microwave sintering in a single-mode cavity. *Journal of the European Ceramic Society*. 2010;**30**:1211-1221
- [15] Xie Z, Yang J, Huang Y. Densification and grain growth of alumina by microwave processing. *Materials Letters*. 1998;**37**:215-220
- [16] Peelamedu RD, Roy R, Agrawal D. Anisothermal reaction synthesis of garnets, ferrites, and spinels in microwave field. *Materials Research Bulletin*. 2001;**36**:2723-2739
- [17] Chatterjee A, Basak T, Ayappa KG. Analysis of microwave sintering of ceramics. *AIChE Journal*. 1998;**44**:2302-2311
- [18] Borrell A, Salvador MD, Peñaranda-Foix FL, Cátala-Civera JM. Microwave sintering of zirconia materials: Mechanical and microstructural properties. *International Journal of Applied Ceramic Technology*. 2013;**10**:313-320
- [19] Cheng J. Study on microwave sintering technique of ceramics materials [thesis]. Wuhan University of Technology; 1991
- [20] Breval E, Cheng JP, Agrawal DK, Gigl P, Dennis M, Roy R, et al. Comparison between microwave and conventional sintering of WC/Co composites. *Materials Science and Engineering A*. 2005;**391**:285-295
- [21] Tian YL, Johnson DL, Brodwin ME. Ultrafine microstructure of Al₂O₃ produced by microwave sintering. In *Ceramic Transactions Vol. I, Ceramic Powder Science 2, Part B*. Westerville, Ohio: American Ceramic Society; 1988. pp. 925-932

- [22] Katz JD, Blake RD. Microwave sintering of multiple alumina and composite components. *American Ceramic Society Bulletin*. 1991;**70**:1304-1308
- [23] Cheng J, Agrawal D, Zhang Y, Roy R. Microwave sintering of transparent alumina. *Materials Letters*. 2002;**56**:587-592
- [24] Binner J, Annapoorani K, Paul A, Santacruz I, Vaidhyanathan B. Dense nanostructured zirconia by two stage conventional/hybrid microwave sintering. *Journal of the European Ceramic Society*. 2008;**28**:973-977
- [25] Goldstein A, Travitzky N, Singurindy A, Kravchik M. Direct microwave sintering of yttria-stabilized zirconia at 2.45 GHz. *Journal of the European Ceramic Society*. 1999;**19**:2067-2072
- [26] Upadhyaya DD, Ghosh A, Gurumurthy KR, Prasad R. Microwave sintering of cubic zirconia. *Ceramics International*. 2001;**27**:415-418
- [27] Rahaman MN. *Sintering of Ceramics*. New York: Taylor & Francis Group, CRC Press; 2007
- [28] Thostenson ET, Chou T-W. Microwave processing: Fundamentals and applications. *Composites. Part A, Applied Science and Manufacturing*. 1999;**30**:1055-1071
- [29] Acierno D, Barba AA, D'Amore M. Heat transfer phenomena during processing materials with microwave energy. *Heat and Mass Transfer*. 2004;**40**:413-420
- [30] Kitchen HJ, Vallance SR, Kennedy JL, Tapia-Ruiz N, Carassiti L, Harrison A, et al. Modern microwave methods in solid-state inorganic materials chemistry: From fundamentals to manufacturing. *Chemical Reviews*. 2013;**114**:1170-1206
- [31] Link G, Mijsch S, Thumm M, Takayama S. Microwave sintering techniques—More than just a different way of heating? *Ceramic Engineering and Science Proceedings*. 2008;**28**:55-66
- [32] Chandrasekaran S, Ramanathan S, Basak T. Microwave material processing—A review. *AIChE Journal*. 2012;**58**:330-363
- [33] Astigarraga-Urquiza J, Astigarraga-Aguirre J. *Hornos de Alta Frecuencia Y Microondas. Teoría, cálculo Y Aplicaciones*. McGraw-Hill; 1995
- [34] Bykov YV, Rybakov KI, Semenov VE. High-temperature microwave processing of materials. *Journal of Physics D: Applied Physics*. 2001;**34**:R55-R75
- [35] Katz JD. Microwave sintering of ceramics. *Annual Review of Materials Science*. 1992;**22**:153-170
- [36] Clark DE. *Microwave Solutions for Ceramic Engineers*. Westerville, Ohio: American Ceramic Society; 2005
- [37] Lasri J, Ramesh PD, Schächter L. Energy conversion during microwave sintering of a multi-phase ceramic surrounded by a susceptor. *Journal of the American Ceramic Society*. 2000;**83**:1465-1468
- [38] Anselmi-Tamburini U, Garay JE, Munir ZA. Fast low-temperature consolidation of bulk nanometric ceramic materials. *Scripta Materialia*. 2006;**54**:823-828

- [39] Hall EO. The deformation and ageing of mild steel: III discussion of results. *Proceedings of the Physical Society Section B*. 1951;**64**:747-753
- [40] Borrell A, Salvador MD, Miranda M, Penaranda-Foix FL, Catala-Civera JM. Microwave technique: A powerful tool for sintering ceramic materials. *Current Nanoscience*. 2014; **10**:32-35
- [41] Goldstein A, Travitzky N, Singurindy A, Kravchik M. Direct microwave sintering of yttria-stabilized zirconia at 2.45 GHz. *Journal of the European Ceramic Society*. 1999;**19**: 2067-2072
- [42] Semenov VE, Rybakov KI. What type of transport phenomena can be induced by microwave field in solids and how these phenomena contribute to materials processing. In: Miyake S, editor. *Novel Materials Processing by Advanced Electromagnetic Energy Sources: Proceedings of the International Symposium, MAPEES'04, 2004, Osaka, Japan*. Oxford: Elsevier; 2005. p. 111-117
- [43] Menezes RR, Kiminami RHGA. Microwave sintering of alumina–zirconia nanocomposites. *Journal of Materials Processing Technology*. 2008;**203**:513-517
- [44] Benavente R, Salvador MD, Penaranda-Foix FL, Pallone E, Borrell A. Mechanical properties and microstructural evolution of alumina-zirconia nanocomposites by microwave sintering. *Ceramics International*. 2014;**40**:11291-11297
- [45] Nightingale SA, Worner HK, Dunne DP. Microstructural development during the microwave sintering of yttria–zirconia ceramics. *Journal of the American Ceramic Society*. 1997; **80**:394-400
- [46] Zhang R, Fu SL, Lu HX, Xu HL, Han DF, Zheng LL. Processes affecting microwave sintering of ZTA ceramics. *Journal of Inorganic Materials*. 2001;**16**:178-182
- [47] Park SS, Meek TT. Characterization of ZrO_2 - Al_2O_3 composites sintered in a 2.45 GHz electromagnetic field. *Journal of Materials Science*. 1991;**26**:6309-6313
- [48] Tsakaloudi V, Papazoglou E, Zaspalis VT. Microwave firing of MnZn-ferrites. *Materials Science and Engineering B*. 2004;**106**:289-294
- [49] Borrell A, Salvador MD, Rayón E, Peñaranda-Foix FL. Improvement of microstructural properties of 3Y-TZP materials by conventional and non-conventional sintering techniques. *Ceramics International*. 2012;**38**:39-43
- [50] García-Gañán C, Meléndez-Martínez JJ, Gómez-García D, Domínguez-Rodríguez A. Microwave sintering of nanocrystalline YTZP (3 mol%). *Journal of Materials Science*. 2006;**41**:5231-5234
- [51] Presenda A, Salvador MD, Penaranda-Foix FL, Catala-Civera JM, Pallone E, Ferreira J, Borrell A. Effects of microwave sintering in aging resistance of zirconia-based ceramics. *Chemical Engineering and Processing—Process Intensification*. 2017;**122**:404-412
- [52] Ai Y, Xie X, He W, Liang B, Chen W. Microstructure and properties of Al_2O_3 - ZrO_2 ceramics prepared by microwave sintering. *Key Engineering Materials*. 2014;**633**:193-197

- [53] Presenda A, Salvador MD, Vleugels J, Moreno R, Borrell A. Fretting fatigue wear behavior of Y-TZP dental ceramics processed by non-conventional microwave sintering. *Journal of the American Ceramic Society*. 2017;**100**:1842-1852
- [54] Borrell A, Salvador MD, Peñaranda-Foix FL, Plaza-Gonzalez PJ, Garcia-Baños B, Garcia-Nieto S. Adaptive microwave system for optimum new material sintering. In: 2013 IEEE MTT-S International Microwave Symposium Digest (IMS); 2013. pp. 1-4
- [55] Vasudevan R, Karthik T, Ganesan S, Jayavel R. Effect of microwave sintering on the structural and densification behavior of sol-gel derived zirconia toughened alumina (ZTA) nanocomposites. *Ceramics International*. 2013;**39**:3195-3204
- [56] Monaco C, Prete F, Leonelli C, Esposito L, Tucci A. Microstructural study of microwave sintered zirconia for dental applications. *Ceramics International*. 2015;**41**:1255-1261
- [57] Beall GH, Pinckney LR. Nanophase glass-ceramics. *Journal of the American Ceramic Society*. 1999;**82**:5-16
- [58] Pelletant A, Reveron H, Chévalier J, Fantozzi G, Blanchard L, Guinot F, Falzon F. Grain size dependence of pure β -eucryptite thermal expansion coefficient. *Materials Letters*. 2012;**66**:68-71
- [59] Chen JC, Huang GC, Hu C, Weng JP. Synthesis of negative-thermal expansion ZrW_2O_8 substrates. *Scripta Materialia*. 2003;**49**:261-266
- [60] Sheu GJ, Chen JC, Shiu JY, Hu C. Synthesis of negative thermal expansion TiO_2 -doped LAS substrates. *Scripta Materialia*. 2005;**53**:577-580
- [61] García-Moreno O, Fernández A, Khainakov S, Torrecillas R. Negative thermal expansion of lithium aluminosilicate ceramics at cryogenic temperatures. *Scripta Materialia*. 2010;**63**:170-173
- [62] García-Moreno O, Fernández A, Torrecillas R. Solid state sintering of very low and negative thermal expansion ceramics by spark plasma sintering. *Ceramic International*. 2011;**37**:1079-1083
- [63] Benavente R, Borrell A, Salvador MD, García-Moreno O, Peñaranda-Foix FL, Catalá-Civera JM. Fabrication of near-zero thermal expansion of fully dense β -eucryptite ceramics by microwave sintering. *Ceramic International*. 2014;**40**:935-941
- [64] Benavente R, Salvador MD, García-Moreno O, Peñaranda-Foix FL, Catalá-Civera JM, Borrell A. Microwave, spark plasma and conventional sintering to obtain controlled thermal expansion β -eucryptite materials. *International Journal of Applied Ceramic Technology*. 2015;**12**(S2):E187-E193
- [65] Benavente R, Salvador MD, Martínez-Amesti A, Fernández A, Borrell A. Effect of sintering technology in β -eucryptite ceramics: Influence on fatigue life and effect of micro-cracks. *Materials Science and Engineering*. 2016;**651**:668-674
- [66] Vanmeensel K, Laptev A, Hennicke J, Vleugels J, Van der Biest O. Modelling of the temperature distribution during field assisted sintering. *Acta Materialia*. 2005;**53**:4379-4388

Sintering Processing of Complex Magnetic Ceramic Oxides: A Comparison Between Sintering of Bottom-Up Approach Synthesis and Mechanochemical Process of Top-Down Approach Synthesis

Zhi Huang Low, Ismayadi Ismail and Kim Song Tan

Additional information is available at the end of the chapter

<http://dx.doi.org/10.5772/intechopen.78654>

Abstract

Sintering is a common synthesis method for the fabrication of ceramics. The widespread use of sintering for the production of complex ceramic oxide especially ferrites has led to a variety of investigations on the subject. Top-down approach synthesis like mechanochemical process has recently been suggested as a promising synthesis method for replacing bottom-up approach synthesis methods like sintering, questioning its necessity for thermal treatment at high temperature. Understanding of sintering mechanism is crucial in order to optimize and enhance the advantages of sintering, which cannot be replaced by other techniques. In general, ferrites with particular set of behaviors require a particular set of microstructural properties influenced by the sintering steps. The main objective of this chapter is to understand how the increase of sintering temperature affects the microstructural evolution, in order to develop a fundamental science understanding for the mechanism of sintering. In the second part of this chapter, presentation of experimental results on sintering of mechanically activated $\text{Ni}_{0.5}\text{Zn}_{0.5}\text{Fe}_2\text{O}_4$ nanoparticles and its effect on microstructural, magnetic, and optical properties was reported. Lastly, a comparative study between sintering (bottom-up approach) and mechanochemical (top-down approach) process is presented.

Keywords: bottom-up approach, sintering, barium hexaferrite, Ni-Zn ferrite

1. Introduction

Sintering is one of the oldest material synthesis methods has existed for thousands of years. Since the introduction of controlled sintering process of ceramic, the methodology has gained

rapid growth and well established as one of the most trustable synthesis method for the production of complex ceramic oxides with desired properties [1]. Sintering is categorized as bottom-up approach synthesis as it involves the construction of nanostructures in materials atom-by-atom, layer-by-layer, from small to large sizes [2]. Since twentieth century, energy efficiency and productivity are two important factors in choosing a particular methodology [3]; therefore, top-down approach synthesis method like mechanochemistry has emerged as one of the most promising candidates to replace known current methodologies like sintering, questioning the necessity for thermal treatment at high temperatures. However, there are advantages of sintering that are irreplaceable by other methodologies. Sintering offers matter transport through diffusion while maintaining the stoichiometry of the ceramic material. Commonly, a single phase ceramic oxide with low porosity can be achieved by sintering of the material to a range of 50–80% of its melting point [1]. With an appropriate sintering temperature, the material does not melt, while atomic diffusion can be activated to achieve a dense, compact, and high crystallinity material, which is essential for the fabrication process. Although the optimization of sintering parameters to achieve complete phases of complex ceramic oxides is crucial; however, the fundamental knowledge behind sintering: the correlation between microstructural properties induced by the thermal activation of sintering, with important behaviors like magnetic and optical properties, is important for the understanding of sintering mechanism.

2. Microstructural aspects of complex magnetic ceramic oxides

Microstructure of complex magnetic ceramic oxides consists of grains, grain boundaries, porosity, and defects structures. As complex as it is microstructural properties influence the behaviors of these complex ceramic oxides. For instance, microstructural properties like surface morphology, atomic arrangement, size and shape affect major macroscopic properties such as magnetic, optical, mechanical, electrical, and many other properties of complex ceramic oxides. These are known as the microstructural dependent behaviors of complex ceramic oxides. Nanomaterials exhibit unique behaviors compared to their bulk counterparts [4].

2.1. Size

There are some important behaviors related to magnetic ceramic oxides, which are size dependent. For instance, magnetic properties and particle, grain, or crystallite size are relevant to each other. When the particles are in nano-size, the percentage of amorphous grain boundary volumes in material is high compared to particles in micron size. The presence of large volume fraction of amorphous phase in the material hinders the exchange interaction between magnetic moments. Therefore, small particles are likely to exhibit weak ferromagnetic, superparamagnetic, and paramagnetic behaviors. Small size polycrystalline nickel zinc ferrite dissipates minimum energy [5]. The magnetocrystalline anisotropy energy, E_A for ferrite can be defined by the following equation:

$$E_A = KV \sin^2 \Theta \quad (1)$$

where K is the anisotropy constant, V is the volume of the crystal, and Θ is the angle between the easy axis and the direction of the field-induced magnetic field. When the grains are small in dimensions or below a critical size, they dissipate minimum energy, therefore, the energy required to create a new domain or shifting the domains is much higher than that required in maintaining the material as single domain. The effect of grain size changed some aspects of magnetic behavior of yttrium iron garnets [6]. Below a critical size, as the volume or size of the grains increases, grain size remains in the single-domain range, therefore, the E_A value increases, the magnetocrystalline anisotropy energy becomes stronger and the coercivity (the energy required to change the direction of the magnetization) increases. After the grain size exceeds the critical size, intergranular domain walls are formed inside the grains, because the energy is not sufficient to maintain relatively big grains as single domains. Therefore, domain walls are created to reduce the overall energy of the system. Grain size has similar impact on the magnetic properties of hard ferrite, $\text{BaFe}_{12}\text{O}_{19}$, which has a critical size as well. Studies defined the critical size as the minimum grain volume that the anisotropy energy is able to overcome thermal agitation [7].

Another important magnetic behavior is the measure or ability of a material to sustain a magnetic field within the material when external field applied. This is known as the magnetic permeability. Magnetic permeability is strongly influenced by the presence of grain boundaries or amorphous surfaces, as they will act as impediments to domain wall movement. Bulk materials have fewer grain boundaries, therefore, higher the permeability. This phenomenon especially noticeable in ferrites as their grain boundaries are thicker [4]. The effect of sintering soaking time on the microstructural properties of nickel zinc ferrite was investigated [8, 9]. Grain size increases with increasing soaking time. The increase of grain size is the main factor that causes the increase of initial permeability. Bulk materials have a low-volume fraction of grain boundary as shown in **Figure 1**. Volume fraction can be represented by:

$$V_{shell} = \frac{\frac{4}{3}\pi R^3 - \frac{4}{3}\pi r^3}{\frac{4}{3}\pi R^3} \times 100\% \quad (2)$$

where V_{shell} is the volume fraction of the structurally disordered boundary region, R is the radius of a particle, and r is the radius of the core region of a particle. If we assume the thickness of the shell

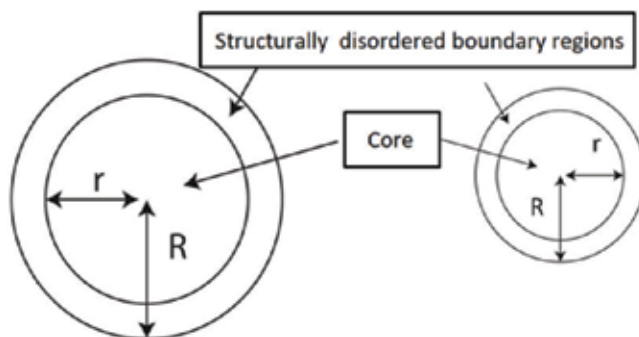


Figure 1. Schematic representation of bulk and nanoparticles, and the definition of R , radius of a particle, and r , radius of the core of a particle.

is approximately 5 nm, for nanoparticles ($R < 100$ nm), the volume fraction of this structurally disordered shell is large ($>10\%$) while for bulk material, the volume fraction of the shell is not significant ($<0.02\%$). As the particles undergo densification and coarsening through increasing sintering temperature, particle size increases from nano-sized to micron-sized. As a result, volume fraction of disordered grain boundary becomes less significant. Therefore, the pinning effects of this disordered boundary region on the domain walls motion is not significant for bulk materials.

2.2. Defects and porosity

Porosity is another microstructural feature that has the pinning effect on the movement of the domain walls. Porosity is abundant in complex magnetic ceramic oxide because it cannot be eliminated by heat treatment. Heat treatment offers grain growth, densification, and boundaries expansion. However, many pores are swept over by grain boundaries and remain within large grain [4]. Porosity and grain size effects sometimes seem inseparable because grain growth and densification happen simultaneously. In case of magnetic properties, saturation magnetization is associated with the following equation [10]:

$$M_s = (1 - p) 4 \pi M_0 \quad (3)$$

where p is the porosity, M_0 is the magnetization extrapolated to zero porosity. Therefore, we can conclude that saturation magnetization is porosity dependent while coercivity is size dependent. Previous study proved that the independence of coercivity from porosity, while saturation magnetization and remanence are independent from grain size effect [10]. In addition to porosity, other defects such as cracks, inclusions, foreign phases, strains, as well as dislocations would alter the magnetic behaviors of ferrites. Defects act as energy wells have a strong pinning effect on the domain wall motion and thus require higher activation energy to detach [4].

2.3. Boundary region

It is believed that boundary region possesses higher energy compared to volume defects. Therefore, boundary region is a highly reactive region, which allows nucleation of new phases. As nanostructured materials have higher surface-to-volume ratio, they are reactive compared to their corresponding bulk materials. In ceramic materials, boundary region between phases and grains governs many properties and processes, for example, as fracture strength, plastic deformation, conductivity, dielectric loss, and phase transformation. All materials have interfacial energy and tension that can be calculated by same thermodynamic formulation [11]. Boundaries act as sinks and sources for the formation of lattice imperfections, diffusion, and phase transformations when deformation occurs. Some behaviors of ceramic oxides such as coercivity and permeability are strongly related to their boundaries [12]. The direction of magnetic moments within the material could be changed easily when the pinning effects of the boundary regions is diminished. Apparent permeability can be expressed as following [13]:

$$\mu_{app} = \frac{(1 - p) \mu_0}{\left(1 + \frac{p}{2}\right) \left(1 + 0.75 \frac{t}{D} \frac{\mu_b}{\mu_0}\right)} \quad (4)$$

where p is the porosity, D is the average grain size, t is the effective thickness of boundary region, μ_b is the permeability of the boundary region, μ_0 is the permeability free from the demagnetizing

field. From the equation, notice that the thickness of boundary region has strong influence on the control of the magnetic properties of ferrites because the thickness of the boundary regions can be altered simply by small amount of additives, impurities, or phase transformations.

3. Ceramic synthesis techniques

Attention has been paid to investigate synthesis techniques and their impacts on new materials, particularly nanostructured and nanocrystalline materials. Synthesis technique is strongly related to behaviors of the investigated nanomaterial because the chosen synthesis technique is responsible for tailoring the atomic and microstructure of the nanostructured material. Numerous published studies have improved our understanding of the effects of synthesis technique on the behaviors of complex magnetic ceramic oxide, especially technologically important hard and soft ferrites [5, 14–16]. Most of the significant findings show that the results are of limited significance unless the microstructures, chemical composition, defects, and atomic arrangement of the investigated ferrite are well-characterized. Generally speaking, the techniques of preparing ferrite are categorized into two: bottom-up and top-down approaches, as shown in **Figure 2**. Bottom-up approach synthesis is a ceramic powder processing approach that engages atoms, ions, molecules or particles as starting building blocks.

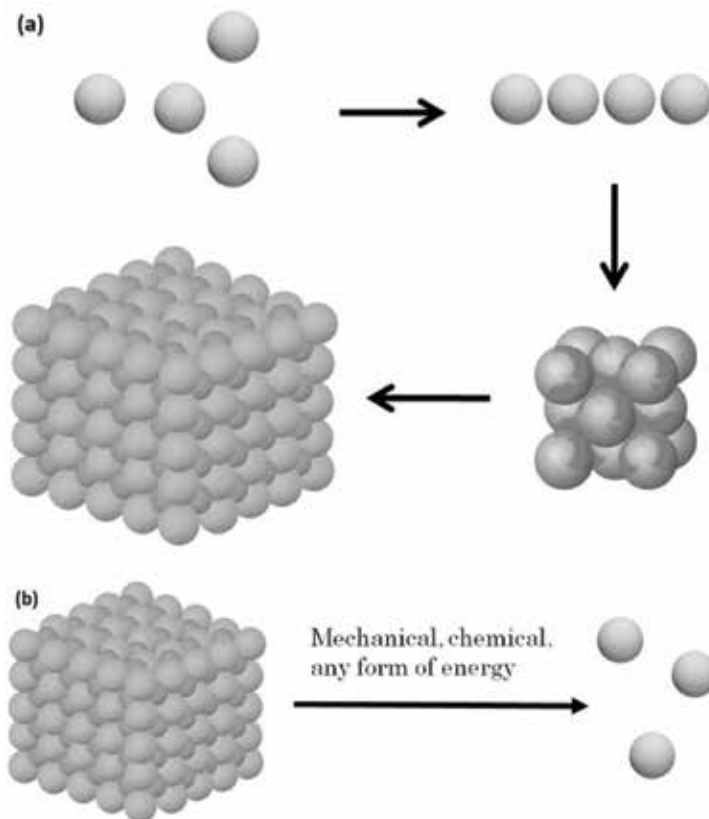


Figure 2. Schematic representations of (a) bottom-up and (b) top-down approaches.

By combining or assembling these building blocks, nanoscale clusters, or corresponding bulk materials are formed. Top-down approach synthesis is a ceramic powder processing approach that begins with micro-structured materials. The approach utilizes mechanical, chemical, or other form of energy to perform structural decomposition to obtain nanoscale materials. Both approaches have its advantages and drawback. For instance, bottom-up approach synthesis such as chemical processes and solid-state routes are capable of producing fine nanocrystalline materials with high purity and homogeneity. However, they have disadvantages like not environmental friendly, high cost of chemical precursors, solvent evaporation, and necessity for thermal treatment at high temperature. On the other hand, top-down approach synthesis like mechanochemical process is considered as green process because it minimizes damage to the environment, fast, economical, and can effectively take nanostructure forms [2]. However, contaminations, defects, and damages that were induced into the material system need to carefully take into account for good material production [15].

4. Ferrites

Ferrites belong to a class of complex magnetic ceramic oxide. The crystal structure of ferrites can be observed as an interlocking network of cations and negatively charged divalent oxygen ions [4]. When a layer of oxygen ions is closely packed lines that connect the centers of these oxygen ions will form a network of equilateral triangles. The second layer of closely packed oxygen ions is arranged in such a way that the centers of these oxygen ions are superimposed with the centers of the equilateral triangles of the first layer. If a similar third layer repeats the same arrangement with the first layer, this arrangement is known as hexagonal close-packed structure in the type of "ababab" stacking sequence. On the other hand, if the third layer arranges in such a way that the centers of the oxygen lie directly over the centers of equilateral triangles adjacent to the ones used for hexagonal close-packed, this will produce a cubic close-packed with a stacking sequence of "abcabc." Then, ferrites are further categorized according to their molar ratio of Fe_2O_3 to other oxide components (modifier oxide) present in the ceramic as presented in **Table 1**.

Type	Structure	Molar ratio of Fe_2O_3 to modifier oxide	Modifier oxide	Example
Magnetoplumbite	Hexagonal	6:1	Group IIA divalent metal oxide. Example: BaO, SrO	$\text{BaFe}_{12}\text{O}_{19}$
Spinel	Cubic	1:1	Transition metal oxide. Example: NiO, ZnO	$\text{Ni}_{0.5}\text{Zn}_{0.5}\text{Fe}_2\text{O}_4$
Garnet	Cubic	3:5	Rare earth oxide	$\text{Y}_3\text{Fe}_3(\text{FeO}_4)_3$

Table 1. Classification of ferrites according to variation in molar ratio of Fe_2O_3 to modifier oxide.

5. Sintering of mechanically activated ferrite powders

Top-down and bottom-up approaches have their own advantages and drawback as mentioned in the previous section. Conventional solid-state process is a bottom-up approach ceramic processing method that involves neither wet chemical reactions nor vapor phase interactions. There are two important processing steps that will affect the quality of the end product: starting powder preparation and heat treatment. The solid-state process is considered as the simplest synthesis route for various ferrites. In the starting powder preparation stage, high-purity raw materials would mix together according to the stoichiometric balance of the final product. This mixing process is being carried out by either dry or wet milling media for a certain period to produce a homogenous distributed starting powder. Then, the starting powder will undergo a heat treatment, typically with the use of a furnace to obtain the final product.

The conventional solid-state process is capable of producing advanced material with unique compositions such as refractory ceramics, glasses, and crystals. Previous research showed that conventional solid-state process was capable of producing particles between 100 nm and 1 micron [16]. However, conventional solid-state process may result in high synthesis temperature because diffusion reaction is limited under low temperature. Besides, this process may produce an incomplete reaction, which results in inhomogeneous products. Other issues of using this process are lack of control of the kinetics and the difficulties of producing desired end products [17]. In order to overcome the drawback of conventional solid-state process, the implementation of mechanical alloying in the starting powder preparation is recommended by many researchers. Apart from the practicality, mechanically activated starting powders exhibit nanostructures and high reactivity. Therefore, it provides an easy, fast, and economical option to produce the desired material. Previous studies showed that starting powder synthesized via mechanical alloying, had a relatively low sintering temperature for the formation of pure, single phase material [5, 7, 18, 19].

6. Experimental results of sintering of mechanically activated soft ferrite $\text{Ni}_{0.5}\text{Zn}_{0.5}\text{Fe}_2\text{O}_4$

6.1. Microstructural properties

X-ray Diffraction (XRD) spectra of $\text{Ni}_{0.5}\text{Zn}_{0.5}\text{Fe}_2\text{O}_4$ after sintering from 600 to 1200°C are presented in **Figure 3**. In view of the results obtained, the occurrence of [121] peak in 600°C spectrum indicated incomplete reaction between raw materials to form a single phase powder. $\alpha\text{-Fe}_2\text{O}_3$ existed as secondary phase at 600°C. The [121] peak shows the existence of secondary phase $\alpha\text{-Fe}_2\text{O}_3$ in the $\text{Ni}_{0.5}\text{Zn}_{0.5}\text{Fe}_2\text{O}_4$ phase. The $\alpha\text{-Fe}_2\text{O}_3$ phase disappeared when the sintering temperature was increased to 700°C. A complete $\text{Ni}_{0.5}\text{Zn}_{0.5}\text{Fe}_2\text{O}_4$ was formed as Zn^{2+} ions diffused into the tetrahedral sites while Ni^{2+} ions occupied the octahedral sites. As the starting powders were mechanically activated by high-energy ball milling by SPEX is the modal name of the dual mixer machine. Which was specially modified to achieve high speeds (approximately 1725 rpm) for the effective production of nanostructured particles; this enables the

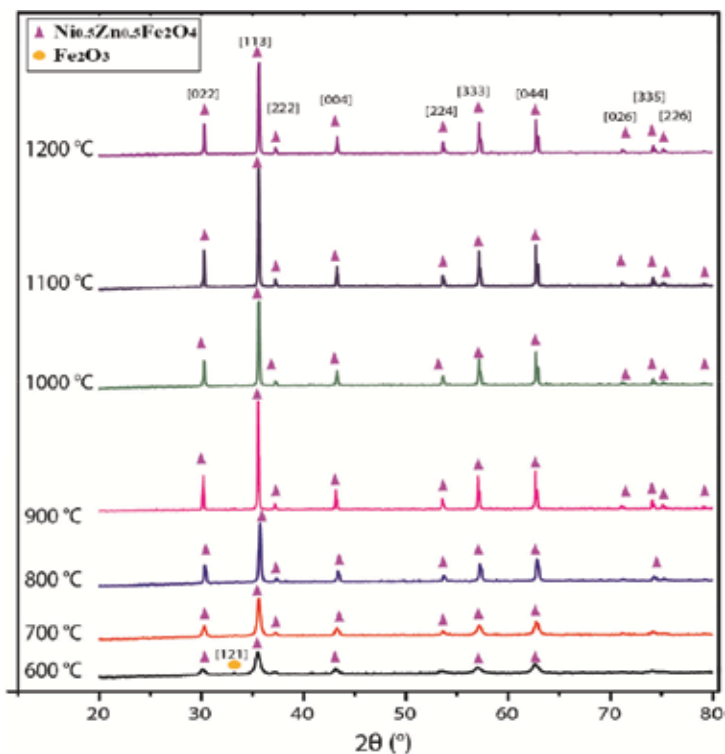


Figure 3. X-ray diffraction patterns of $\text{Ni}_{0.5}\text{Zn}_{0.5}\text{Fe}_2\text{O}_4$ sintered from 600 to 1200°C.

formation of single phase at a lower sintering temperature. It is worth mentioning that the synthesis temperature for single phase Ni-Zn ferrite for refluxing method is between 950 and 1150°C [20]; sol-gel technique requires more than 1000°C [21]; co-precipitation method requires 550–1000°C [22]. The intensity of the Bragg peaks increased, and the peak widths decreased with increasing sintering temperature indicating the increase of crystallinity and particle size.

Structural information was obtained from Rietveld refinement. The increase of lattice parameters and unit cell volume was observed. As shown in **Figure 4**, as the sintering temperature increased, the unit cell volume expanded, and Zn^{2+} ions diffused into the interstitial sites; this was crucial for the reaction as interstitial diffusion is the most important lattice diffusion mechanism [1]. Further increasing of sintering temperature (>900°C), a decrease in lattice parameters and unit cell volume was observed. This could be due to the small amount of Zn^{2+} ions evaporated from the lattice [8]. This is because zinc has a low-boiling point of 907°C. Mechanically activated starting material has high lattice strain as defects and inhomogeneity could be introduced into the system. This is known as the second order stress, which it modifies the materials by one grain to another or from one part of the grain to another on a microscopic scale. There was also first order stress induced by milling. This type of stress modifies the material uniformly across the entire material [23], causing a macroscopic variation on the material. By increasing the sintering temperature, relaxation can be attained for macro and micro stresses induced during milling.

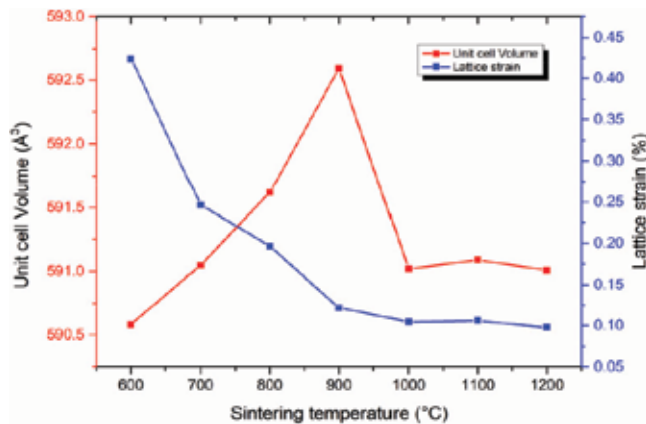


Figure 4. Unit cell volume and lattice strain as a function of sintering temperature.

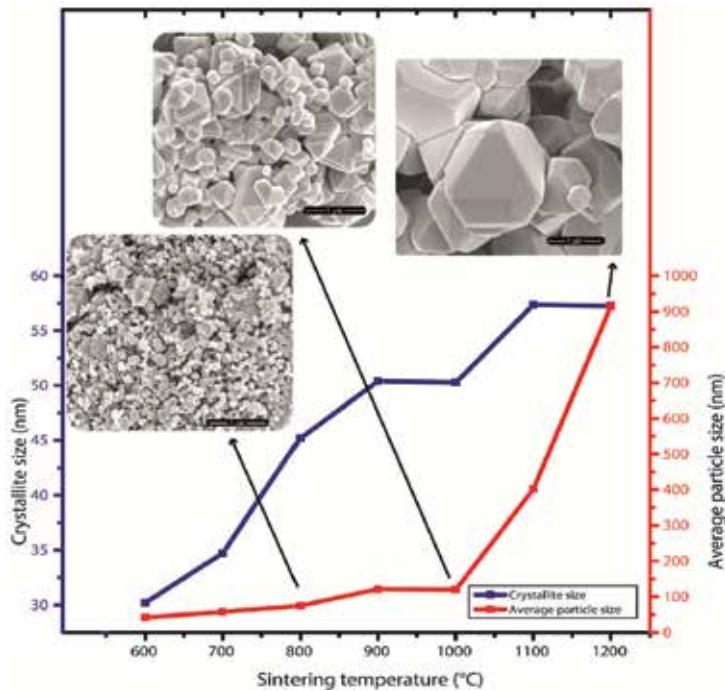


Figure 5. Average particle size and crystallite size as a function of sintering temperature; the evolution of morphology is shown in the inserted field emission scanning electron microscope (FESEM) micrographs.

Figure 5 shows the evolution of particle size, crystallite size, and morphological properties of $\text{Ni}_{0.5}\text{Zn}_{0.5}\text{Fe}_2\text{O}_4$ with elevating sintering temperature. As a whole, bottom-up synthesis of soft ferrite, $\text{Ni}_{0.5}\text{Zn}_{0.5}\text{Fe}_2\text{O}_4$ acquires three stages of sintering. Initial stage of sintering can be observed for samples sintered at 600-, 700-, and 800°C. Phenomena such as rearrangement

of particles and necking structure can be observed at this stage. At the intermediate stage (900-, 1000-, and 1100°C), further increase of sintering provides sufficient thermal energy for nanoparticles to move closer. Grain boundaries are formed. However, the most significant observation for intermediate stage is the formation of interconnected pores. Finally, the sample sintered at 1200°C exhibited the final stage of sintering. Isolated pores are observed, and rigid crystal structure is visible. The coarsening and densification of particles are observed with increasing sintering temperature.

6.2. Three stages of sintering

The activation energy of particle growth of sintering is strongly related to the size evolution of the particles [24]. Size-dependent activation energy can be represented by the plot of log particle size (D) versus the reciprocal of absolute temperature ($1/T$) of $\text{Ni}_{0.5}\text{Zn}_{0.5}\text{Fe}_2\text{O}_4$ [25]. Three distinct stages of sintering can be observed in **Figure 6**. Activation energy is the lowest at initial stage, indicating the particles are nano-sized, which exhibit relatively largest surface area. Small thermal energy is enough to initiate the particle growth. Through intermediate and final stages, particle size increases, therefore, the activation energy for particle growth increases hence higher thermal energy is required for the densification and coarsening mechanisms in sintering [26]. As a summary during initial stage, particles rearranged themselves so that they

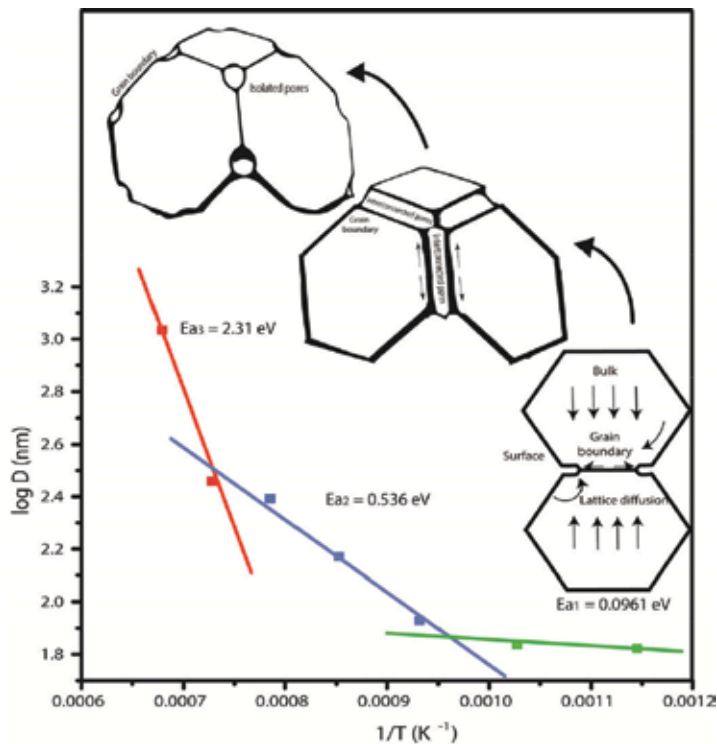


Figure 6. Plot of log D versus the reciprocal of absolute temperature ($1/T$) of $\text{Ni}_{0.5}\text{Zn}_{0.5}\text{Fe}_2\text{O}_4$ showing three stages of sintering.

are in tangential contact. This is to activate the material transport mechanism through diffusion. During this process, necking structures are formed between particles. At intermediate stage, densification occurs and the pores shrink to reduce their cross-section. As a result, interconnected pores are formed at the boundary regions. Densification and coarsening continue to occur; eventually, the pores become unstable and isolated at the final stage of sintering [1].

High resolution transmission electron microscopy (HRTEM) is utilized to identify some unique features of each stage in terms of atomic arrangement, structural information, and defects like grain boundaries. In **Figure 7a**, a lattice spacing of 2.53 Å was measured for $\text{Ni}_{0.5}\text{Zn}_{0.5}\text{Fe}_2\text{O}_4$, corresponding to (113) lattice plane. A few particles rearrange themselves in such a way that they are in tangential contact. The contact points between particles are the material transport paths that allow diffusions to occur at early stage of sintering. In **Figure 7b**, it can be seen that the spheres begin to coalesce. The radius of the necking structure has reached a value of >0.50 of the particle radius. This indicated that at sintering temperature of 800°C, the particles are near the end of an initial stage of sintering [1].

In **Figure 8a**, it can be observed that two particles were brought together, and they are undergoing deformation in response to surface energy reduction. Massive lattice diffusion and material transport occur between these particles. In **Figure 8b**, grains adopt the shape of polyhedron with multiple faces, and the edge of the particle appears to have a clean

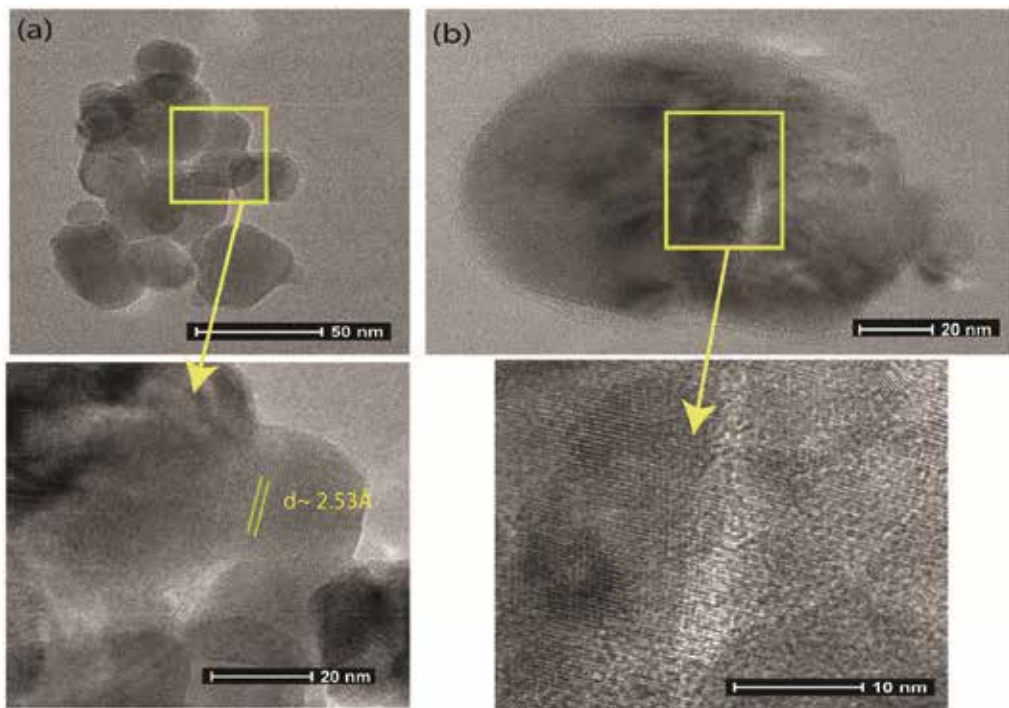


Figure 7. High resolution transmission electron microscopy (TEM) images for $\text{Ni}_{0.5}\text{Zn}_{0.5}\text{Fe}_2\text{O}_4$ nanoparticles sintered at (a) 600°C, and (b) 800°C (initial stage of sintering).

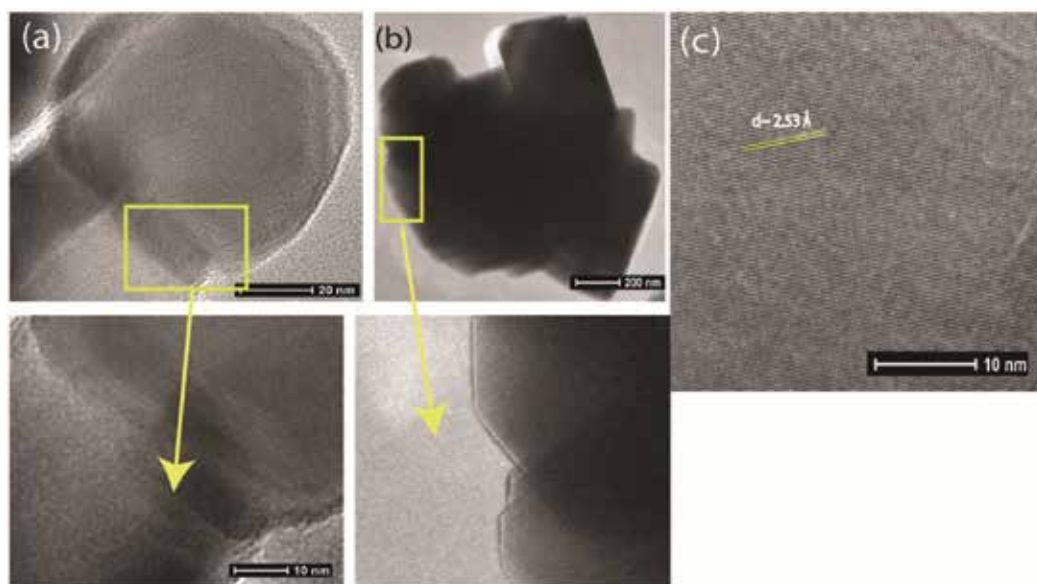


Figure 8. High resolution TEM images for $\text{Ni}_{0.5}\text{Zn}_{0.5}\text{Fe}_2\text{O}_4$ nanoparticles sintered at (a) 900°C, (b) 1100°C (intermediate stage of sintering), and (c) 1200°C (final stage of sintering).

crystalline surface, where amorphous phase diminishes at 1100°C. In the final stage of sintering (**Figure 8c**), a homogeneous atomic arrangement, with (113) lattice plane is formed.

6.3. Microstructural related properties of sintered $\text{Ni}_{0.5}\text{Zn}_{0.5}\text{Fe}_2\text{O}_4$

Figure 9a shows the M-H hysteresis loops of $\text{Ni}_{0.5}\text{Zn}_{0.5}\text{Fe}_2\text{O}_4$ sintered at various temperatures. The magnetic parameters are extracted from hysteresis loops. All the samples sintered from 600 to 1200°C exhibited less slanting, narrow sigmoid hysteresis loop. This indicates that the preparation of raw powder with modified high-speed mechanical alloying increases the reactivity of nanoparticles. Ferromagnetic phase exists in the sample even at low sintering temperatures such as 600 and 700°C. **Figure 9b** shows the plot of maximum magnetization at 10 kOe, $M_{10\text{kOe}}$ against sintering temperature. In view of the results obtained, the $M_{10\text{kOe}}$ values increase with increasing sintering temperature. At low sintering temperature, small particles exhibit surface distortion due to the interaction of transition metal ions in the lattice with oxygen atoms, causing a reduction in the resultant magnetic moment. This phenomenon is normally predominant in ultrafine particles because of their large surface to volume ratio. This effect becomes less influential at high sintering temperature as particle size increases. Volume fraction of amorphous phase decreases with increasing sintering temperature. Thus, the exchange interaction between particles increases with increasing volume fraction of crystalline phase. As a result, strong ferromagnetic behaviors are strengthened with erect, narrow, and well-defined sigmoid hysteresis loops are observed with increasing temperature. Coercivity has an indirect relationship with particle size. At low sintering temperature, there are amorphous phase and defects like grain boundaries in the sample. Therefore, the magnetocrystalline anisotropy is low because the crystalline volume fraction is low. Below a critical size ($D_c \approx 90$ nm), coercivity increases with average particle size. As the sintering temperature increases, the crystalline volume fraction increases, the magnetocrystalline

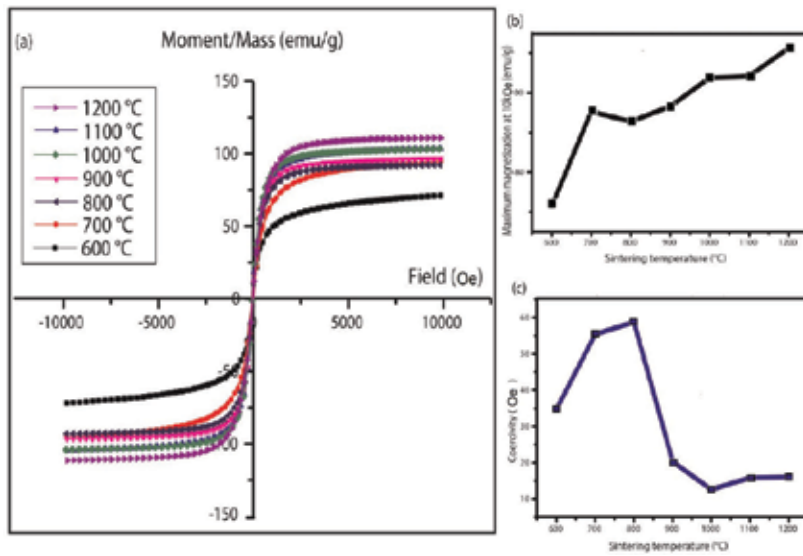


Figure 9. Magnetic parameters of bottom-up synthesis $\text{Ni}_{0.5}\text{Zn}_{0.5}\text{Fe}_2\text{O}_4$: (a) hysteresis loops at different sintering temperature, (b) plot of M_{10kOe} versus sintering temperature, (c) plot of coercivity versus sintering temperature.

anisotropy is enhanced. To change the orientation of magnetic moment, higher energy is required to overcome this magnetocrystalline anisotropy energy. Therefore, below D_c coercivity increases with increasing average particle size. Above this D_c , high magnetocrystalline anisotropy is not favorable in terms of energy level [27]. In order to reduce the overall energy of the system, domain walls are created causing the coercivity to decrease.

In **Figure 10**, a red shift of optical property is observed with increasing sintering temperature. It can be seen that the increase of crystallite is accompanied with the decrease of optical bandgap values (red-shift). This is thought to be due to size-dependent quantum confinement effect. Quantum confinement effect can be observed when the crystallite size is in the same order as the wavelength of the electron. The energy level at the microscopic level can be described by the expression [28]:

$$E = \frac{(hk)^2}{2m} \quad (5)$$

where h is the Planck constant, k is the wave factor ($k = 2\pi/\lambda$), m is the mass of electron. When the crystallite size is small, the wave vector k can be expressed as [28]:

$$k = \frac{2\pi}{\lambda} = \frac{n\pi}{a} \quad (6)$$

where a is the crystallite size of the material and n is an integer. Based on Eqs. 5 and 6, the value of wave vector k has an inversely proportional relationship with the crystallite size. The crystallite size increased with increasing sintering temperature resulting in decrease of wave vector k value. When we substitute $n = 1, 2, 3$, and so on, for Eqs. 5 and 6, the difference between two consecutive energy becomes smaller. Therefore, energy bandgap values decrease with increasing crystallite size. This phenomenon happens when the motion of electrons is restricted in a nano-scale size.

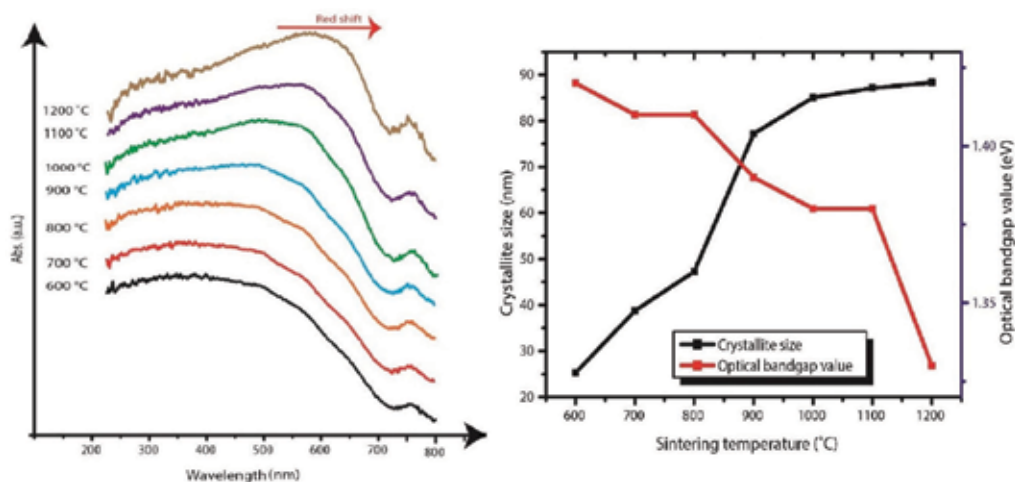


Figure 10. Optical properties of $\text{Ni}_{0.5}\text{Zn}_{0.5}\text{Fe}_2\text{O}_4$ nanoparticles sintered at different sintering temperature.

7. Comparative study of bottom-up and top-down approach synthesis

Sample with similar particle size, synthesized via mechanochemical process with optimized parameters [29] is chosen as a candidate for this comparative study with two parameters were chosen, which were milling at 8 hours (top-down approach) and sintering synthesis at 900 °C (bottom-up approach). **Figure 11** shows the XRD diffraction patterns milled at 8 hours and sintered at 900 °C $\text{Ni}_{0.5}\text{Zn}_{0.5}\text{Fe}_2\text{O}_4$ nanoparticles. Nanoparticles that milled 8 hours exhibit a superimposition of broad diffraction reflections on the broad diffraction maximum or “hump,” indicating the presence of a highly disordered phase. Nanoparticles that sintered at 900 °C exhibit a single phase pattern with sharp Bragg peaks.

Figure 12. shows the field emission scanning electron microscope (FESEM) micrographs and particle size distribution for nanoparticles synthesized by different synthesis approaches. As can be seen, nanoparticles that sintered at 900 °C have a narrower size distribution compared to nanoparticles that milled at 8 hours. Commercial nanoparticles are uniform in size. Densification mechanism of sintering can be seen in **Figure 12b**. Small and large particles coexisted for both bottom-up and top-down approaches synthesized nanoparticles. However, particles with rigid and clear grain boundaries can be observed in sintered particles while top-down approach synthesized particles are agglomerated particles with randomly shaped boundaries.

Figure 13 shows the M-H hysteresis loops of $\text{Ni}_{0.5}\text{Zn}_{0.5}\text{Fe}_2\text{O}_4$ nanoparticles synthesized via different synthesis approaches. Nanoparticles that milled at 8 hours exhibited complex disordering in structure. Therefore, it possesses canted spin arrangement that has significant implications on its magnetism. The maximum magnetization at 10 kOe is lower compared to nanoparticles that sintered at 900 °C. On the other hand, nanoparticles that sintered at 900 °C exhibited low coercivity with high saturation magnetization (the magnetization at 10 kOe had

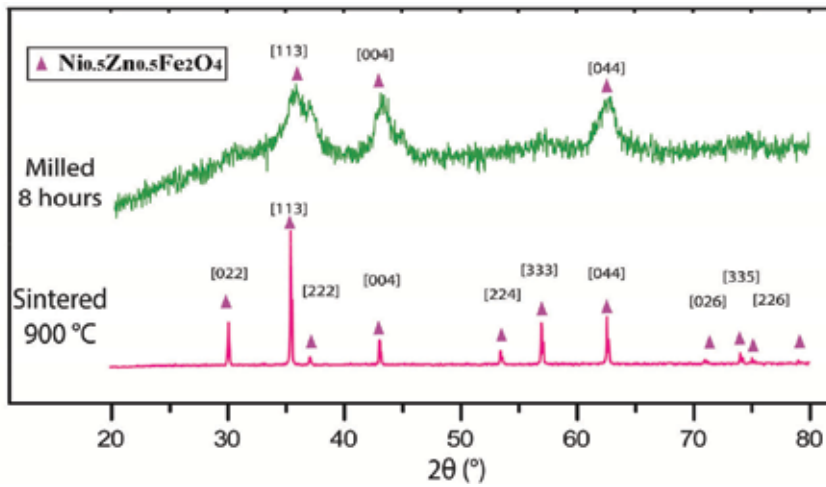


Figure 11. X-ray diffraction patterns of $\text{Ni}_{0.5}\text{Zn}_{0.5}\text{Fe}_2\text{O}_4$ nanoparticles synthesized by different synthesis approaches.

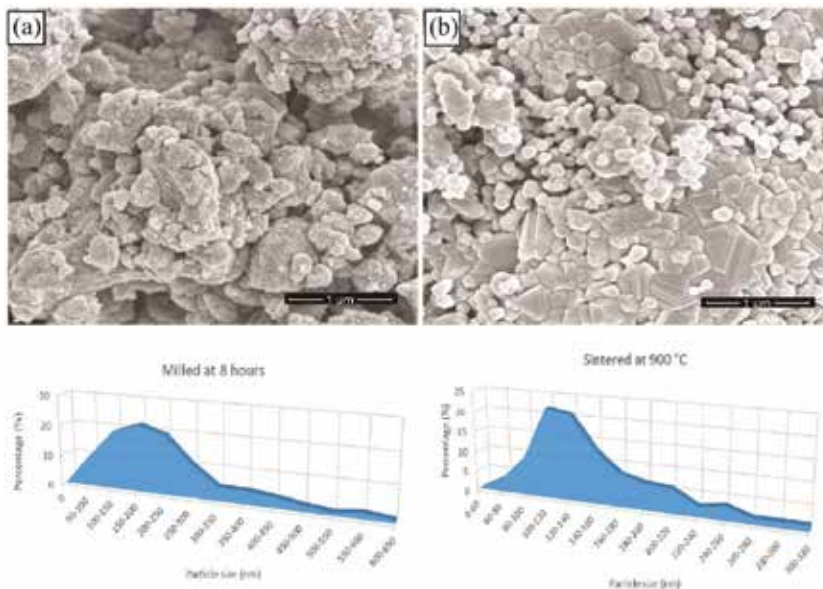


Figure 12. FESEM micrographs and particle size distribution for (a) milled at 8 hours and (b) sintered at 900°C.

saturated). This indicated that the formation of single phase nickel zinc ferrite that exhibits soft ferrite magnetic properties. The optical bandgap values were 1.39–1.30 eV for sintered at 900°C and milled at 8 hours nanoparticles, respectively. Both bottom-up and top-down approaches synthesized nanoparticles exhibit same order optical bandgap value. It is evident that optical bandgap is a size-dependent behavior. However, defects that induced during mechanochemical process reduced the optical bandgap value of nanoparticles that milled at 8 hours. This is attributed to structural disorder bandgap narrowing effect.

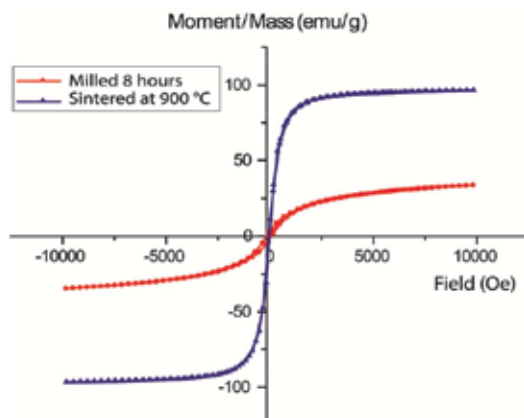


Figure 13. M-H hysteresis loops of $\text{Ni}_{0.5}\text{Zn}_{0.5}\text{Fe}_2\text{O}_4$ nanoparticles synthesized by different synthesis approaches.

8. Conclusions

As most common approach for the fabrication of ceramic material, sintering shows some irreplaceable advantages. Sintering provides control on processing variables like sintering temperature, to achieve required microstructure for a particular set of properties. The synthesis temperature for single homogeneous phase can be lowered by mechanically activates the starting materials. Three stages of sintering mechanism can be observed in the experimental data of Ni-Zn ferrite. The observed evolutionary relationship between microstructural, magnetic, and optical properties can be used to develop a useful framework for designing a sintering condition for final microstructure with desired properties. From the comparative study of top-down and bottom-up approaches carried out, we concluded that different synthesis methods produced ceramic materials with different behaviors. Top-down approach synthesis method has the ability to produce nanocrystalline particles, which then must be compacted without losing the refined microstructural properties, with high uniformity in terms of size, and morphological properties. This remains a challenge to this approach otherwise it is a versatile method. Bottom-up approach synthesis method is capable of producing particles with refined microstructures, which then high-purity single phase particles must be produced with particle size below 100 nm. This is relatively more difficult as single phase can only be achieved when sufficient heat energy is provided, and typically single phase particles are produced at high sintering temperature where particle growth is unavoidable.

Acknowledgements

We would like to dedicate this chapter and show our gratitude to the late Assoc. Prof. Dr. Mansor Hashim from Universiti Putra Malaysia, Malaysia for sharing his pearls of wisdom with us during the course of this research.

Author details

Zhi Huang Low¹, Ismayadi Ismail^{1*} and Kim Song Tan²

*Address all correspondence to: ismayadi@upm.edu.my

1 Materials Synthesis and Characterization Laboratory, Institute of Advanced Technology, Universiti Putra, Malaysia, Serdang, Selangor Darul Ehsan, Malaysia

2 Advanced Imaging Centre, Malaysian Rubber Board, RRIM Sungai Buloh, Selangor, Malaysia

References

- [1] Rahaman MN. Sintering of Ceramics. Boca Raton: CRC Press; 2007
- [2] Sopicka-Lizer M. High-Energy Ball Milling Mechanochemical Processing of Nanopowders. Boca Raton, Florida: CRC Press; 2010
- [3] Holdren JP. Science and technology for sustainable well-being. *Science*. 2008;**319**:424-434
- [4] Goldman A. Modern Ferrite Technology. 2nd ed. Pittsburgh, PA, USA: Springer; 2006
- [5] Idza IR, Hashim M, Rodziah N, Ismayadi I, Norailiana AR. Influence of evolving microstructure on magnetic-hysteresis characteristics in polycrystalline nickel–zinc ferrite, $\text{Ni}_{0.3}\text{Zn}_{0.7}\text{Fe}_2\text{O}_4$. *Materials Research Bulletin*. 2012;**47**(6):1345-1352
- [6] Rodziah N, Hashim M, Idza IR, Ismayadi I, Hapishah AN, Khamirul MA. Applied surface science dependence of developing magnetic hysteresis characteristics on stages of evolving microstructure in polycrystalline yttrium iron garnet. *Applied Surface Science*. 2012;**258**(7):2679-2685
- [7] Shafie MSE, Hashim M, Ismail I, Kanagesan S, Fadzidah MI, Idza IR, Hajalilou A, Sabbaghizadeh R. Magnetic M–H loops family characteristics in the microstructure evolution of $\text{BaFe}_{12}\text{O}_{19}$. *Journal of Materials Science: Materials in Electronics*. 2014;**25**(9):3787-3794
- [8] Ismail I, Hashim M, Matori KA, Alias R, Hassan J. The transition from paramagnetic to ferromagnetic states as influenced by evolving microstructure of $\text{Ni}_{0.5}\text{Zn}_{0.5}\text{Fe}_2\text{O}_4$. *Journal of Superconductivity and Novel Magnetism*. 2012;**25**(1):71-77
- [9] Bera J, Roy PK. Effect of grain size on electromagnetic properties of $\text{Ni}_{0.7}\text{Zn}_{0.3}\text{Fe}_2\text{O}_4$ ferrite. *Physica B: Condensed Matter*. 2005;**363**(1-4):128-132
- [10] Igarashi H, Okazaki K. Effects of porosity and grain size on the magnetic properties of NiZn ferrite. *Journal of the American Ceramic Society*. 1977;**60**(1-2):51-54
- [11] Kingery WD. Plausible concepts necessary and sufficient for interpretation of ceramic grain-boundary phenomena: I, grain-boundary characteristics, structure, and electrostatic potential. *Journal of the American Ceramic Society*. 1974;**57**(1):1-8

- [12] Dho J, Lee EK, Park JY, Hur NH. Effects of the grain boundary on the coercivity of barium ferrite $\text{BaFe}_{12}\text{O}_{19}$. *Journal of Magnetism and Magnetic Materials*. 2005;**285**(1-2):164-168
- [13] Rikukawa H. Relationship between microstructures and magnetic properties of ferrites containing closed pores. *IEEE Transactions on Magnetics*. 1982;**18**(6):1535-1537
- [14] Ibrahim IR, Hashim M, Nazlan R, Ismail I, Wan Ab Rahman WN, Abdullah NH, Idris FM, Shafie MSE, Zulkimi MMM. Grouping trends of magnetic permeability components in their parallel evolution with microstructure in $\text{Ni}_{0.3}\text{Zn}_{0.7}\text{Fe}_2\text{O}_4$. *Journal of Magnetism and Magnetic Materials*. 2014;**355**:265-275
- [15] Suryanarayana C. *Mechanical Alloying and Milling*. New York: Marcel Dekker; 2004
- [16] Benito G, Morales MP, Requena J, Raposo V, Vázquez M, Moya JS. Barium hexaferrite monodispersed nanoparticles prepared by the ceramic method. *Journal of Magnetism and Magnetic Materials*. 2001;**234**(1):65-72
- [17] Zahi S, Daud AR, Hashim M. A comparative study of nickel-zinc ferrites by sol-gel route and solid-state reaction. *Materials Chemistry and Physics*. 2007;**106**(2-3):452-456
- [18] Hajalilou A, Hashim M, Ebrahimi-Kahrizangi R, Kamari HM. Influence of evolving microstructure on electrical and magnetic characteristics in mechanically synthesized polycrystalline Ni-ferrite nanoparticles. *Journal of Alloys and Compounds*. 2015;**633**:306-316
- [19] Low ZH, Hashim M, Ismail I, Kanagesan S, Ezzad Shafie MS, Idris FM, Ibrahim IR. Development of magnetic B-H hysteresis loops through stages of microstructure evolution of bulk $\text{BaFe}_{12}\text{O}_{19}$. *Journal of Superconductivity and Novel Magnetism*. 2015;**28**(10):3075-3086
- [20] Yan W, Li Q, Zhong H, Zhong Z. Characterization and low-temperature sintering of $\text{Ni}_{0.5}\text{Zn}_{0.5}\text{Fe}_2\text{O}_4$ nano-powders prepared by refluxing method. *Powder Technology*. 2009;**192**(1):23-26
- [21] Zahi S, Hashim M, Daud AR. Synthesis, magnetic properties and microstructure of Ni-Zn ferrite by sol-gel technique. *Journal of Magnetism and Magnetic Materials*. 2007;**308**(2):177-182
- [22] Chen DG, Tang XG, Wu JB, Zhang W, Liu QX, Jiang YP. Effect of grain size on the magnetic properties of superparamagnetic $\text{Ni}_{0.5}\text{Zn}_{0.5}\text{Fe}_2\text{O}_4$ nanoparticles by co-precipitation process. *Journal of Magnetism and Magnetic Materials*. 2011;**323**(12):1717-1721
- [23] Cullity BD, Stock SR. *Elements of X-Ray Diffraction*. 3rd ed. United Kingdom: Pearson, Prentice Hall; 2011
- [24] Phuoc TX, Chen R-H. Modeling the effect of particle size on the activation energy and ignition temperature of metallic nanoparticles. *Combustion and Flame*. 2012;**159**(1):416-419
- [25] Jarcho M, Bolen CH, Thomas MB, Bobick J, Kay JF, Doremus RH. Hydroxylapatite synthesis and characterization in sense polycrystalline forms. *Journal of Materials Science*. 1976;**11**:2027-2035

- [26] Kang SJL. Sintering Densification, Grain Growth, and Microstructure. London, United Kingdom: Elsevier; 2005
- [27] Skomski R, Sellmyer DJ. Intrinsic and extrinsic properties of advanced magnetic materials. *ChemInform*. 2006;**37**(47):1
- [28] Fox M. *Optical Properties of Solids*. 2nd ed. United States: Clarendon Press Oxford; 2010
- [29] Low ZH, Chen SK, Ismail I, Tan KS, Liew JYC. Structural transformations of mechanically induced top-down approach BaFe₁₂O₁₉ nanoparticles synthesized from high crystallinity bulk materials. *Journal of Magnetism and Magnetic Materials*. 2017;**429**:192-202

Sintering Temperature Effect on Microstructure and Magnetic Evolution Properties with Nano- and Micrometer Grain Size in Ferrite Polycrystals

Raba'ah Syahidah Azis,
Muhammad Syazwan Mustaffa and
Nuraine Mariana Mohd Shahrani

Additional information is available at the end of the chapter

<http://dx.doi.org/10.5772/intechopen.78638>

Abstract

The morphology and evolution of magnetic properties in multisample sintering (MSS) of yttrium iron garnet ($Y_3Fe_5O_{12}$, YIG) and single-sample sintering (SSS) of nickel zinc ferrite ($Ni_{0.6}Zn_{0.4}Fe_2O_4$, NZF) were studied in detail, focusing on the parallel evolving relationship with their dependences on sintering temperature. Sintering is an important process in ferrite fabrication which involved the process of transforming a noncrystalline powder into a polycrystalline solid by heating process. Under the influence of heat, the surface area is reduced through the formation and growth of bond between the particles associated with reduction in surface energy. This makes the particles move closer, grains to form by the movement of grain boundaries to grow over pores, and results in decreasing the porosity and increasing the density of the sample. Technological applications, especially in electronics applications, require high-density nanostructured ferrites, integrated by sintering from nanoparticles. The evolution from low to high sintering temperature will result in the transition from disordered to ordered ferromagnetism behavior. Multisample sintering (MSS) of yttrium iron garnet ($Y_3Fe_5O_{12}$, YIG) and single-sample sintering (SSS) of nickel zinc ferrite ($Ni_{0.6}Zn_{0.4}Fe_2O_4$, NZF) have been used as a studied material in this research work.

Keywords: MSS yttrium iron garnet ($Y_3Fe_5O_{12}$, YIG), SSS nickel zinc ferrite ($Ni_{0.6}Zn_{0.4}Fe_2O_4$, NZF), microstructure, magnetic properties

1. Introduction of garnet and spinel ferrites

Garnet ferrites with composition ($A_3B_5O_{12}$) structure have unique electromagnetic, magneto-optical, mechanical, and thermal properties [1]. Garnet ferrite comprises three crystallographic lattice (a, b, and c) sites. Among these lattice sites, the $24Fe^{3+}$, $16Fe^{3+}$, and $24R^{3+}$ ions occupy the [b] tetrahedral, (a) octahedral, and {c} dodecahedral sites, respectively, whereas oxygen ions are distributed to the interstitial sites [2]. However, R is the rare earth ions such as Ce, Gd, Y, and Nd. The general formula for rare earth garnets is $R_3Fe_5O_{12}$, whereas the ion distribution in rare earth garnets are $[Fe_2](Fe_3)\{R_3\}O_{12}$ represented tetrahedral, octahedral, and dodecahedral sites, respectively [3]. As for Ni-Zn ferrite, it has a spinel ferrite structure. Spinel ferrite crystallizes in the cubic structure. Spinel ferrites have the general formula $M(Fe_2O_4)$, where M is usually a divalent cation such as manganese (Mn^{2+}), nickel (Ni^{2+}), cobalt (Co^{2+}), zinc (Zn^{2+}), copper (Cu^{2+}), or magnesium (Mg^{2+}). The unit cell of spinel ferrites consists of 32 oxygen, 16 trivalent iron, and 8 divalent metal ions. The most important feature of the unit cell is that its array of oxygen ions leaves open two kinds of interstices, which can be filled by the metal ions. These interstices are referred to as tetrahedral or A sites and octahedral or B sites. The sintering process plays a prominent role in the fabrication of ceramics. Almost all ceramic bodies must be fired at elevated temperatures to produce a microstructure with the desired properties. This widespread use of sintering process has led to a variety of approaches to the subject. The criteria that should be met before sintering can occur are the mechanism for material transport and source of energy to activate and sustain this material transport. The relationship between microstructural properties with the effect of sintering temperature toward magnetic characteristics of MSS of yttrium iron garnet ($Y_3Fe_5O_{12}$, YIG) and SSS of nickel zinc ferrite ($Ni_{0.6}Zn_{0.4}Fe_2O_4$, NZF) is the focus of interest in this research work.

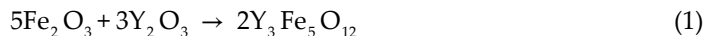
2. Brief overview of preparation methods

2.1. Preparation of hematite (Fe_2O_3)

About 100 g of mill scale was weighed using digital weighing balance. The mill scale was used as Fe_2O_3 source for preparing YIG. The mill scale was crushed by wet milling process for 48 h to obtain the precise sized powder. The magnetic particles were poured into a glass tube filled with 90–100°C distilled water in the presence of 1 T external magnetic field. Due to the weak susceptibility of ferromagnetic particles, FeO (wustite) presumably would drop to the bottom of the tube, and the Fe_3O_4 (magnetite) and Fe_2O_3 (hematite) would be attracted to the surface close to the poles. This separation was sorted out based on the Curie temperature of FeO, Fe_2O_3 , and Fe_3O_4 particles [4, 5]. The one that has been used for Fe_2O_3 production is the bottom particles. The powder was oxidized using furnace at 500°C for 9 h in air. The yield of oxidation, Fe_2O_3 , was sieving to obtain a fine powder and used as a raw material in preparing YIG.

2.2. Preparation and characterization of MSS of YIG

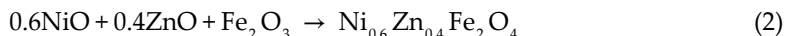
The starting raw powder materials of yttrium oxide (Y_2O_3) (99.9% purity, Alfa Aesar) and Fe_2O_3 which derived from mill scale (Curie separation technique) were mixed according to the stoichiometric ratio based on Eq. 1:



The raw materials were mixed using an agate mortar for about 1 h. The mixing operation is necessary to combine the starting materials into a thoroughly homogeneous mixture. The mixing powder then was milled by using high-energy ball mill (SPEX8000D) with the ball to the powder weight ratio (BPR) of 10:1 for 9 h. After milling, polyvinyl alcohol with 1 wt.% PVA was added in the powder as a binder for giving strength to the pressed compact and was lubricated with 0.3 wt.% of zinc stearate. The mixture powder was pressed with 300 MPa into a toroidal shape. Then, the samples were sintered at different sintering temperatures from 500 to 1400°C for 9 h in air. The evolution of microstructural properties of the sample was determined by using a NovaNano 230 FESEM. The distribution of grain sizes was obtained by taking at least 200 different grain images and estimating the mean diameters of individual grains for each sample using J-image software. The magnetization studies were performed at room temperature using a LakeShore 7404 vibrating sample magnetometer with a maximum magnetic field of 11 kG. The variations of complex permeability were measured using an Agilent HP4291A Impedance Analyzer in the range of 1 MHz to 1.8 GHz.

2.3. Preparation and characterization of SSS of nickel zinc ferrite ($Ni_{0.6}Zn_{0.4}Fe_2O_4$, NZF)

The starting raw powder materials of nickel oxide (NiO), zinc oxide (ZnO), and iron oxide (Fe_2O_3) (>99% purity, Alfa Aesar) were mixed according to the stoichiometric ratio based on Eq. 2:



The mixed material was crushed by using a SPEX8000D HEBM machine at room temperature. The raw mixed powders were milled according to 10:1 ball to the powder weight ratio (BPR) for 6 h. The milled powder was granulated by using polyvinyl alcohol (1 wt.% PVA) as a binder and 0.1 wt. % zinc stearate was added as a lubricant. The previously granulated powder was then uniaxially pressed into toroidal form with pressure of 440 MPa. The single toroidal sample was repeatedly sintered from 600 up to 1200°C with an increment of 25°C under ambient air condition for 10 h. The evolution of microstructural properties of the sintered toroid was studied using a NovaNano 230 FESEM. The distribution of grain sizes was measured by taking at least 200 different grain images and estimating the mean diameters of individual grains for each sample using J-image software. The saturation induction, B_s , and coercivity, H_c , were determined from a $B-H$ hysteresis loop which was obtained via a Linkjoin Technology MATS 2010SD Static Hysteresis graph. The frequency variations of the complex permeability were measured using an Agilent HP4291A Impedance Analyzer in the range of 1 MHz to 1.8 GHz.

3. Microstructure and magnetic properties of MSS yttrium iron garnet and SSS nickel zinc ferrite

3.1. MSS of yttrium iron garnet (YIG)

The samples undergo grain growth or the increase in size of grains when sintering at higher temperature. Sintering can be defined as removal of the pores between starting particles accompanied by shrinkage of the component combined with growth together and formation of strong bonds between adjacent particles [6, 7]. **Figure 1** shows the FESEM micrograph of samples sintered at different sintering temperatures. The micrograph of the sample sintered at 500, 600, and 700°C revealed that the sample encounters initial stage of sintering. The initial stage of sintering involves rearrangement of the powder particles and formation of strong bond or necks at the contact point between particles [8]. At 500 and 600°C, the sample showed nearly the same evolution trend, where the sample sintered at 500–600°C showed slight particle growth and rearrangement of the particles. After sintering at 700 and 800°C, the sample undergoes the formation of necks between particles. This can be noticed with the existence of dumbbell shape in the micrograph at these sintering temperatures. The red-dotted circles in **Figure 1** at 700°C indicate the necking structure between the particles. SEM micrograph of the samples sintered at 900, 1000, and 1100°C exhibits intermediate stage of sintering. Intermediate sintering is the stage where the size of the necks grows, the amount of porosity decreases substantially, and the particles move closer [9]. At this range of temperature, grain boundaries are formed and move so that some grains grew at the expense of others. Grain growth becomes increasingly active as the pore structure collapses. The pinning effect of the pore diminishes as they shrink and occupy less grain boundary area. Further sintering at 1200, 1300, and 1400°C corresponds to the final stage of sintering. The grains with the hexagonal structure are observed in this range of temperature. At this stage, the pores diminished and are slowly eliminated by diffusion of vacancies from the pores along the grain boundaries. The grain boundaries are regions of more open crystal structure than the grain themselves. Thus, the diffusion along grain boundary is more rapid. Reducing the grain boundary area by the grain growth lowers the energy of the system to a more stable state. From the results, it is believed that a mass transport mechanism started with atomic surface diffusion at relatively low temperature and continued to occur by the grain boundary diffusion, resulting in formation of necking, contact growth, pore elimination, and grain growth.

The magnetization versus magnetic field ($M-H$) curve of the sintered samples is measured at room temperature, as shown in **Figure 2**, and the corresponding saturation magnetization, M_s versus sintering temperature is given in **Table 1**. The saturation magnetization reached 0.597, 0.792, 0.259, and 0.069 emu/g at 500, 600, 700, and 800°C, respectively. These values could be related to the presence of weak ferromagnetic behavior of α -Fe₂O₃ and YFeO₃ and a significant amount of amorphous phase [10]. Moreover, such trend can also be associated with the mixture of disordered and ordered magnetism. The samples sintered from 500 to 800°C contained only weak magnetic phase as the magnetization in this temperature range is almost zero. It represents a very small amount of ordered magnetism in these samples. In addition, the smaller value of saturation magnetization in smaller grain size at this region temperature is attributed to the fine greater fraction of surface spins in the particles that tends to be canted with a smaller net moment. At 700 and 800°C, orthoferrites and hematite show

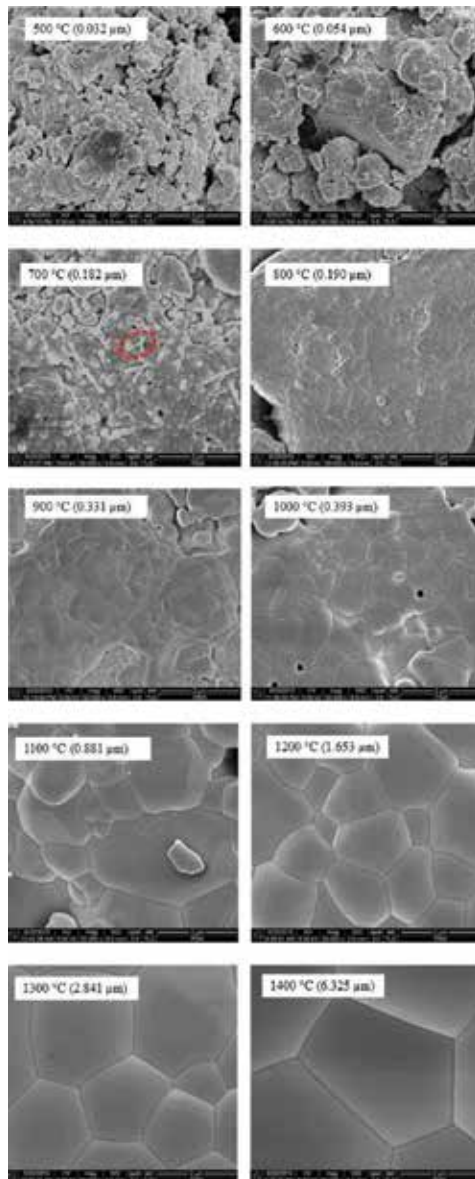


Figure 1. FESEM micrograph of MSS of YIG sintered from 500 to 1400°C.

the weak ferromagnetic behavior. The weak ferromagnetism arises from the low symmetry of the magnetic unit cell, producing a spin-canted structure of Fe sublattices. The weak ferromagnetic behavior of α -Fe₂O₃ is due to a slight disorder of the spin axis from exact antiparallelism. The increase in saturation magnetization for the sample sintered from 900 to 1100°C appears to be established by the initial formation of ferrimagnetic YIG phase at 900°C from the amorphous phase, while the sintering temperature at 1100°C shows only a single phase of YIG exist. This trend is characterized by a remarkable transformation from mixture of disordered and ordered to completely ordered arrangements of the magnetic moments in the sample.

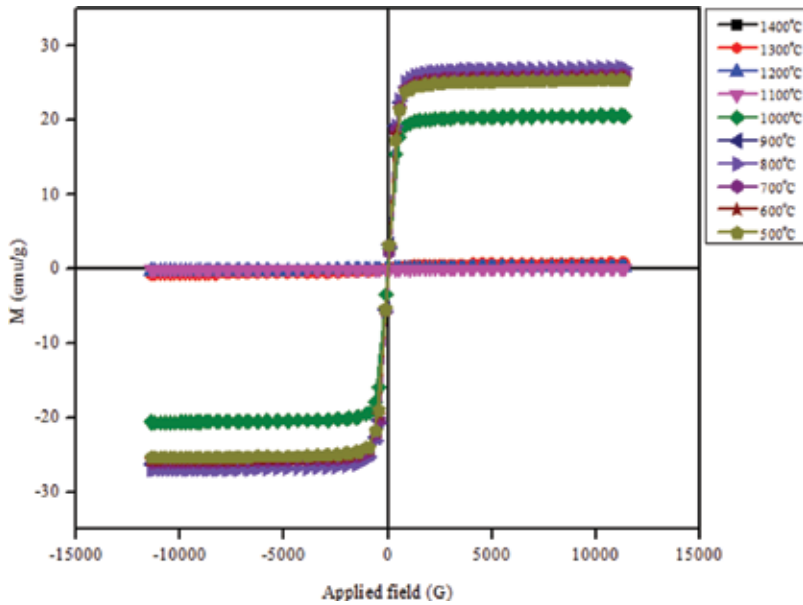


Figure 2. Magnetization curve of MSS of YIG sintered from 500 to 1400°C.

Sintering Temperature (°C)	Saturation magnetization, M_s (emu/g)	Saturation magnetization, M_s (emu/cm ³)	Coercivity, H_c (G)	Grain sizes (μm)
500	0.597	2.790	107.97	0.032
600	0.792	3.744	95.902	0.054
700	0.259	1.233	71.519	0.182
800	0.069	0.329	78.175	0.190
900	20.650	98.998	20.508	0.331
1000	26.282	126.322	8.564	0.393
1100	27.074	132.116	6.750	0.881
1200	26.086	127.550	3.605	1.653
1300	25.770	127.203	1.467	2.841
1400	25.466	130.157	3.715	6.325

Table 1. Saturation magnetization, M_s , and coercivity, H_c , of MSS of YIG sintered from 500 to 1400°C.

The sample sintered at 900°C exhibits the saturation magnetizations lower than the value of 26.8 emu/g, and at 1000°C, the saturation magnetization is close for the usual YIG ceramic, 26.8 emu/g [11]. This should be the contribution from the smallness of YIG present at 900°C and the basis of well-crystalline YIG with poor yttrium iron perovskite (YFeO₃) phase with high grain boundary content at 1000°C. The maximum saturation magnetization (27.074 emu/g) can be achieved at 1100°C. This value is higher as the amorphous phase is diminished due to the larger grain size and increasing bulk volume fraction of YIG. Thus, a strong interaction of magnetic moment within domains occurred due to exchange force. The powder sintered from 1200 to 1400°C shows a decreasing value of magnetization. The decrease of magnetization is

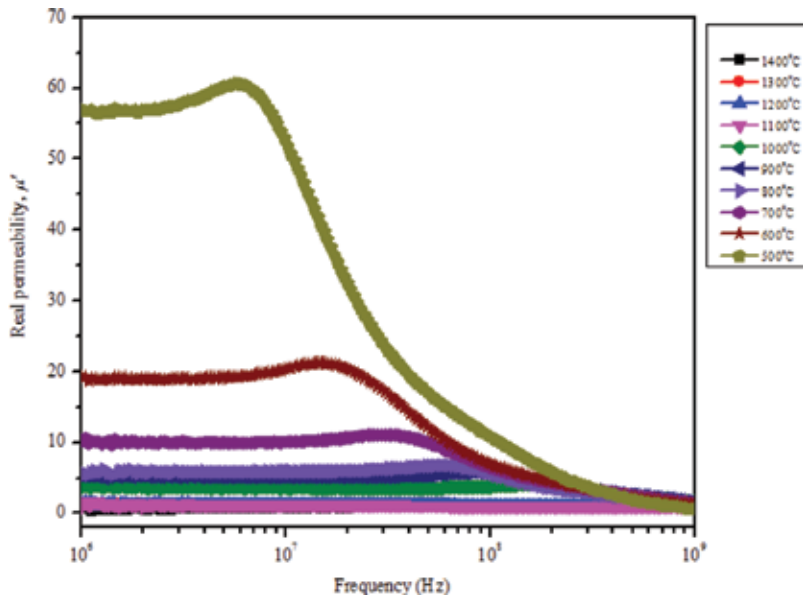


Figure 3. Real permeability, μ' , of MSS of YIG sintered from 500 to 1400°C.

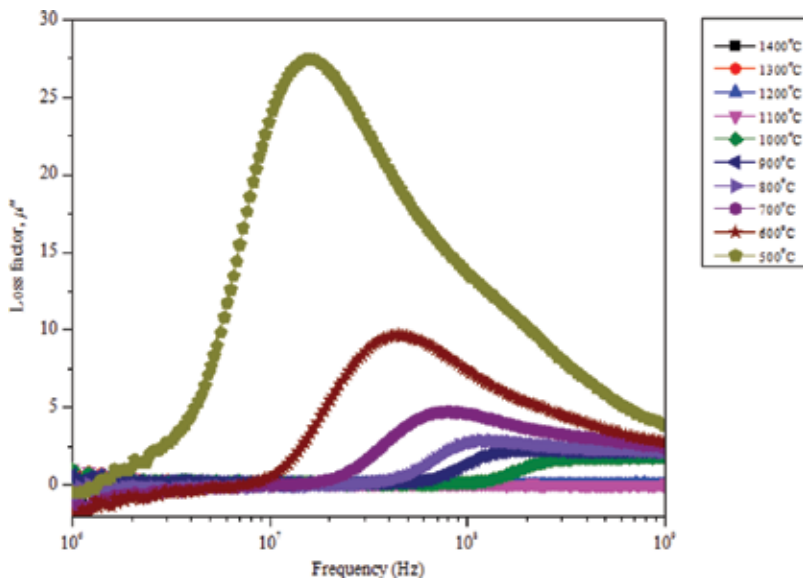


Figure 4. Loss factor, μ'' , of MSS of YIG sintered from 500 to 1400°C.

mainly connected with oxygen gas surface interaction at higher sintering temperature. For larger grains, magnetization can follow the easy magnetization directions in the single grains, and domains can be formed within the grains. Thus, the magnetization process is determined by the magnetocrystalline anisotropy of the crystallites. For very small grains, ferromagnetic

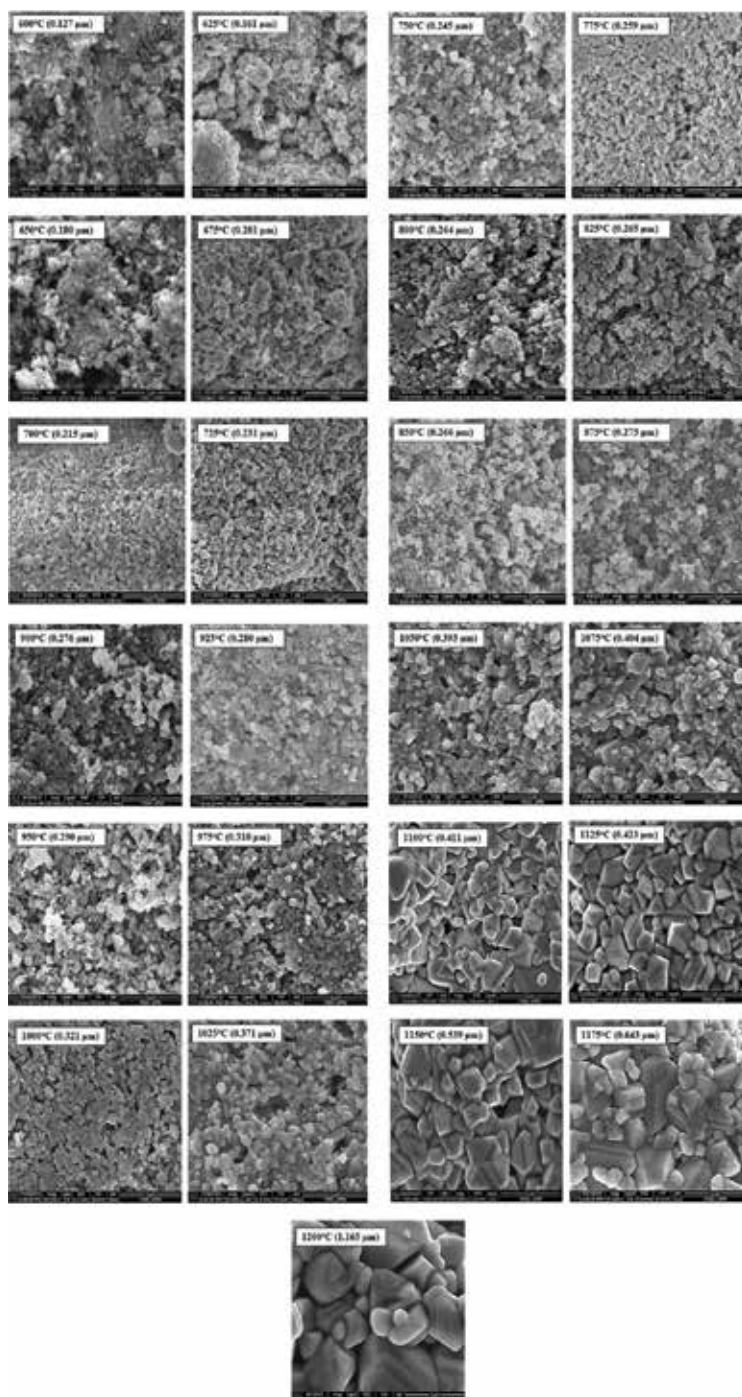


Figure 5. FESEM micrograph of SSS of $\text{Ni}_{0.6}\text{Zn}_{0.4}\text{Fe}_2\text{O}_4$ sintered from 600 to 1200°C.

exchange interaction more and more forces the magnetic moments to align parallel, thus impeding the magnetization to follow the easy direction of each individual grain.

Complex permeability consists of two components: the real permeability, μ' , and loss factor, μ'' . The room temperature of real permeability and loss factor of sintered samples are measured from 1.0 MHz to 1.8 GHz. The sample shows the μ' value is increased to a maximum value and then decreases rapidly to a very low value (**Figure 3**). The same trend of the loss factor is observed in **Figure 4**. The samples show the increment of permeability loss factor with the rise in frequency and attain the maximum value at particular frequency and decrease with further increase in frequency. From both figures (**Figures 3 and 4**), it can be seen that the μ'' maximizes, while the μ' drops off at 10 MHz because of the occurrence of a magnetic resonance. The sample sintered at 500–800°C has low values of the real permeability and does not show the trend of permeability as same as the higher temperature because of the presence of amorphous phase. The increase of μ' value with sintering temperature after 900°C and above is due to the increasing of grain sizes which correspondingly reduce the grain boundaries inside the sample. As the crystallinity and phase purity increase with increasing sintering temperature, the magnetic mass is increased and makes the movement of the domain wall easier. The increase in the sintering temperature also results in the decrease of magnetic anisotropy by decreasing the internal stress and crystal anisotropy [12]. Hence, the hindrance of the movement of domain wall is reduced and increases the value of μ' .

The loss factor, μ'' , is the imaginary part of initial permeability. The permeability loss factor arises due to the lag between the magnetization or flux induction and external applied field [6]. The main types of losses encounter in ferrites are the hysteresis loss, eddy current loss, and residual loss. Otsuki et al. [13] reported that the larger grain size increases the eddy current loss because of the easier movement of domain wall in the larger grain. The fraction of larger grains that are occupied with domain wall also increases hysteresis losses. Hysteresis loss can be minimized if one reduces the hindrance to the domain wall motion by reducing the pinning center to the domain wall movement such as volume fraction of pores, impurities and dislocations, and internal strain inside the sample. The hysteresis loss becomes less important in the high-frequency range due to spin rotation at higher frequency. The eddy current loss is important at higher frequency because of the circulating current induced in the sample due to the change of magnetic field which leads to the energy losses. However, in the polycrystalline YIG, the eddy current losses can be neglected due to high resistivity of YIG. Residual loss is also important in the high-frequency range. To reduce the residual loss, the complex permeability has to be made to peak at the high frequency as possible by using fine-grained sample.

3.2. SSS of nickel zinc ferrite ($\text{Ni}_{0.6}\text{Zn}_{0.4}\text{Fe}_2\text{O}_4$)

SEM micrographs for single-sample sintering (SSS) of $\text{Ni}_{0.6}\text{Zn}_{0.4}\text{Fe}_2\text{O}_4$ are shown in **Figure 5**. The increased average grain size shows the microstructural evolution of the sample. The microstructural evolution can be described by adapting the stages of sintering which are three major stages involved in this process:

- i. Initial stage sintering involves rearrangement of the powder particles and formation of a strong bond or neck at the contact points between particles [14].
- ii. Sample sintered from 600 to 1050°C shows an intermediate stage of sintering, where the size of the neck grows, the amount of porosity decreases substantially, and particles move closer leading to shrinkage of the component. Grain boundaries and grains are formed and move so that some grains grow at the expense of others. This stage continues while the pore channels are connected (open porosity) but is considered over when the pores are isolated (closed porosity).
- iii. Final stage sintering occurred in the sample sintered from 1075 to 1200°C. In this stage, the pores become closed and are slowly eliminated generally by diffusion of vacancies from the pores along grain boundaries with only a little densification of the component. The grain boundaries are regions of more open crystal structure than the grains themselves so that diffusion along them is more rapid. Grain size increases during this stage.

The developments of $B-H$ hysteresis loops are shown in **Figure 6**. The hysteresis properties of polycrystalline nickel zinc ferrite (**Table 2**) are very sensitive to the structure and volume fraction of the complete phase, and also to the grain size. The trends of loops are discussed below:

- i. 600–1000°C: narrowly bulging but linear-looking shape which consists of weak ferromagnetic phase + paramagnetic phase (amorphous phase) + superparamagnetic phase (crystalline phase and small particles). At this stage, the hysteresis shape is significantly dominated by paramagnetic phase because it does not show the properties associated with ordered magnetism. It shows very slight hysteresis with low saturation induction, B_s indicating the low degree of crystallinity and a small amount of ferromagnetic phase. The magnetic moments begin to line up in the direction of applied field with a complex process such as domain growth, domain walls motion, and domain rotation [15–18].
- ii. 1025–1125°C: slanted sigmoid shape which consists of moderate ferromagnetic phase + paramagnetic phase. As sintering temperature increased, paramagnetic states decreased, and at 1025°C, a moderately ferromagnetic state appeared. With further sintering, there is an increase in the volume fraction of grains, yielding more magnetic crystalline mass which would exhibit stronger ferromagnetism with negligible paramagnetic phase (amorphous phase) arising from nickel zinc ferrite phase formation. They have higher B_s values indicating that higher ferromagnetic phase crystallinity is formed [15–18].
- iii. 1150–1200°C: erect, narrower, and well-defined sigmoid shape which consists of strong ferromagnetic phase. At this stage, strong ferromagnetism state was very dominant with negligible superparamagnetism and paramagnetism due to their high volume fraction of the complete Ni-Zn ferrite phase, high density, large grain size, and low amount of microstructure defects which allow easy domain wall movement in the magnetization and demagnetization process [15–18].

Figure 7 shows the real permeability, μ' results plotted against the frequency in the range of 1.0 MHz to 1.8 GHz. The real permeability remains almost unchanged at low frequency, rises

slightly, and then drops sharply when the frequency gets to a certain high value, which is called the cutoff frequency. The magnetic permeability and the cutoff frequency, f_c , confirm the Snoek's relation [19] by using Eq. 3:

$$\mu_i f_c = \text{Constant} \quad (3)$$

The real permeability increase with sintering temperature can be attributed to increase in density and grain size with sintering temperature [20]. At higher sintering temperature, with increased grain size, a fewer number of grain boundaries would be present, and diminished grain boundary caused the existence of very mobile domain walls thus increasing the permeability value of the $\text{Ni}_{0.6}\text{Zn}_{0.4}\text{Fe}_2\text{O}_4$. During grain growth, pores become fewer which act as barrier to domain wall motion due to pinning of the wall. Besides that, the increase in sintering temperature results in a decrease of the magnetic anisotropy by decreasing the internal stress and crystal anisotropy, which reduces the hindrance to the motion of domain walls [17, 21–23].

The same trend is seen in the case of variation in loss factor, μ'' , with respect to frequency as shown in **Figure 8**. The loss factor was observed first to remain constant with frequency, attain the maximum value at a particular frequency, and then decrease with increase in frequency. The loss factor increased with the increasing sintering temperature and grain size. When the grain size increases, more domain walls exist in the grain. Therefore, the domain walls can move easily in the larger grain. When the grain is large, which means a

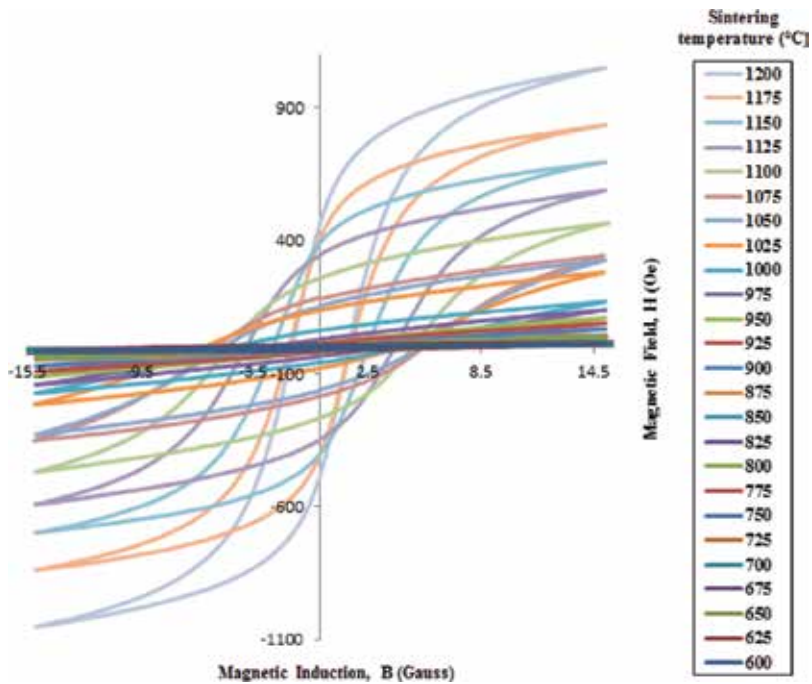


Figure 6. *B-H* hysteresis loop of SSS of $\text{Ni}_{0.6}\text{Zn}_{0.4}\text{Fe}_2\text{O}_4$ sintered at 600 to 1200°C.

Sintering temperature (°C)	Average grain size, D (μm) ($\pm 0.01 \mu\text{m}$)	Saturation induction, B_s (Gauss) ($\pm 5 \text{ G}$)	Coercivity, H_c (Oe) ($\pm 0.01 \text{ Oe}$)
600	0.127	16.96	1.38
625	0.161	17.08	1.81
650	0.180	18.22	1.92
675	0.201	19.22	2.00
700	0.215	20.90	2.02
725	0.231	21.20	2.13
750	0.245	24.64	2.29
775	0.259	32.84	2.84
800	0.264	36.65	2.99
825	0.265	37.36	3.11
850	0.266	42.20	3.17
875	0.275	46.56	3.21
900	0.276	69.83	3.37
925	0.280	91.11	3.44
950	0.290	110.10	3.58
975	0.310	141.10	3.82
1000	0.321	172.50	4.58
1025	0.371	248.90	5.13
1050	0.393	328.20	5.20
1075	0.404	348.00	5.32
1100	0.411	467.70	4.84
1125	0.423	590.50	3.98
1150	0.539	697.50	2.50
1175	0.643	837.50	1.60
1200	1.165	1052.00	1.33

Table 2. Average grain size, saturation induction, B_s , and coercivity, H_c , of SSS of $\text{Ni}_{0.6}\text{Zn}_{0.4}\text{Fe}_2\text{O}_4$ sintered from 600 to 1200°C.

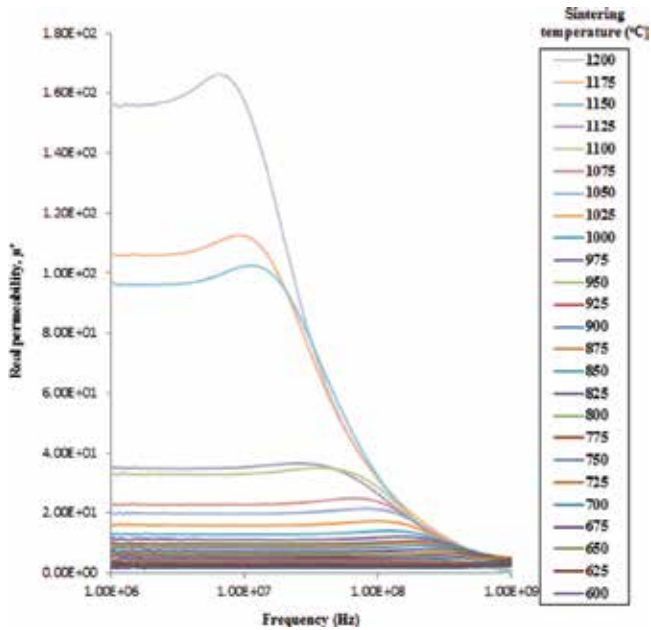


Figure 7. Real permeability, μ' , of SSS of $\text{Ni}_{0.6}\text{Zn}_{0.4}\text{Fe}_2\text{O}_4$ sintered from 600 to 1200°C.

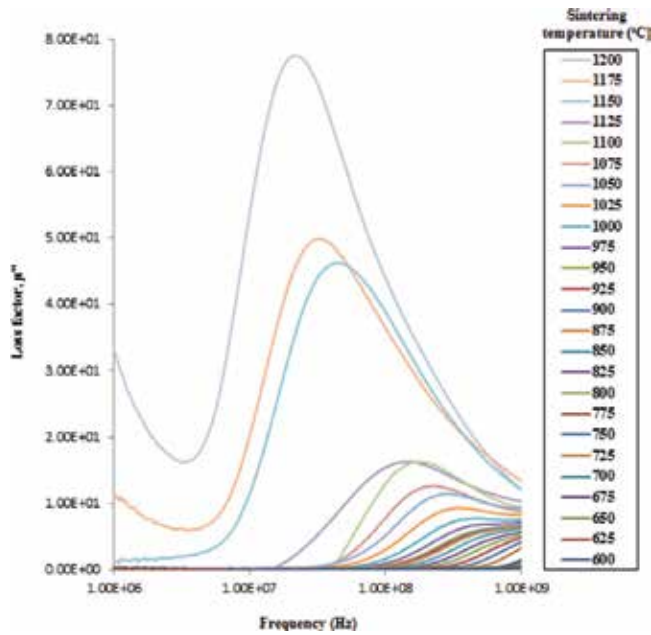


Figure 8. Loss factor, μ'' , of SSS of $\text{Ni}_{0.6}\text{Zn}_{0.4}\text{Fe}_2\text{O}_4$ sintered from 600 to 1200°C.

decrease in the number of grain boundaries; it will not strongly impede the eddy current flows. Thus, larger eddy current is induced [17, 23–25]. Usually, small grains with prominent grain boundaries lead to higher resistivity, the eddy current loss of which is negligible. The losses in ferrites are associated with rotational resonance and domain wall relaxation. Rotational resonance is usually observed at higher frequencies, while domain wall relaxation is observed at lower frequencies [12, 26, 27]. The major contribution to the magnetic losses in ferrites is due to hysteresis losses, which are based on the damping phenomena associated with spin rotations and irreversible wall displacement. In the high-frequency range, the hysteresis losses become less important because the wall displacement is mainly damped and the losses would be most due to spin rotation [13, 22, 28]. Comparing **Figures 7** and **8**, it is observed that the off-resonance frequency region of μ'' firstly occurred and was later followed by the μ'' . The lag in this process was due to μ' being in phase with the external field, whereas μ'' was out of phase with the external field [29].

4. Conclusion

MSS YIG and SS NZF have been prepared via mechanical alloying technique. The samples were sintered at various sintering temperatures in order to study the influence of sintering temperatures on the microstructure and magnetic properties. Increasing sintering temperature will enhance the grain size with less grain boundaries. This extrinsically increases the real magnetic permeability, μ' , loss factor, μ'' , and the saturation magnetization, M_s . The higher magnetic permeability represents the high frequency losses due to the presence of grain boundaries as impediments to domain wall motion. The large M_s reduces the coercivity,

H_c as the increasing the multidomain grain size. The magnetic hysteresis and complex permeability graph can be categorized into three distinct groups which represent the formation of a paramagnetic state to a moderate ferromagnetic state and then to a strong ferromagnetic state with microstructural changes at varied sintering temperatures.

Acknowledgements

The authors are thankful to Putra Research Grants, Universiti Putra Malaysia and Fundamental research Grants (FRGS), Ministry of Science and Technology Malaysia (MOSTI) for financial assistance. Also thanks to the Department of Physics, Faculty of Science, UPM and the Materials Synthesis and Characterization Laboratories (MSCL), ITMA, UPM for the measurements facilities.

Author details

Raba'ah Syahidah Azis^{1,2*}, Muhammad Syazwan Mustaffa¹ and Nuraine Mariana Mohd Shahrani²

*Address all correspondence to: rabaah@upm.edu.my

1 Department of Physics, Faculty of Science, Universiti Putra Malaysia, UPM, Serdang, Selangor, Malaysia

2 Materials Synthesis and Characterization Laboratory (MSCL), Institute of Advanced Technology, Universiti Putra Malaysia, UPM, Serdang, Selangor, Malaysia

References

- [1] Joseyphus RJ, Narayanasamy A, Nigam AK, Krishnan R. Effect of mechanical milling on the magnetic properties of garnets. *Journal of Magnetism and Magnetic Materials*. 2006;**296**:57-64. DOI: 10.1016/j.jmmm.2005.04.018
- [2] Park MB, Cho NH. Structural and magnetic characteristics of yttrium iron garnet (YIG, Ce:YIG) films prepared by RF magnetron sputter techniques. *Journal of Magnetism and Magnetic Materials*. 2001;**231**:253-264. DOI: 10.1016/S0304-8853(01)00068-3
- [3] Xu H, Yang H, Xu W, Feng S. Magnetic properties of Ce, Gd substituted yttrium iron garnet ferrite powders fabricated using a sol-gel method. *Journal of Materials Processing Technology*. 2008;**197**:296-300. DOI: 10.1016/j.jmatprotec.2007.06.061
- [4] Azis RS, Hashim M, Saiden NM, Daud N, Shahrani NN. Study the iron environments of the steel waste product and its possible potential applications in ferrites. *Advances in Materials Research*. 2015;**1109**:295-299. DOI: 10.4028/www.scientific.net/AMR.1109.295

- [5] Azis RS, Hashim M, Yahya N. High purity iron oxide α -Fe₂O₃ from mill scale using Curie temperature separation technique (2002). *Journal of Solid State Science and Technology*. 2002;**9**(1):87-90
- [6] Paladino AE, Maguire EA. Microstructure development in yttrium iron garnet. *Journal of the American Ceramic Society*. 1970;**53**(2):98-102. DOI: 10.1111/j.1151-2916.1970.tb12019.x
- [7] Heister W. Magnetic properties and grain structure of Mn-Zn ferrites. *Journal of Applied Physics*. 1959;**30**:22-24. DOI: 10.1063/1.2185902
- [8] Shahrani NMM, Azis RS, Hashim M, Hassan J, Zakaria A, Daud N. Effect of variation sintering temperature on magnetic permeability and grain sizes of Y₃Fe₅O₁₂ via mechanical alloying technique. *Materials Science Forum*. 2015;**846**:395-402. DOI: 10.4028/www.scientific.net/MSF.846.395.
- [9] Shahrani NMM, Azis RS, Hashim M, Hassan J, Abbas Z, Daud N, Sulaiman S, Muda NNC, Azizan AAH, Musa MA. Effect of sintering temperature on crystallography and microstructure of yttrium iron garnet via mechanical alloying technique. *Journal of Solid State Science and Technology Letters*. 2015;**16**(1-2):67-72
- [10] Musa MA, Azis RS, Osman NH, Hassan J, Dihom MM. Structural and magnetic properties of yttrium aluminum iron garnet (YAlG) nanoferrite prepared via auto-combustion sol-gel synthesis. *Journal of the Australian Ceramic Society*. 2018;**54**(1):55-63. DOI: 10.1007/s41779-017-0126-7
- [11] Huang H, Gong H, Tang D, Tan OK. Synthesis and characterization of yttrium aluminum garnet by high-energy ball milling. *Optical Materials*. 2009;**31**:716-719. DOI: 10.1016/j.optmat.2008.07.006
- [12] Nazlan R, Hashim M, Abdullah NH, Ibrahim IR, Ismail I. Influence of milling time on the crystallization, morphology and magnetic properties of polycrystalline yttrium iron garnet. *Advanced Materials Research*. 2012;**501**:324-328. DOI: 10.4028/www.scientific.net/AMR.501.324
- [13] Zhao H, Zhou J, Bai Y, Gui Z, Li L. Effect of bi-substitution on the dielectric properties of polycrystalline yttrium iron garnet. *Journal of Magnetism and Magnetic Materials*. 2004;**280**:208-213. DOI: 10.1016/j.jmmm.2004.03.014
- [14] Azizi A, Sadrnezhad SK. Effects of annealing on phase evolution, microstructure and magnetic properties of mechanically synthesized nickel-ferrite. *Ceramics International*. 2010;**36**:2241-2245. DOI: 10.1016/j.ceramint.2010.06.004
- [15] Idza IR, Hashim M, Rodziah N, Ismayadi I, Norailiana AR. Influence of evolving microstructure on magnetic-hysteresis characteristics in polycrystalline nickel-zinc ferrite Ni_{0.3}Zn_{0.7}Fe₂O₄. *Materials Research Bulletin*. 2012;**47**:1345-1352. DOI: 10.1016/j.materresbull.2012.03.007

- [16] Ismayadi I, Hashim M, Khamirul AM, Alias R, Hassan J. The transition from paramagnetic to ferromagnetic states as influenced by evolving microstructure of $\text{Ni}_{0.5}\text{Zn}_{0.5}\text{Fe}_2\text{O}_4$. *Journal of Superconductivity and Novel Magnetism*. 2012;**25**(1):71-77. DOI: 10.1007/s10948-011-1201-x
- [17] Ismail I, Hashim M, Kanagesan S, Ibrahim IR, Nazlan R, Wan Ab Rahman WN, Abdullah NH, Mohd Idris F, Bahmanrokh G, Shafie MSE, Manap M. Evolving microstructure, magnetic properties and phase transition in a mechanically alloyed $\text{Ni}_{0.5}\text{Zn}_{0.5}\text{Fe}_2\text{O}_4$ single sample. *Journal of Magnetism and Magnetic Materials*. 2014;**351**:16-24. DOI: 10.1016/j.jmmm.2013.09.041
- [18] Mustaffa MS, Hashim M, Azis RS, Ismail I, Kanagesan S, Zulkimi MM. Magnetic phase-transition dependence on nano-to-micron grain-size microstructural changes of mechanically alloyed and sintered $\text{Ni}_{0.6}\text{Zn}_{0.4}\text{Fe}_2\text{O}_4$. *Journal of Superconductor and Novel Magnetism*. 2014;**27**:1451-1462. DOI: 10.1007/s10948-013-2453-4
- [19] Goldman A. *Modern Ferrite Technology*. New York: Van Nostrand Reinhold; 1990
- [20] Nakamura TO. Electromagnetic properties of Mn-Zn ferrite sintered ceramics. *Journal of Applied Physics*. 1996;**79**:7129-7233. DOI: 10.1063/1.361482
- [21] Verma A, Goel TC, Mendiratta RG. Frequency variation of initial permeability of Ni-Zn ferrites prepared by the citrate precursor method. *Journal of Magnetism and Magnetic Materials*. 2000;**210**:274-278. DOI: 10.1016/S0304-8853(99)00451-5
- [22] Ismayadi I, Hashim M. Sintering temperature dependence of evolving morphologies and magnetic properties of $\text{Ni}_{0.5}\text{Zn}_{0.5}\text{Fe}_2\text{O}_4$ synthesized via mechanical alloying. *Journal of Superconductivity and Novel Magnetism*. 2012;**25**:1551-1561. DOI: 10.1007/s10948-012-1468-6
- [23] Jahanbin T, Hashim M, Khamirul AM, Waje SB. Influence of sintering temperature on the structural, magnetic and dielectric properties of $\text{Ni}_{0.8}\text{Zn}_{0.2}\text{Fe}_2\text{O}_4$ synthesized by co-precipitation route. *Journal of Alloys and Compounds*. 2010;**503**:111-117. DOI: 10.1016/j.jallcom.2010.04.212
- [24] Waje SB, Hashim M, Wan Yusoff WD, Abbas Z. Sintering temperature dependence of room temperature magnetic and dielectric properties of $\text{Co}_{0.5}\text{Zn}_{0.5}\text{Fe}_2\text{O}_4$ prepared using mechanically alloyed nanoparticles. *Journal of Magnetism and Magnetic Materials*. 2010;**322**:686-691. DOI: 10.1016/j.jmmm.2009.10.041
- [25] Jahanbin T, Hashim M, Matori KA. Comparative studies on the structure and electromagnetic properties of Ni-Zn ferrites prepared via co-precipitation and conventional ceramic processing routes. *Journal of Magnetism and Magnetic Materials*. 2010;**322**:2684-2689. DOI: 10.1016/j.jmmm.2010.04.008
- [26] Vajargah SH, Hosseini HRM, Nemati ZA. Preparation and characterization of nanocrystalline misch-metal-substituted yttrium iron garnet powder by the sol-gel combustion process. *International Journal of Applied Ceramic Technology*. 2008;**5**:464-468. DOI: 10.1111/j.1744-7402.2008.02241.x

- [27] Goldman A. Modern Ferrite Technology. Pittsburgh: Springer Science and Business Media, Inc; 2006
- [28] Verma A, Chatterjee R. Effect of zinc concentration on the structural, electrical and magnetic properties of mixed Mn-Zn and Ni-Zn ferrites synthesized by the citrate precursor technique. *Journal of Magnetism and Magnetic Materials*. 2006;**306**:313-320. DOI: 10.1016/j.jmmm.2006.03.033
- [29] Goldman A. Handbook of Modern Ferromagnetic Materials. Massachusetts: Kluwer Academic Publishers; 1999

Application

Conventional Sintering Effects on the Microstructure and Electrical Characteristics of Low-Voltage Ceramic Varistor

Mohd Sabri Mohd Ghazali,
Muhamad Syaizwadi Shaifudin,
Wan Rafizah Wan Abdullah,
Wan Mohamad Ikhmal Wan Mohamad Kamaruzzaman,
Maria Fazira Mohd Fekeri and
Muhamad Azman Zulkifli

Additional information is available at the end of the chapter

<http://dx.doi.org/10.5772/intechopen.78652>

Abstract

Conventional, free or pressure less sintering is the simplest technique which involves heating of a powder compact, previously prepared at ambient temperatures, without applying any external pressure. It can be conducted with various box furnaces or tube furnaces under different atmospheres (oxidizing, reducing, inert, and vacuum). Through the use of this method, a highly applicable varistor can be mass produced. Varistors are of a particular interest for modern surge protection of over-voltage. Nowadays, ZnO ceramic varistors are most favorable in electronic industry due to their excellent electrical characteristics and high energy handling capabilities. By optimizing the method during sintering process, the number of potential barriers formed can be controlled thus improving the capability of the low-voltage varistor.

Keywords: conventional sintering, microstructure, electrical properties, low-voltage varistors

1. Introduction

Sintering or firing of ceramic materials is the heat treatment to provide the energy to the ceramic powder particle to bond together to remove the porosity exist from compaction

stages. The sintering process involves strengthening of powder compact by heating to a high temperature. During sintering process, the ceramic powders of the separate particles disperse to the neighboring powder particles. The sintering process reduces the surface energy of the particles by decreasing their vapor-solid interfaces. The pores take places in the disc/pellet where it diminishes, resulting in densification of the compact ceramic powders, and increases its mechanical properties. The porosity will be decrease from the effect of sintering temperature and time. Sintering will be improved if a liquid phase takes part in the process and a long time and high temperature are needed for the dispersion happens in solid state.

Sintering can result in high-strength bonds, particularly in ceramic materials with a crystalline structure. Sintering is the final step in the ceramic fabrication process where it will provide ceramic powders with density. The sintering operation is carried out in many stages such as heating up, annealing at specified temperature and cooling. The atmosphere, temperature and duration need to be chosen carefully for ceramic materials in order to provide a ceramic material with particular characteristics. The required characteristics of ceramic material are needed to design processing methods that will provide this required properties. The aim of sintering process is to increase the mechanical strength of the material and to prevent deformation and cracking of samples. Sintering of ceramic powder compacts will undergo several significant changes including chemical reactions in the solid state such as decomposition, oxidation and phase transformations. The sintering proceeds in different ways for different ceramic materials to provide densification of ceramic powder compact to improve the properties of the material [1].

Fabrication of varistor ceramics is normally achieved via conventional solid-state ceramic fabrication method by applying sintering temperature. Varistor is a solid state electronic ceramic component used to protect electronic devices against overvoltage surges. Varistor are of particular interest to modern surge protection, which commonly made from zinc oxide. The application of ZnO varistor as high or low-voltage varistors is related to the presence of potential barriers and improves their microstructure, which can be controlled during sintering [2]. The sintering temperature has a prominent effect on the electrical characteristics of varistor ceramics where the process will contribute to the formation of a multi-phase microstructure and promoting the formation of potential barriers and also gives rise to a distinctive microstructure of ZnO varistor ceramics [3, 4]. ZnO varistor ceramics with minor additions of other oxides exhibit nonlinear electrical characteristic and, therefore are widely used as varistors devices to protect electronic equipment against overvoltage [5]. Conventional preparation of varistors are preparing of powder by weighing, milling, mixing and spray drying the milled of different metal oxide materials. After that, for electrical characterization the powder is pressed into disc-shapes (pellets) form with predetermined thickness in order to obtain a desired application. Finally, the pressed powder, which is the green pellets, will be expose to heat treatment by using conventional sintering at different sintering temperature, time and atmosphere, in order to improve their microstructure and electrical properties for desired application and method.

The sintering temperature of ceramic compact powder will transforms into a dense body with varistor characteristics. The physical properties are mostly developed during sintering,

which involves the final densification of the ceramic material at high temperature. Sintering process of varistor ceramic was commonly achieved at three stages. At the first stages, a liquid phase is formed due to the dispersion and the homogeneous distribution of the dopants and contribute to the grain growth at the second stage. For the second stage at the end the of the process which is for in the beginning of the last stage, the grain growth, crystallization of the secondary and spinel phase, formation of the potential barriers, and retraction of the liquid phase from the two grain boundaries to the triple junctions are taking place [6]. The sintering process gives a microstructure with conductive ZnO grains and improves the grain boundaries with additive. The sintered varistor pellets was then silver paste for electrical characteristics. This processing method is still preferred in varistor industries due to their low cost of production, processing viability, only need basic instrumentation tools for preparation of varistors, reduce risks and hazards leads to the attraction of this processing method.

2. Tailoring the properties of grain and grain boundaries during the fabrication process

As one of the most widely used electronic tool in the world, designing and tailoring the microstructure of ceramic play a big role in determining their properties for a specific application. Nowadays, the usage of modern ceramic can be seen almost virtually in any modern devices. In fact, without the existence of ceramic, there would not be a \$2 trillion global industry today [7]. The only reason it manages to come this far is none other because of its capability to fit in various emergence of new products. Thus, researching and discovering a better method to tailor the properties of ceramic on the atomic level are of a great importance to future generation of technology. The focused of this topic will be dealing on the subject of tailoring the properties of grain and grain boundaries of ZnO ceramic varistor by reviewing previous related studies.

Zinc oxide is an interesting and useful material, which produces various applications such as optical devices, sensors, FET devices, SAW devices, and varistor by a few processing procedure. Between all of them, the effects of varistor with using zinc oxide have become interesting nowadays [8]. Zinc oxide based varistor (ZnO) is one of material electronic semiconductor ceramic that have properties high energy absorption which capable to defend electronic device from excess voltage flow that sent to the electronic components that will cause breakdown [9]. Commonly, sintered zinc oxide ceramics produce their own microstructure with numerous grains and grain boundaries. The microstructure unit consists of grain–grain and boundary–grain, which is 3-dimensional series and parallel connection and it is distributed into entire bulk. Pure zinc oxide will show a linear voltage (V)–current (I) connection that obey the Ohm's Law [10]. However, the main features of ZnO possess the attribute of non-linear current-voltage (I - V) with a grain size suitable for enhancement to improve the breakdown voltage of a varistor. By decreasing the grain size below 10 μm the material become qualified to be applied in high voltage application while larger grain size ($>30 \mu\text{m}$) is fitting for low-voltage application [10].

There are several factors, which contribute to controlling specific desired microstructure properties of ZnO ceramic varistor such as the temperature of sintering, hold time, addition of impurities (dopant), and so on [11]. By selecting a suitable combination of these factors during the fabrication process will an acceptable result is produced. For this topic, tailoring the microstructure of ceramic through a conventional method will be discussed and explained. The fabrication of ceramic generally begins with ceramic powder is processed into a compact form and pass through a heat treatment (sintering) where the structure starts to significantly change [12]. Changes include phase transformation and chemical reaction such as oxidation and decomposition. In different term, sintering is a diffusional process that occurred when the temperature of the material is increase to half or three quarters of its melting temperature [13]. Frankly, sintering can be considered as one of the major step in developing a desired outcome of a ceramic since during this process the densification begins to take place. The step is crucial due to density affect desirable properties such as dielectric constant and mechanical strength [14]. Detailed explanation on densification will be further explained later in the subtopic.

2.1. Process of powder through solid-state route

Necessity to understand the importance of an appropriate techniques in the powder preparation is derived from a fact that the step will determine the outcome properties of the finished product. The process usually begins by setting a specific ratio of chemical composition without any presence of impurities with smallest grain size possible. By selecting a smaller and better developed material, the capability of the powder to produce a desired microstructure will significantly increase. Several studies have suggested the method of applying particle growth technique as well as disintegrating the grained materials as means to create smaller size powder [15]. However, such technique mostly required the researcher to spend large amount of money to obtained specific equipment with no real capability for mass production.

Previously, a technique consisting of ball mills are generally selected to fulfill the role of crushing the powder into fine form. Not only the technique is easier to operate, but the mechanism is also relatively simple. Moreover, it has wider control on the powder distribution by choosing a proper size and shape of the mill balls [16]. Nowadays, with the advance of technology the technique has been further develop and a better technique known as high energy ball milling has been introduced. The new technique is more adaptable and able to deal with lower particle size unlike the previous version where it can only function up till the micron size particle. By constantly colliding the particles of powder with the mill balls and bowl will result in mechanical energy, which promotes the phase reaction among the reactant reducing the size of particles to the size of nano. The use of the technique will also ensure the mixed oxide powder are evenly and homogenously mix up. Reportedly, the usage of high energy ball milling is a promising approach for the starting mixture of powder in the varistor ceramic preparation [17].

The mixed powder will later undergo calcination process where the materials are subjected to high temperature for the purpose of removing humidity and gases [18]. Due to

its function of dispelling unwanted composition, sometimes the process is also called as a purification process. The process will begin by increasing the temperature inside the furnace slowly until it reached the designated values usually above 500°C and below 900°C in an average spent of 2 hours [19]. After the heating process is finished, the inside furnace is cooled down slowly and turned off at specific temperature. Point to be noted is the temperature used in this step does not exceed the value of sintering temperature of the later procedure.

The process will then proceed with remilling the mixed powder while adding binder for the purpose of increasing the mechanical strength of green ceramic body. Binder such as polyvinyl alcohol (PVA) are commonly added in a small quantity and mix together using mortar and pestle [20]. There is supposedly an ideal method suggested i.e. through the use of spray-dry system. However, the disadvantages are it requires longer time, difficult to clean the mobile parts and mostly applied for a large amount of mixed powder. Thus, using agate-mortar is not only simpler but also proves to be fully functional. Selecting a suitable binder is also a key in producing a good pellet with adequate electrical properties. A good binder must yield high density and high fired strength, which are essential to increase the electrical properties of the ceramic varistor [21]. PVA is extensively chose in various study mainly due to its high affinity for adsorption reaction when reacts with dispersed oxide particle in water.

The following procedure is pressing where the finalized mixed powder is pressed under a high pressure forming a pellet or disk. The thickness of pellet depends upon the application to be tested. If for the purpose of producing an applicable low voltage ceramic varistor, the thickness is under 1.5 mm while above is for high voltage application. After the pellet is formed, then it will be sintered with the goal of converting a compact porous powder into a well-structured grain form possessing the desired mechanical and electrical properties. The optimum range of temperature used in the process is still debatable since many studies revealed different result when testing different substance under different temperature. But, the range of the best temperature generally falls between 800 and 1200°C [4, 22]. The sintering procedure sometimes continue to pre-sintering step where the products are once again sintered under the same condition due to the previous step unable to produce the desired grain structure or have some defects. By repeating the process, the structure will be further enhance result in superior mechanical and macro properties.

Conventional sintering technique can be considered as one of the commercially accepted method presently. Although there are other better methods such as sol-gel, hydrothermal and co-precipitation but this method is much more simple, faster and easier to use while ensuring a decent quality output.

2.2. Microstructure and electrical properties

Microstructure is defined as structure of material that is extremely small in size. The structure of material can only be observed by using 25× magnification of microscope. The importance of understanding the microstructure lies in its capability to affect physical properties of material,

which is metals, ceramics and composite and also polymers. Such physical properties include strength, toughness, ductility, corrosion resistance, temperature behavior, and hardness or wear resistance [23]. Moreover, it is important to carefully decide the scale of magnification during conducting observation on microstructure since the characteristic of material microstructural may have a huge distinct when observed from various length scales. In ZnO-based varistor, the microstructure refers to the grain and grain boundaries.

Nowadays, all of the electrical and electronic devices have varistor's help. ZnO-based varistor is usually used due to its ability to surge protection from overvoltage current. This is because, ZnO provide an electrostatic potential that act as a barrier between the grains in the sintered body of an electronic tools. Generally, the production of ZnO based varistor is prepared by the addition of additive, which is needed to improve the efficiency varistor for further application [12]. Through the sintering process, ZnO based varistor will form a polycrystalline structure that consist of semiconductor ZnO grains after sintering process [9].

Typically, ZnO is a material that controlled by grain boundaries. It is expected that the properties of the samples will be modified due to the many defect present. Microstructurally, the doped-ZnO samples consist of a very high conductive n-type ZnO grains that is surrounded by an electrically insulating regions of grain boundary. Increasing the sintering temperature up to limited temperature will cause the average size of grain gradually increased. This will reduce the discontinuity between the grains that happen when the microstructure became more compact with less grain boundaries. Due to the increasing of sintering temperature, larger driving forces for internal atomic diffusion enhance the grain growth and pore elimination [5].

In general, the structure of the grains, grain boundaries morphology, density and also distribution of second phase are some of the factors influenced the electrical properties of ZnO such nonlinear coefficient (α), breakdown field (E_b), leakage current density (J_l), and barrier height (ϕ_b) [11, 24]. The mechanical, magnetic piezoelectric and electrical properties of ceramic also will improve if the grain size is smaller which also can help to enhance the application of ceramics [5]. The parameter of the sintering process such as temperature and hold time is really important in getting grain structure. In order to form ceramic with good varistor characteristic, a homogeneous distribution of dopant and correct concentration of oxygen is necessary, as the conductivity of zinc oxide depends on oxygen defect in the structure [11]. Methods that involve during sintering process are important to investigate in order to achieve the solids microstructure and final properties [25].

2.3. Densification

Density is defined as the amount of substance that occupies a defined volume at stated pressure and temperature. In the production of ceramic varistor, density is one of the essential component, which requires a special concern. Without a good control on the development of density, the material will not be able to achieved its desired performance [25]. If we take a look generally on the densification step occurred during sintering, the process can be considered to be divided in three stages i.e. initial, intermediate and final stage. During the first stage, when the particles of powder are exposed to sintering force it begins to rotate and slide into a stable

arrangement. The movement of the particle will cause the microstructure to shrink contributing to the overall increase in the density. Moreover, the stage also leads the particles to form necks between one another as shown in **Figure 1** as the interparticle contact is increased. The first stage is assumed to finish when the extent of neck growth of particle reach to 0.4 and 0.5 of its total radius.

The intermediate stage starts immediately right after the end of the first when the pores of the powder have achieved their equilibrium configuration. Although the particles have begun to develop at this point, the overall density is still low with the pores are mostly linked to one another. Thus, in the second stage the densification will cause the length of cross section between the pores to significantly reduce which eventually result in the pores develop into an unstable state and break away. The second stage can in fact be regards as the major stage out of the three. With the particles are fully individualize, the final stage will take place. At this section, the sintering process generally covers the elimination of isolated pores present in the powder increasing the total density to its theoretical value. Furthermore, the growth of grains is also reach its crucial step at this point where larger grains will exponentially increase by sacrificing smaller grains [27].

The importance of densifying the green bodies of ceramic varistor lies in the formation of continues 3D structure for further selected application. The mechanisms, which are generally responsible for densification, are migration of grain boundaries and diffusion of grain boundaries where the first oversee the last stage of the whole sintering process. Migration of grain boundary refers to the movement of boundary, which separates different grain body through diffusion of atoms from one body to another. Several factors act as the driving force impacting the movement such as strain and elastic energy. The second mechanism of grain boundary diffusion will further densify the ceramic varistor until it reaches highest density capable by the mixed materials [28].

Additionally, the whole densification process can also be seen in three different scales i.e. global, microstructure and atomic scale. Through global scale it shows the densification process which occurred because of surface energy minimization which leads to grain boundaries replacing solid–gas interface. The second scale of microstructure focused on the differences in pressure and concentration gradient due to the presence of vacancies that act as a driving force for the transfer of mass. Finally, the atomic scale reveals the condition of all atoms either in a convex or concave surfaces where there is higher concentration of atoms on the surface of

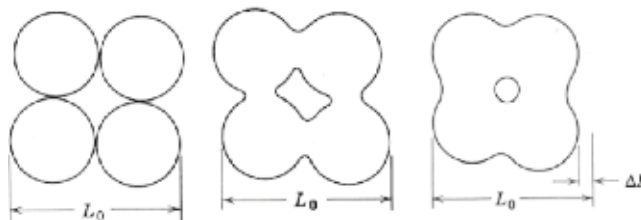


Figure 1. Diagrammatic depiction of (a) powder compact, (b) partial densification of neck growth and (c) fully densified neck growth [26].

concave than convex. The movement on this scale can be seen as a flow of atom from higher place (higher concentration) to the lower region with the upper region having more energy and mobility [29].

Up to date, several researches have shown the relationship between sintering temperature and how it affects the densification of ceramic varistor. Such example includes decreasing in sintering temperature cause an increase in pores, which directly decrease the density and vice versa [8, 30, 31]. The truth is each material has its own properties that cause this kind of situation to happen. Thus, for every material present and included in the production of ceramic varistor it requires an elaborate investigation to determine their specific characteristics before any conclusion can be made.

2.4. Sintering technology

Sintering is the densification of powder compact with the help of thermal treatment. It is also the key for processing the ceramic and powder metallurgical [32]. Sintering can be divided by two categories, which is conventional sintering and advanced sintering. Advanced sintering included spark plasma sintering (SPS), hot pressing sintering and microwave sintering. Unfortunately, some of the technique produce different final product that might not help the economy due to it possessing a non-viable property. Thus, the conventional method is considered to be more appealing for the purpose of mass producing ceramic product since it has lower cost maintenance. For conventional method, minimum grain growth can be controlled by maximization the last density that determine by the heating curve. By controlling the procedure of the heating curve, high densification of grain size can be controlled [25].

2.4.1. Conventional sintering

Conventional sintering technology is the simplest form in sintering that also known as pressureless sintering. It only involves heating of the powder compact after prepared at ambient temperatures without any external pressure applied during the process. Nanostructured ceramic materials that have dense properties normally acquire nanopowder that have undergo pressing process, which is done through a pressure assisting method. The pressure assisted method includes hot pressing, sinter forging, hot isostatic pressing, and others [33]. Hot pressing technique can also use to produce the mixture of two or more types of metals powder base product that can be improved the mechanical properties. When using the hot pressing method, some of the ceramic materials are found to be densified even at lower temperature when compared to conventional method. The benefits in using hot pressing sintering technique are firstly improving the densification kinetic and limited of grain development, where disadvantages are the end product have limited geometry and equipment needed highly in cost [34].

2.4.2. Microwave sintering

Generally, it has been 3 decades since the microwave sintering of ceramics have been introduced. Respectively, it has some superiority, which is fast processing and heating selective.

Furthermore, the processed materials are mostly enhanced via inhibition of the grain for it to develop while reducing the processing time and energy required to complete the process. The application of microwave technology is not really something new in the field of processing and material science. Its applications are actually widely applied in various field such as calcination, drying of ceramic and decomposition of gaseous species. Processing materials it is only limited to only 2000 ceramics with the use of microwave, polymeric materials, semi-conductors and inorganic. The advantages of this sintering technique are great microstructure control, improved the material mechanical properties, the product have no limit geometry and reduce the manufacturing cost due to low temperature, energy used and processing time. Microwave sintered sample also reported that hardly reveal any development and cobalt does not exhibit any dissolution of tungsten while there are nearly 20% dissolved in cobalt binder phase in the conventional sintering. The researcher also found that sample that sintered in microwave always showed improvement in mechanical properties compared to the conventional sintered one [34].

2.4.3. Spark plasma sintering

Spark Plasma Sintering or in a more complex Pulsed Electric Current Sintering (PECS) is a new technology in the field of metals, ceramics and composite fabrication starting from powders. With the nanostructured features, it has the potential of densifying powders while avoid it become rough which follow the densification routes [34]. This spark plasma sintering mechanism has been investigated in the 1960s and began to be used in metal powder compressed. But there is no wider use of it since the price of the equipment are very expensive coupled with inferior efficiency in sintering. To heat the specimens, the use of pulsed direct current is commonly used in these systems. SPS consist of several parts of uniaxial pressure machine where the water-cooled punches also work as electrodes, a pulsed DC generator a water cooled reaction chamber, position, pressure and temperature regulation system. The relatively low homogenous temperature and short duration required for this technique because it is really suitable for the preservation and nanocrystalline densification feature in the ceramics material. Nowadays SPS is widely used due to the possibility in performing a fast consolidation of ceramic that tough to sinter and composite ceramics during decreased temperature [33].

3. Low-voltage ZnO-based varistor

Zinc oxide (ZnO) ceramic materials are commonly used for overvoltage protection in electronic industry. ZnO varistor ceramic is nonlinear electrical component and high energy handling capabilities. Low-voltage varistor are now highly demand for surge protection in electronic devices with fast response, highly nonlinear current–voltage properties and energy absorption capabilities. The performance of low-voltage ZnO varistors can be improve by increasing the grain size, which allows the decreased grain boundary per unit volume and improves the nonlinear electrical characteristics. Low-voltage varistors are improved when their thickness is decrease to increase the size of ZnO grains. However the strength and energy absorption

capabilities of the thin ZnO varistor are very poor due to its small volume [35]. In addition to grains size and the additives, sintering temperature is an important parameter in the manufacture process of varistor-based ceramics. Low-voltage ZnO varistors are now being used for surge protection in integrated circuits and in automobiles. The electrical properties of low-voltage ZnO varistors are based on their composition and microstructure. Optimizing the process, the composition and microstructure of conventional varistors are used to achieve low-voltage varistor. Therefore, it is important to find a new method to fabricate high performance varistors without reducing their thickness.

In low-voltage ZnO varistors, the most influence additives are titanium oxide (TiO_2) which can greatly improve the grain growth of ZnO, thus is commonly used as a grain growth enhancing additive to produce low-voltage ZnO varistors. But, the doping of TiO_2 reduces the degree of nonlinearity [36]. The degree of nonlinearity (α) is used to explain the characteristics of varistor ceramics with excellent surge withstanding capabilities. The coefficient α is the measure of efficiency of the device, the higher its values the more is the effectiveness of device in protecting a circuit from overvoltage [37]. The nonlinearity strongly depends on the microstructure and directly affects their electrical properties that can be adjusted by the means of sintering process. The performance of microstructure and electrical characteristics of varistor ceramic can be improve by adding additives by thermal treatment. A unique properties of grain boundaries is formed in the ceramics during sintering and they are responsible for determining the nonlinear electrical characteristics of varistor component. The chemical composition, sintering temperature, sintering time, heating and cooling rates are variables that can be adjust fundamentally to control the electrical performance of ZnO varistors [38].

The sintering temperature reaction between ZnO and additives lead to the formation of different phases in the ZnO grain boundary and the nonlinear properties are ascribe to the formation of potential barriers at the ZnO grain boundaries. The performance of ZnO-based components is sensitive to the presence of additive even though their amount is very small and the processing environment has significant effect on the microstructure of varistor ceramics. Development of specific microstructure at varying sintering condition in ZnO based varistor ceramics will determine its electrical characteristics especially at varistor voltage of the ceramic device, since it is directly related to the grain size and grain boundary of ZnO varistor ceramics. Therefore, the temperature at which these reactions take place will lead to different grain sizes, and different electrical properties will be obtained when fabricating the varistor device [39]. Industrially, varistor manufacturing is commonly by the conventional solid-state preparation method and ZnO varistors were manufactured through a high-temperature reaction called sintering. A dense varistor product was normally obtained through the sintering process, since the varistor performance depends on the final sintered microstructures, the sintering process must be carefully carried out. For sintering, the varistor powder needs to be hard-pressed to ceramic discs/pellets and should be heated at a temperature in the range of 1100–1250°C [40, 41]. The improvement of ZnO varistor with excellent electrical properties and high energy handling capability can be obtain through grain size control by using nanosize-doped ZnO powder and manage the excess of grain growth by step sintering process.

3.1. Barium titanate and calcium manganite as additive

A new processing technique in the production of low-voltage ZnO varistor are now being investigated for overvoltage protection in low-voltage electronic due to highly demand. The breakdown voltage (varistor voltage) is directly proportional to the number of ZnO grains in series between the electrodes, therefore, it can be achieve by decreasing the thickness of the disc/pellet or increase the size of ZnO grains. However, the thin ZnO varistor are weak, thus by using additives or improve their processing technique are important to optimize the performance of low-voltage varistor ceramics. In low-voltage varistor, a grain growth-enhancer titanium oxide (TiO_2) is mostly used and can influence the degree of non-linearity of conduction. As barium titanate (BaTiO_3) consist of TiO_2 , its addition can attribute to the formation of grain growth [42]. BaTiO_3 is one of the members of perovskite (ABO_3) family that has wide applications in electronic industry. Doping with BaTiO_3 on ZnO based varistor ceramics has significant effect due to the rich variety of physical properties such as high-temperature superconductivity and colossal magnetoresistance observed in these compounds makes them very attractive from both fundamental and applied perspectives.

Perovskite oxides have attracted much attention due to their structure properties formed by substitution make it outstanding functional materials which is exhibit various properties and one of the important usages of perovskite oxides is in the capacitor application because of their excellent dielectric properties [43]. The combination of varistor-capacitor characteristics makes it a promising material in the field of overvoltage protection of electronic devices. The presence of large BaTiO_3 grains on the ZnO microstructures will greatly improve the electrical properties of the varistor since BaTiO_3 as the doping of ZnO based varistor possess the ability to control the microstructural development of the ceramic. According to previous research reveals that the heavily ZnO doping on the BaTiO_3 ceramic are very interesting for the purpose of capacitor-varistor integration [44]. BaTiO_3 is a prototypical ferroelectric material with a tetragonal distortion characteristic of the cubic perovskite structure. The ferroelectric distortion is facilitated by the large size of the Ba cation. Barium titanate is a good candidate for a variety of applications due to its excellent dielectric, ferroelectric, and piezoelectric properties [45]. It is extensively used in the electronic industry as capacitor and positive temperature coefficient of resistivity (PTCR) sensors.

The used of calcium manganite (CaMnO_3) as additive material to produce low-voltage varistor is extensively studied due to their unique properties that make them attractive in enhancing the performance of the existing materials. Perovskite manganite AMnO_3 , where A is an alkaline earth metal such as Ca, Sr., Ba and Pb, has been the subject of intense research during the last decade and it has a significant effect on the microstructure of ZnO varistor ceramics [4]. In addition, the varistors prepared from ZnO with CaMnO_3 perovskite as the only forming additive, exhibit voltage-limiting electrical properties while the combination of perovskite structure CaMnO_3 with the microstructure of ZnO varistor ceramics is simple consisting of only ZnO grain and CaMnO_3 as intergranular layer [46].

Additive of CaMnO_3 on the microstructure of ZnO varistor ceramics shows a good properties in order to produce low-voltage varistors. The combination of ZnO with perovskite manganite gives multifunctional properties for low-voltage electrical characteristics with large

nonlinear coefficients, which is suitable for semiconductor electronic and magnetoelectric devices due to magnetotransport properties of polycrystalline multi-phase ceramic [47]. The influence of perovskite CaMnO_3 as the only additives in the microstructure of ZnO varistor ceramics shows a significant effect on the electrical characteristics of low-voltage ZnO based varistor and with the new formulation for low-voltage ceramic varistor containing CaMnO_3 as varistor former in spinel phase and doping elements of rare-earth also shows a potential to be used as doping low-voltage varistor [48]. The new generation of varistor that introduced perovskite as additive and as varistor former, make this device less use of additives as compared to first generation, which is use bismuth oxide as a varistor former [49–52].

3.2. Effects of ZnO + perovskite on the development of microstructure

The further improvement of the electrical characteristics is associated to the ability to control the microstructural development in the ceramic materials. The used of barium titanate (BaTiO_3) as an additive on the microstructure and grain growth in the ZnO varistor ceramics shows a significant effect, where it contains titanium oxide (TiO_2) which has mostly used as grain growth enhancer and can influence the nonlinear coefficient of varistor. BaTiO_3 is a ceramic material with a characteristic of the cubic perovskite structure and facilitated by the large size of the Ba cation. The displacement of atoms in BaTiO_3 as a function of an external electric field will induce to a nonlinear behavior. ZnO- BaTiO_3 -based varistor ceramic sintered at 1300°C enhances their grain size and improves microstructural uniformity. The microstructure consists of two phase which is ZnO grain (primary phase) and inter-granular phase with concentration of BaTiO_3 solid solution in the ZnO grain boundaries. The BaTiO_3 as additive increase the grain size of ZnO compared to the sample without BaTiO_3 at the same sintering temperature. From the microstructure, the ZnO grains reveal high concentration of additives with BaTiO_3 element. The distribution of the chemical elements is homogeneous except near the grain boundaries where the solid solutions are located. The inhomogeneity is characterized by a strong concentration in the grain boundaries, which contain of excess BaTiO_3 in ZnO microstructure. The secondary phase is located near triple-grain junctions and nodal points in the grain boundaries with the high concentration of the additives. The competition between dissolution and segregation of the BaTiO_3 into the grain boundaries of ZnO are present and this chemical and physical reaction depends on the sintering temperature and amount of concentration between them. From **Figure 2**, the microstructure of ZnO doped with BaTiO_3 is shown to be larger as the sintering temperature is increase from 900 to 1300°C .

Additive of calcium manganite (CaMnO_3) on the ZnO based varistor reveals the presence of ZnO as dominant in the microstructure and the secondary phase formed at the grain boundaries and also at the triple point junction which consist of CaMnO_3 as varistor former for grain growth. The ionic radii of Mn^{2+} is larger than ZnO^{2+} ions, therefore, it segregated at the grain boundaries as secondary phases. However this phase reduces when the sintering temperature was increased to 1300°C due to the reactive melting of CaMnO_3 . The non-uniformity of the grain structure of ZnO- CaMnO_3 based varistor ceramics are reduce when the sintering temperature are increase which a uniform grains are present and free from abnormal grain growth by doping of CaMnO_3 as an additive. ZnO ceramics doped with perovskite phase of

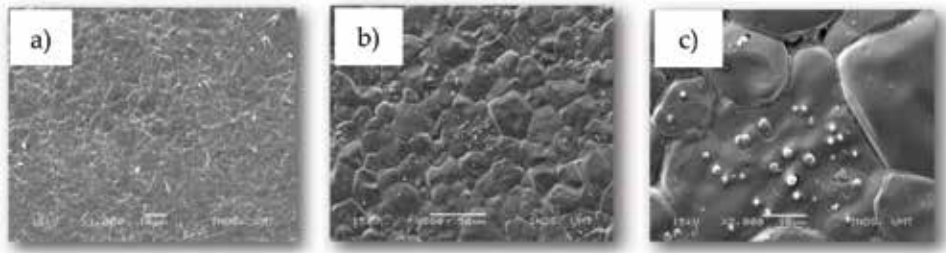


Figure 2. SEM micrographs of ZnO-BaTiO₃ at sintering temperature in (a) 900°C, (b) 1100°C and (c) 1300°C.

CaMnO₃ as the additive improves the microstructure with the support of sintering process. The sintering temperature influences the microstructure of ZnO-CaMnO₃ by segregate of CaMnO₃ dopants at grain boundaries with the increase in sintering temperature.

3.3. Effects of ZnO + perovskite on the electrical properties

The incorporation of large barium titanate (BaTiO₃) grains on the ZnO microstructures will greatly improve the electrical properties of the varistor since BaTiO₃ as the doping of ZnO based varistor possess the ability to control the microstructural development of the ceramic. The effect of BaTiO₃ on the electrical properties can be seen clearly with the increase of BaTiO₃ content as the additive and the varistor voltage increase significantly with BaTiO₃. The varistor voltage is enhanced with the increase of the number of active grain boundaries because of the decrease of ZnO grain size with increasing of BaTiO₃ percentage. It is well known that titanium oxide (TiO₂) are commonly used to produce low-voltage varistor, since BaTiO₃ consist of TiO₂ it will increase the grain size but restrict the nonlinear properties. When the grain size are increase it lowering the varistor voltage with the increase in of BaTiO₃ concentration at the grain boundaries. The present of TiO₂ in the perovskite structure BaTiO₃ act in inverse since nonlinear coefficient (α) increases with the addition of BaTiO₃. The varistor sintered at 1300°C decreases the varistor voltage due to the homogeneous microstructure of grain boundaries and increasing the grain size compared to varistor sintered at temperature 1250°C that possess high varistor voltage. The breakdown voltage of current-voltage characteristics for ZnO varistor is much better with BaTiO₃. For low-voltage ZnO varistors it can be improve by increasing the grain size, which allows the decreased grain boundary per unit volume and improves the nonlinear electrical characteristics. The addition of perovskite structure BaTiO₃ is attribute to the formation of potential barriers at the grain boundaries where the large grain size of BaTiO₃ will greatly increase the grain size and the present of Barium will contribute to the increase in nonlinearity of ZnO varistor, since it more dominant in comparison with the effect of titanium oxide. The used of BaTiO₃ as an additive for grain growth will produce a suitable range of varistor voltage with the conventional sintering technology in order to produce low-voltage varistor.

In addition, the perovskite manganite CaMnO₃ as an additive changes the breakdown voltage of the ZnO varistor system. It presents a good electrical properties for low-voltage varistor

with large nonlinearity coefficients [47] and surpasses the results as reported by using ZnO-Bi₂O₃ based and ZnO-Pr₆O₁₁ based varistor [53, 54]. The low-voltage nonlinearity originates as a result of higher concentration of manganese present at the grain boundary layer regions, being charge compensated by zinc vacancies [47]. The effect of sintering temperature on microstructure and electrical properties of low voltage varistor ceramics fabricated from a mixture of ZnO with CaMnO₃ perovskite gives a broad idea to researcher for their further research on production of low-voltage varistor [55]. The effect sintering temperature at certain composition of this additives can exhibit a voltage-limiting in the electrical properties of ZnO varistor. The varistor sintered at 1200°C provided low varistor voltage per thickness of the ZnO ceramics for low voltage varistor [4].

4. Overview

The preceding chapter in this book has presented the best available knowledge the conventional sintering effects as a driving force on the microstructure and electrical characteristics of low-voltage ceramic varistor. The aim of this chapter is to provide sufficient knowledge related to sintering technology that has been used for ceramic varistors fabrication industry. Almost the past century there has been a discovery of ceramic varistors and a few decade later, a varistor with simple formulation of ZnO-Bi₂O₃ based varistor was successfully fabricated in industries and start from that, varistor have been growing, whereas, ZnO-perovskite introduced. At the heart of this magnificent semiconductor device is the sintering technology- a way of heat treatment to make the ceramic varistor become compacted and less porosity.

The methodology in this chapter present low-voltage ZnO based varistor and its additives. The discussion part elaborates the recent studies related to microstructure and electrical properties of ZnO-perovskite based varistor as compared in citation to first generation and second generation, which are ZnO-Bi₂O₃ based and ZnO-Pr₆O₁₁ based varistor; respectively. The discussion concludes with driving force through sintering process in solid-state route, the desired low voltage ZnO-Bi₂O₃ and ZnO-perovskite based varistor with favorable nonlinearity coefficient, α , is successfully fabricated.

5. Conclusion

The effects of conventional sintering on the microstructure and electrical properties of low-voltage ceramic varistor in this chapter are describe based on their useful properties which are determined by their properties of grain and grain boundaries during the fabrication process. The processing technique through solid-state route shows a significant effect with sintering process in the microstructural development of ZnO varistor ceramics. The densification of sintered ceramic varistor can be controlled by using different sintering technology in order to improve their microstructure and electrical properties especially for production of low-voltage varistor. It was also determined that a steady increase in sintering temperature and time until certain limitations results in larger size of grains which in turn will decrease the grain

boundary per unit volume improving the nonlinear parameters. Moreover, the low-voltage ZnO varistor ceramics can be improved by using suitable additives such as Barium Titanate and Calcium Manganite since it exhibits perovskite structure where these materials possess the ability to control the microstructure development during sintering process.

Author details

Mohd Sabri Mohd Ghazali^{1,3*}, Muhamad Syaizwadi Shaifudin¹,
Wan Rafizah Wan Abdullah², Wan Mohamad Ikhmal Wan Mohamad Kamaruzzaman¹,
Maria Fazira Mohd Fekeri¹ and Muhamad Azman Zulkifli¹

*Address all correspondence to: mohdsabri@umt.edu.my

1 Advanced Nano Materials (ANoMa) Research Group, Nano Research Team, School of Fundamental Science, Universiti Malaysia Terengganu, Kuala Nerus, Terengganu, Malaysia

2 School of Ocean Engineering, Universiti Malaysia Terengganu, Kuala Nerus, Terengganu, Malaysia

3 Institute of Biodiversity and Sustainable Development, Universiti Malaysia Terengganu, Kuala Nerus, Terengganu, Malaysia

References

- [1] Sutharsini U, Thanishaichelvan M, Singh R. Two-step sintering of ceramics. In: *Sintering of Functional Materials*. Rijeka, Croatia: InTech; 2018
- [2] Souza FL, Gomes JW, Bueno PR, Cassia-Santos MR, Araujo AL, Leite ER, Varela JA. Effect of the addition of ZnO seeds on the electrical properties of ZnO-based varistors. *Materials Chemistry and Physics*. 2003;**80**(2):512-516
- [3] Anas S, Mangalaraja RV, Poothayal M, Shukla SK, Ananthakumar S. Direct synthesis of varistor-grade doped nanocrystalline ZnO and its densification through a step-sintering technique. *Acta Materialia*. 2007;**55**(17):5792-5801
- [4] Lakin II, Zakaria A, Abdollah Y, Umaru D. Effect of sintering temperature on microstructure and electrical properties of ZnO+ CaMnO₃ ceramics used in low voltage varistors. *Digest Journal of Nanomaterials and Biostructures*. 2015;**10**(1):189-197
- [5] Norailiana AR, Azmi BZ, Ismayadi I, Hashim M, Ibrahim IR, Nazlan R, Mohd Idris F. Parallel development of microstructure and electrical properties in doped-zinc oxide. *Journal of Materials Science and Surface Engineering*. 2017;**5**(2):528-532
- [6] Anas S, Mahesh KV, Maria MJ, Ananthakumar S. Sol-gel materials for varistor devices. In: *Sol-Gel Materials for Energy, Environment and Electronic Applications*. Cham: Springer; 2017. pp. 23-59

- [7] The American Ceramic Society. Ceramics in electronics [internet]. 2014. Available from: <http://ceramics.org/learn-about-ceramics/ceramics-in-electronics-2> [Accessed: May 01, 2018]
- [8] Nahm CW. Effect of sintering temperature on microstructure and varistor properties of Zn-VO-based ceramics incorporated with Mn-Nb-Tb. *Transactions of Nonferrous Metals Society of China*. 2015;**25**:4040-4045
- [9] Umaru D, Zakaria A, Abdullah CAC, Lakin II, Abdollahi Y. Effect of sintering temperature on V_2O_5 doped $ZnO-Bi_2O_3-Sb_2O_3-MnO_2$ based varistor ceramics: Microstructure and electrical. *Digest Journal of Nanomaterials & Biostructures (DJNB)*. 2016;**11**:707-714
- [10] Daneu N, Gramc NN, Rečnik A, Kržmanc MM, Bernik S. Shock-sintering of lowvoltage ZnO-based varistor ceramics with $Bi_4Ti_3O_{12}$ additions. *Journal of the European Ceramic Society*. 2013;**33**:335-344
- [11] Tak S K, Shekhwat M S, Mangal R. Electrical property of conventionally sintered ZnO. In: *International Journal of Modern Physics: Conference Series*; 2013. pp. 501- 510
- [12] Chen GH, Chen X, Kang XL, Yuan CL. Sintering temperature dependence of varistor properties and impedance spectroscopy behavior in ZnO based varistor ceramics. *Journal of Materials Science: Materials in Electronics*. 2015;**26**:2389-2396
- [13] Liu PS, Chen GF. *Porous Materials Processing and Applications*. 1st ed. Oxford: Butterworth-Heinemann; 2014. p. 21
- [14] Peirson B. Comparison of specific properties of engineering materials [internet]. 2005. Available from: www2.gvsu.edu/peirsonb/spec_prop.pdf [Accessed: May 01, 2018]
- [15] Leszek H. *Semiconductor Ceramics Grain Boundary Effects*. 1st ed. Warsaw: Ellis Horwood; 1994. p. 4
- [16] Sharma P, Sharma S, Khanduja D. On the use of ball milling for the production of ceramic powders. *Materials and Manufacturing Processes*. 2015;**30**:1370-1376
- [17] Dong X, Tang DM, Lei J, Yuan HM, Zhao GP, Cheng XN. Effects of high-energy ball milling oxide-doped and varistor ceramic powder on ZnO varistor. *Transactions of Nonferrous Metals Society of China*. 2012;**22**:1423-1431
- [18] Yongvanich N, Visuttipitukkul P, Leksuma P, Vutcharaammatt V, Sangwanpanit P. Sinterability and microstructure of Bi-added SnO_2 nanomaterials by precipitation method. *Journal of Metals, Materials and Minerals*. 2010;**20**:67-72
- [19] Milošević O, Vasović D, Poleti D, Karanović LJ, Petrović V, Uskoković D. Progress in preparation of ZnO based varistor ceramics. In: Dragan PU, Hayne P, Richard MS, editors. *Science of Sintering*. 1st ed. Boston: Springer; 1989. pp. 117-126
- [20] Gholizadehsangesaraki S, Begum S, Nainar, M A M, Kothandapani Z. Effect of binder on mechanical and physical characterization of titanium dioxide based varistor. In: *Electronic Manufacturing Technology Symposium (IEMT)*; 2012. p. 1-5

- [21] Begum S, Karim ANM, Hashmi MSJ. Characterization and performance evaluation of zinc oxide varistor blocks processed by latex binders. *Journal of the American Ceramic Society*. 2008;**91**:3216-3221
- [22] Akinnifesi JO, Akinwunmi OO. Effect of sintering temperature on the microstructure and electrical characteristics of low clamping voltage zinc oxide- based ceramic varistor. *Journal of Materials Science Research*. 2015;**4**:40-48
- [23] Corrosionpedia. Microstructure [internet]. 2014. Available from: <https://www.corrosionpedia.com/definition/777/microstructure> [Accessed: May 01, 2018]
- [24] Pillai SC, Kelly JM, McCormack DE, Ramesh R. Effect of step sintering on breakdown voltage of varistors prepared from nanomaterials by sol gel route. *Advances in Applied Ceramics*. 2006;**105**:158-160
- [25] Chinelatto ASA. Mechanisms of microstructure control in conventional sintering. In: Lakshmanan A, editor. *Sintering of Ceramics*. 1st ed. Boca Raton: CRC Press; 2007. pp. 401-422
- [26] Fahrenholtz WG. Ceramic engineering 111 sintering [internet]. 2004. Available from: web.mst.edu/~billf/labrpt.pdf [Accessed: May 01, 2018]
- [27] Shi JL. Solid state sintering of ceramics: Pore microstructure models, densification equations and applications. *Journal of Materials Science*. 1999;**34**:3801-3812
- [28] Ubenthiran S. Two-step sintering of ceramics. In: Shishkovsky I, editor. *Sintering of Functional Materials*. 1st ed. London: IntechOpen; 2018. pp. 3-21
- [29] Rawlings RD, Wu JP, Boccaccini AR. Glass-ceramics: Their production from wastes–A review. *Journal of Materials Science*. 2006;**41**:733-761
- [30] Chu MY, DeJonghe LC, Lin MKF, Lin FJT. Precoarsing to improve microstructure and sintering of powder compacts. *Journal of the American Ceramic Society*. 1991;**74**:2902-2911
- [31] Bernik S, Cheng L, Podlogar M, Li G. Low-temperature sintering of ZnO–Bi₂O₃- based varistor ceramics for enhanced microstructure development and current- voltage characteristics. *Ceramics–Silikáty*. 2018;**62**:8-14
- [32] Advance ceramics and powder metallurgy. Advance Sintering Technology [Internet]. 2014. Available from: <https://www.mtm.kuleuven.be/Onderzoek/Ceramics> [Accessed: May 01, 2018]
- [33] Khalil AK. Advanced Sintering of Nano-Ceramic Materials, *Ceramic Materials –Progress in Modern Ceramics*. Prof. Feng Shi, editor. Saudi Arabia, Egypt: InTech; 2012. 228 p
- [34] Henriques B, Soares D, Teixeira JC, Silva FS. Effect of hot pressing variables on the microstructure, relative density and hardness of sterling silver (Ag-Cu alloy) powder compacts. *Materials Research*. 2014;**17**:664-671
- [35] Wang Q, Qin Y, Xu GJ, Chen L, Li Y, Duan L, Cui P. Low-voltage ZnO varistor fabricated by the solution-coating method. *Ceramics International*. 2008;**34**(7):1697-1701

- [36] Wang MH, Hu KA, Zhao BY, Zhang NF. Electrical characteristics and stability of low voltage ZnO varistors doped with Al. *Materials Chemistry and Physics*. 2006;**100**(1):142-146
- [37] Surthi S, Kotru S, Pandey RK. Low-voltage varistors based on La–Ca–Mn–O ceramics. *Materials Letters*. 2002;**57**(4):887-893
- [38] Simões AZ, Ries A, Perazolli L, Longo E, Varela JA. Nonlinear electrical behaviour of the Cr₂O₃, ZnO, CoO and Ta₂O₅-doped SnO₂ varistors. *Ceramics International*. 2006;**32**(3):283-289
- [39] Peiteado M, Fernandez JF, Caballero AC. Processing strategies to control grain growth in ZnO based varistors. *Journal of the European Ceramic Society*. 2005;**25**(12):2999-3003
- [40] Gupta TK. Application of zinc oxide varistors. *Journal of the American Ceramic Society*. 1990;**73**(7):1817-1840
- [41] Senda T, Bradt RC. Grain growth in sintered ZnO and ZnO-Bi₂O₃ ceramics. *Journal of the American Ceramic Society*. 1990;**73**(1):106-114
- [42] Kharchouche F, Belkhiat S, Belkhiat DEC. Non-linear coefficient of BaTiO₃-doped ZnO varistor. *IET Science, Measurement & Technology*. 2013;**7**(6):326-333
- [43] Li J, Wu K, Jia R, Hou L, Gao L, Li S. Towards enhanced varistor property and lower dielectric loss of CaCu₃Ti₄O₁₂ based ceramics. *Materials & Design*. 2016;**92**:546-551
- [44] Han JH, Lee DH, Kim DY. Fabrication of low-voltage ZnO varistors by a two-step process. *Journal of the European Ceramic Society*. 1995;**15**(4):371-375
- [45] Mahbub R, Fakhru T, Islam MF. Enhanced dielectric properties of tantalum oxide doped barium titanate based ceramic materials. *Procedia Engineering*. 2013;**56**:760-765
- [46] Vijayanandhini K, Kutty TRN. Low-voltage varistors from ZnO+ CaMnO₃ ceramics. *Applied Physics Letters*. 2006;**88**(12):123513
- [47] Vijayanandhini K. Nonlinear Electrical and Magneto transport Properties of ZnO/ Perovskite Manganite Ceramic Composites [thesis]. Bangalore, India: Indian Institute of Science; 2009
- [48] Zulkifli MA, Ghazali MSM, Abdullah WRW, Zakaria A, Ahmad Z. Preliminary characteristic of electrical non-linearity co doped CaMnO₃-ZnO based Varistor ceramics. *Jurnal Teknologi*. 2016;**78**(3):327-331
- [49] Sabri MGM, Azmi BZ, Rizwan Z, Halimah MK, Hashim M, Sidek HAA. Application of direct current and temperature stresses of low-voltage ZnO based varistor ceramics. *American Journal of Applied Sciences*. 2009;**6**(8):1591
- [50] Sabri MGM, Azmi BZ, Rizwan Z, Halimah MK, Hashim M, Zaid MHM. Effect of temperature treatment on the optical characterization of ZnO-Bi₂O₃-TiO₂ varistor ceramics. *International Journal of Physical Sciences*. 2011;**6**(6):1388-1394
- [51] Ghazali MSM, Zakaria A, Abdullah WRW, Hafiz MZM, Matori KA. Effect of Co₃O₄ doping on nonlinear coefficient in Zn-Bi-Ti-O Varistor ceramics. *Advanced Materials Research*. 2015;**20**:1107

- [52] Ghazalia MSM, Abdullah WRW, Zakaria A, Rizwand Z, Matoric KA, Mohd MH. Effect of MnO_2 doping on nonlinear Coefficient of Zn-Bi-Ti-O Varistor ceramics. *Jurnal Teknologi*. 2016;78(3):185-190
- [53] Ghazali M S M, Abdullah W R W, Zakaria A, Zulkifli M A, Zaid M H M, Rizwan Z. Effect of Co_3O_4 doping and sintering temperature on optical energy band gap properties in Zn-Bi-Ti-O varistor ceramics. In: *AIP Conference Proceedings*; September 2017; Melville. New York: AIP Publishing; 2017. p. 1-8
- [54] Wan Abdullah WR, Zakaria A, Ghazali MSM. Synthesis mechanism of low-voltage praseodymium oxide doped zinc oxide varistor ceramics prepared through modified citrate gel coating. *International Journal of Molecular Sciences*. 2012;13(4):5278-5289
- [55] Zulkifli MA, Ghazali MSM, Abdullah WRW, Zakaria A, Ahmad Z, Umar R. Effect of erbium-calcium manganite doping on microstructure and electrical properties of zinc oxide based varistor ceramics. *Journal of Fundamental and Applied Sciences*. 2017;9(25):298-307

Nanostructured Pure and Doped Zirconia: Synthesis and Sintering for SOFC and Optical Applications

Mythili Prakasam, Sorina Valsan, Yiyang Lu,
Felix Balima, Wenzhong Lu, Radu Piticescu and
Alain Largeteau

Additional information is available at the end of the chapter

<http://dx.doi.org/10.5772/intechopen.81323>

Abstract

Zirconia is a multifunctional material with potential applications in wide domains. Rare-earth doped zirconia and stabilized zirconia yield interesting properties based on the phase transitions induced by the sintering conditions. Zirconia nanopowders were prepared by hydrothermal technique. Synthesis methods of zirconia with various rare earths are discussed here. An overview of the sintering of zirconia-based ceramics is presented in particular for SOFC and sensors and optical applications.

Keywords: sintering, solid oxide fuel cell, optical ceramics, hydrothermal synthesis

1. Introduction

Zirconia (ZrO_2) is one of the materials well known for multifunctional applications [1–8]. Commonly employed application domains of ZrO_2 are refractories [9], oxygen sensors [10], and fuel cell membranes [11] due to the high O_2 diffusivity, structural [12], and biomedical applications [13] due to its high strength and toughness. ZrO_2 with its higher birefringence than alumina [14] makes it to be employed in miniature optical devices. Two crystallographic transformations are experienced by ZrO_2 between room temperature and its melting point ($\sim 2715^\circ C$) such as monoclinic to tetragonal [15] at $\sim 1170^\circ C$ and tetragonal to cubic [16] at $\sim 2370^\circ C$. The high temperature tetragonal and cubic forms are stabilized with different elements, such as Mg, Ca, Sc, Ce, and Y [17]. Existence of Cubic ZrO_2 until room temperature, which is named FSZ (fully stabilized zirconia), can be observed with concentration of 8% Ytria [18]. Stabilized

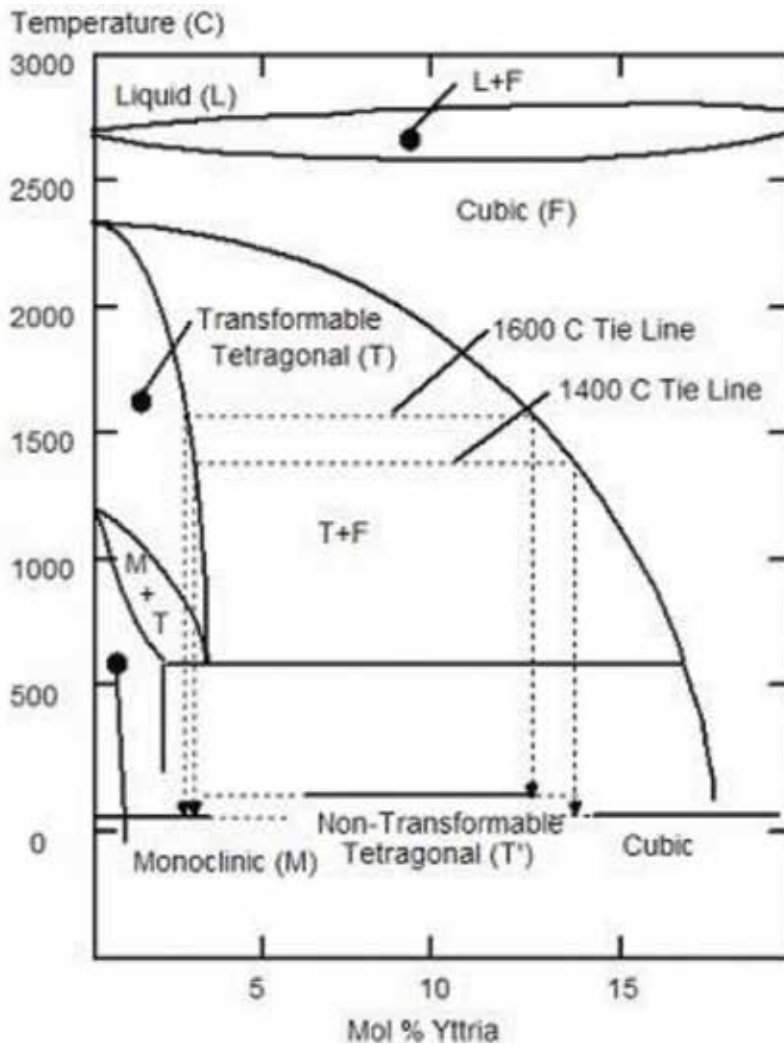


Figure 2. Phase diagram of zirconia with yttria stabilization.

The transition from tetragonal to monoclinic phase is done with a volume increase of about 4% leading to microcracking that drastically affects the mechanical properties. Therefore, the stabilization of cubic or tetragonal phase on larger temperature ranges is required for safety application. The tetragonal or cubic phase can be stabilized (e.g., the temperature of the “*c* → *t*” transition may be decreased) by inducing such additives as MgO, CaO, Y₂O₃, and other rare earth oxides, etc. The doping elements affect not only the structural and mechanical properties but also optical and electrical behavior. Synthetically, the binary system of ZrO₂ may be classified into different systems as specified by Haberkro et al. [22]: systems forming cubic solid solutions in the rich ZrO₂ domain: ZrO₂-MeO (Me = Mg, Cr, Co, Cu), ZrO₂-Me₂O₃ (Me = Fe, Cr, La), ZrO₂-Me₃O₄ (Me = Fe, Mn), ZrO₂-MeO₂ (Me = Th, Ce); systems with the formation of other types of solid solutions in the rich ZrO₂ domain: HfO₂-ZrO₂, TiO₂-ZrO₂, etc.; and

systems with no interactions between the components, e.g., ZnO–ZrO₂, Al₂O₃–ZrO₂. Zirconia ceramic materials are known as important candidates for functional and structural applications. Stabilized Y₂O₃–ZrO₂ ceramics (YSZ) is the most common solid electrolyte used in various applications as oxygen sensors or fuel cells in automotive industry, metallurgical, glass and cement industries, gas pumps for removing oxygen traces from the gases used in special industrial processes, and fuel cells. Their utilization opened a new way for optimization of oxygen (air)/fuel ratios and made automotive and industries more environment friendly due to its adequate level of oxygen ion conductivity and desirable stability in both oxidizing and reducing atmospheres [23]. In principle, these sensors use the Nernst voltage generated by the difference of two different ion concentrations (with different partial pressures) on the sides of an electrolyte, which generate an electrical potential. This voltage is proportional to the natural logarithm of the ratio of the two different ion concentrations according to the Nernst equation:

$$\Delta U = \frac{k_B T}{e_0} = \ln \frac{c_1}{c_2} \quad (1)$$

where k_B is the Boltzmann constant ($= 1.38 \times 10^{-23}$ J/K), T is the absolute temperature in K, e_0 is the elementary charge (1.602×10^{-19} C), and c_i is the ion concentration on the two sides of the solid electrolyte in mol/kg. The mechanism of zirconia partial oxygen pressure sensors is basically described below. At temperatures higher than a certain activation value depending on the composition and structure, zirconia partly dissociates to produce oxygen ions, which can be transported through the material when a voltage is applied. Due to this process, zirconia behaves like a solid electrolyte for oxygen. If two different oxygen pressures exist on either side of a zirconia material, the Nernst voltage can be measured across that element. Generally, ZrO₂-8 mol%Y₂O₃ (YSZ) solid electrolytes exhibiting a conductivity of about $0.1 \Omega^{-1} \text{ cm}^{-1}$ at 1000°C and about $3 \times 10^{-5} \Omega^{-1} \text{ cm}^{-1}$ at 400°C corresponding to an activation energy of 96 kJ mol⁻¹ are used.

2.1. Rare earth doped zirconia phases

To improve the ionic conductivity and sensors' quality factors in a large temperature range, different approaches were proposed: partial or total replacement of Y₂O₃ with Sc₂O₃ having a maximum corresponding to the composition (Y_{0.5}Sc_{0.5})*0.3 Zr_{0.7}O_{1.85}. The main limitation of this approach is the decrease of conductivity observed with holding time due to the structural modifications [24]. The development of planar sensors using ceramic membranes and multipackaging technology in place of classical bulk sintered materials shows the ability to increase the efficiency of the thermal transfer but has limited effect on the ionic conductivity of the material itself [25]. In this case, the technology is the main limiting factor, since complex additives are required to control the dispersibility of the ceramic powders [26]. Reducing the diffusion and transport distances using nanocrystalline membranes and thin films, Kosacki et al. found that nanocrystalline YSZ thin films with mean grain sizes in the range 10–200 nm materials exhibited two-three orders of magnitude increase in conductivity compared to polycrystalline and single crystalline materials [27]. An activation energy in the range 0.85 ± 0.05 eV for bulk conductivity with a corresponding grain boundary conductivity of 1.0 ± 0.1 eV for nanocrystalline 2–3 mol% Y₂O₃ doped ZrO₂ ceramics with average grain particle in the range 35–50 nm was reported. It was also reported that yttria doped tetragonal

zirconia (YTZP) ceramics have lower activation energy for the ion conduction opening the field for their utilization at lower temperatures [28]. A comprehensive review with respect to the structure, chemistry, design and selection of materials, underlying mechanisms, and performance of each SOFC component, which opens up the future directions toward pursuing SOFC research, was recently proposed in [29].

Zirconia co-doped with different rare earth elements has been intensively studied during recent period due to the versatility of these materials in various optoelectronic devices and biomaterials. Some examples are summarized below. A single step, rapid microwave driven solution combustion technique was used to obtain luminescent, cubic ZrO_2 : Eu^{3+} nanophosphors [30]. Zirconia doped with selected trivalent rare earth oxides was successfully obtained by a complex polymerization method and may be considered promising candidates for white light-emitting applications [31]. ZrO_2 : Eu^{3+} nanocrystals were synthesized by hydrothermal technique. Effects of Eu^{3+} doping and annealing on the morphology, crystal structure, and fluorescence properties of the resultant nanocrystals were investigated. Nanocrystals with tetragonal or cubic structure may find potential applications as the raw material for producing the transparent ceramics with efficient fluorescence properties [32]. Zirconium oxide powders doped with terbium, synthesized by hydrothermal route from a highly basic solution, were used to determine the role of the basic agent (NaOH, KOH, or LiOH) utilized to carry out the hydrothermal synthesis on their morphology, crystalline structure, photoluminescent, or cathodoluminescent properties [33]. Scandia-stabilized zirconia powder (ScSZ) was synthesized by a microwave-hydrothermal method. The structure of the ScSZ powder changed from a tetragonal to a cubic phase, and accordingly, the powder conductivity was increased from 90.55 to 120.56 mS/cm by the introduction of the mineralizer solutions ($\text{KOH} + \text{K}_2\text{CO}_3$) during the microwave-hydrothermal processing [34]. Un-doped and rare earth (Dy and Ce)-doped ZrO_2 nanoparticles NPs were synthesized by coprecipitation method, showing no toxicity and possessing good antibacterial ability [35]. The thermal stability of zirconia up to very high temperatures explains also its intensive use in energy generation applications as coatings or sintered bulk pieces. Thermal barrier coatings (TBCs) have proved to be a key technology in thermal stability, and their use to achieve surface temperature reduction of the underlying super alloys surpass all other achievements in the field of material technologies that have taken place in last three decades [36].

2.2. Zirconia nanopowder synthesis

The technique most often used to prepare zirconia powders is the sol-gel route. The sol-gel process makes it possible to manufacture an inorganic polymer by simple chemical reactions and at a temperature close to room temperature. The synthesis is carried out from precursors. They are either liquid or solid and are mostly soluble in common solvents. The simple chemical reactions at the base of the process are triggered when the precursors are brought into contact with water. To prepare the pure zirconia powders [37–41], the precursor used is zirconium n-propoxide ($\text{Zr}(\text{OC}_3\text{H}_7)_4$, 70% diluted in n-PrOH) [42]. Sol-gel synthesis can also be carried out to obtain zirconia powders doped with 3% of Yttria [43].

Another technique used in the synthesis is coprecipitation [44]. It is a simultaneous precipitation of two substances, and it is used for the preparation of 8YSZ. To do this, we must precipitate Zr^{4+} and Y^{3+} . The synthesis of the powders can also be obtained by pyrolysis of spray

aerosol (spray-pyrolysis). This process involves injecting the spray containing the precursor solution into a combustion chamber where the particles are quickly ignited. This technique makes it possible to obtain zirconia powders doped with Ytria [45] and in particular doped with 8YSZ [46]. It is also possible to use a hydrothermal route to synthesize zirconia powders [47]. Hydrothermal synthesis allows the production of crystalline fine powders to deagglomerate. These qualities are suitable for the preparation of fine oxide/oxide composites by simultaneous synthesis of the two phases. The last technique that can be used is a homogeneous precipitation method of zirconium oxychloride, yttrium, urea, which is used as a precipitating agent, and polyacrylic acid, which is used as a dispersing agent [48].

2.2.1. Synthesis methods for RE doped ZrO_2 , with accent on hydrothermal synthesis

The so-called triangle synthesis, properties, and applications must be fully exploited to obtain assessed materials for specific applications. The properties of nanostructured materials depend on the atomic structure, composition, microstructure, defects, and interfaces, which are controlled by thermodynamics and kinetics of the synthesis. Different synthesis routes for manufacturing of nanomaterials were proposed. Generally, they may be classified as physical, chemical, and combined routes. Other classification considers the top-down approach from the macroscale to the nanoscale or conversely by assembly of atoms or particles using the bottom-up approach. Chemical reactions for material synthesis can be done in solid (conventional synthesis route), liquid, or gaseous state. For solid state reactions, diffusion of atoms depends on the temperature of the reaction, and transport across grain boundaries and grain growth at elevated temperature reactions may lead to solids with large grain size. Compared to solid-state synthesis, diffusion in the liquid or gas phase is typically and advantageously many orders of magnitude larger than in the solid phase; thus, the synthesis of nanostructured materials can be achieved at lower temperatures, reducing the detrimental grain growth.

Synthesis route	Solid-state process	Coprecipitation	Hydrothermal	Sol-gel	Spray pyrolysis
Composition control	Poor	Good	Excellent	Medium	Excellent
Morphology control	Poor	Medium	Good	Medium	Good
Particle size (nm)	>1000	>100	10–100	>10	>10
Hard agglomerates	Medium	High	Low	Medium	Low
Impurities (%)	0.5–1	Max. 0.5	Max. 0.5	0.1–0.5	0.1–0.5
Additional steps	Calcinations, milling	Calcinations, milling	No	Calcinations, milling	No
Scalability	Industrial	Industrial	Demonstration	Demonstration	R&D
Environmental impact	High	Moderate	Low	High	Moderate

Table 1. A comparison between main synthesis routes for obtaining doped zirconia materials.

Although many laboratory-scale reactions can be scaled up to economically produce large quantities of materials, the laboratory-scale reaction parameters may not be linearly related to that of large-scale reaction. The synthesis parameters such as temperature, pH, reactant concentration, and time should be ideally correlated with factors such as supersaturation, nucleation and growth rates, surface energy, and diffusion coefficients in order to ensure the reproducibility of reactions. A comparison between the main procedures used for the synthesis of doped zirconia materials is presented in **Table 1** from the point of view of scalability.

The main advantages of the hydrothermal synthesis are one step process for powder synthesis or oriented ceramic films; minimized consumption energy; closed-flow system; relatively high deposition rate; products with much higher homogeneity than solid state processing; products with higher density than gas or vacuum processing (faster growth rate); and versatility: oxides, nonoxides, organic/biologic materials, and hybrid materials with different morphologies may be obtained [49].

3. Classical sintering of rare earth doped zirconia

Different theoretical and empirical models for solid state sintering were used for modeling the density of sintered zirconia nanomaterials using classical pressing and sintering technology, however being limited by the complexity of the structural modifications during the compaction process. A study on the influence of the synthesis and processing parameters on the ion conduction of YTZP nanomaterials and the characteristics of gauges for pressure sensors was performed [50]. YTZP powders (ZrO_2 doped with 3.5 mol% Y_2O_3) obtained by hydrothermal treatment of the precursor suspensions in a Teflon autoclave for various times at temperatures around 250°C using ammonia as mineralizing agent were used in the sintering studies.

Powders with very high specific surface area (195–200 m^2/g) and pycnometric density in the range 5–5.2 g/cm^3 were used. YTZP powders obtained via the hydrothermal procedure having the microstructure and properties described before were used (**Figure 3**) to obtain compact materials via two methods:

- Bulk material by pseudo-axial pressing and sintering.
- Tape casting of membranes followed by drying and sintering.

The sintered bulk material was obtained by pseudo-biaxial pressing at 100 MPa followed by sintering in air. To eliminate the chemically bonded water, powders have been additionally attrition milled for 2 hours in acetone before addition of sintering additives. The optimal sintering parameters were estimated from the dynamic sintering curves obtained by the heating stage microscopy (**Figure 4**). Two shrinkage intervals can be clearly observed, the first from room temperature to approximately 550°C related to thermal decomposition of binders (polyvinyl alcohol PVA) and the second at 1400°C corresponding to sintering, with a total shrinkage of 28% at 1400°C. Compacts with densities higher than 96% of the theoretical and grain sizes around 200 nm have been obtained.

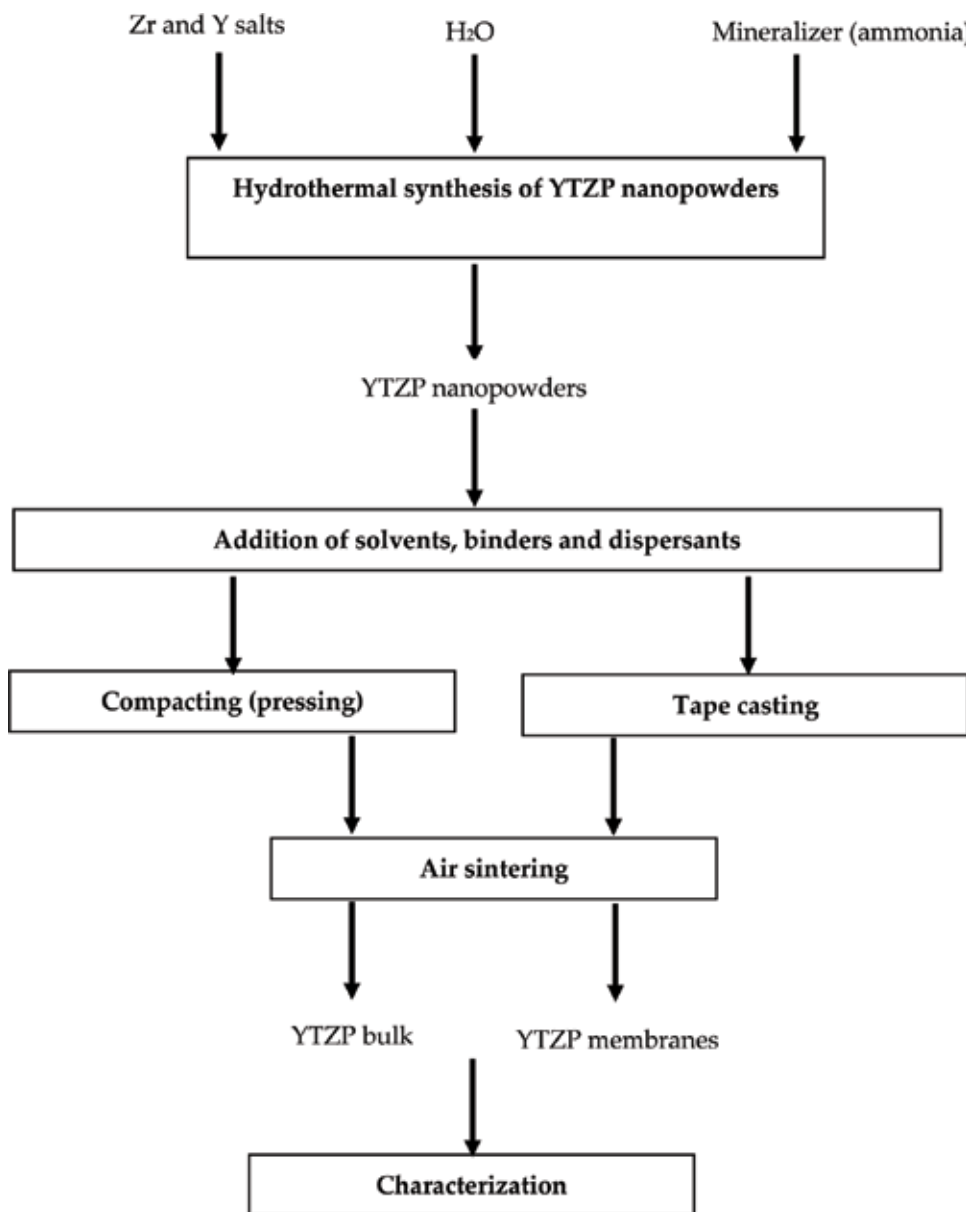


Figure 3. Schematic flow sheet for obtaining of YTZP materials for sensors application.

The effective ionic conductivity of YTZP bulk materials was measured using impedancemetry measurements. The contributions of bulk and grain boundaries on the total ionic conductivity were calculated from the impedance spectra of samples. The results on the activation energy of ionic conduction are presented in **Table 2** below.

The model developed suggest that grain boundaries increase the total ionic conductivity of yttria-doped zirconia due to a “short circuit effect,” leading to an apparent conductivity

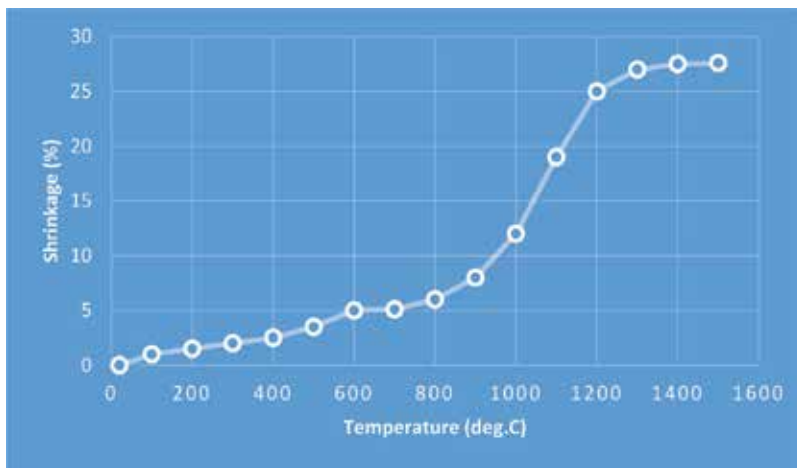


Figure 4. Dynamic sintering curves of YTZP nanopowders.

Y ₂ O ₃ mol% in YTZP	Grain sizes (nm)	Microstructure	Activation energy of ionic conductivity (kJ/mol)
7.5	625	Polycrystalline	110
3	524	Polycrystalline	97.5
3	393	Polycrystalline (0.25% Al ₂ O ₃ (grain growth inhibitor))	86
4	603	Polycrystalline	90
3		Single crystal	84

Table 2. Activation energy of ionic conductivity in YTZP nanomaterials.

higher than of single crystals of similar composition. This effect increases with decreasing grain sizes and may practically neglect large micrometric grain sizes.

3.1. New sintering methods of rare earth doped zirconia

Various sintering techniques [51] have been employed till date for the fabrication of YSZ transparent ceramics. Most prevalently used techniques are hot isostatic pressing [52], spark plasma sintering (SPS) [53], and microwave sintering [54]. Different approaches have been employed for obtaining transparent ceramics [55] of YSZ either by means of dopant, high pressure, two-step load application procedure, or pre compaction followed by vacuum sintering and hot isostatic pressing. Kim et al. [56] studied the effects of the sintering conditions of dental zirconia ceramics on the grain size and translucency by comparing the microwave sintering and classical sintering. Jiang et al. [57] analyzed the effects of sintering temperature and particle size (40 and 90 nm) on the 3YSZ (YSZ with 3% Y₂O₃) dental ceramic because 3% Y₂O₃ gives higher mechanical strength than 8% Y₂O₃. Fang et al. [58] showed enhanced densification of zirconia containing ceramic matrix composites by microwave processing. Tamburini

et al. [59] reported on high pressure SPS, whereas Casolco et al. [60] used a traditional die set-up and two-step load application procedure. Klimke et al. and Krell et al. [14, 61] used CIP followed by HIP, whereas Tosoh [62] Corporation and their team used sintering aid such as TiO_2 to obtain transparent 8YSZ (YSZ with 8% Y_2O_3). The addition of TiO_2 is reported to decrease the mechanical strength [63] of 8YSZ transparent ceramics with low transparency.

Zirconia powders doped with 3 mol% Y_2O_3 and co-doped with 3 mol% Y_2O_3 -6 mol% CeO_2 have been selected for preliminary sintering tests using a field assisted method [64]. The hydrothermally synthesized powders after were mixed with a solution containing 6 wt% polyvinyl alcohol as binder and spray dried using a LabPlant spray drier system (air speed of 3.5 m/s at evacuation and feeding rate of 617 ml/h using a 0.5 mm nozzle). Rapid analysis by optical micrographs of all investigated samples revealed the presence of rounded particles with sizes ranging from a few microns to tens of microns. The powder morphology was maintained after the heat treatment for 2 hours at 500°C to remove the PVA binder, and they have been further used in FAST sintering tests, using a thermal mechanical simulator—Gleeble 3800, with fully integrated digital closed-loop control thermal and mechanical testing system makes highly accurate process control possible. The tests were conducted with variation of different key parameters, such as pressure, maximum temperature, and holding time, where the temperature range applied was 1100 – 1300°C , with pressure range of 75–125 MPa and holding time of 120–240 second.

The relative density of the sample was calculated to 99.47%, which was under the sintering condition at 1300°C and 125 MPa, with $25^\circ\text{C}/\text{S}$ heat rate and 120 Sholding time. It may be observed that no open porosity exists, which indicates that a fully dense bulk material was achieved (Figure 5).

Flash sintering is also a new sintering method that attracted significant attention for rapid densification of ceramics at low sintering temperatures, allowing to retain the fine grains and control the dielectric and mechanical properties. Flash sintering of yttria-stabilized zirconia at temperatures $<600^\circ\text{C}$ with a constant heating rate of $25^\circ\text{C}/\text{min}$ leads to dense ceramics

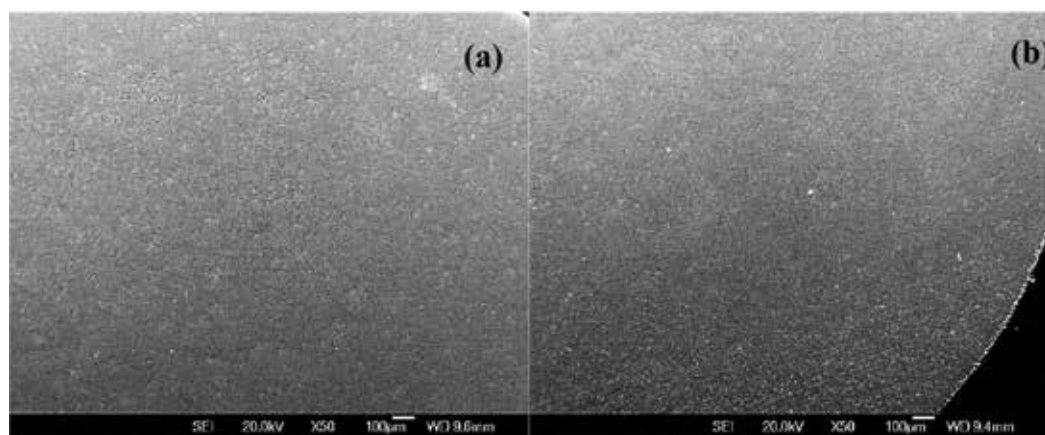


Figure 5. SEM micrographs of sintered samples (a) ZrO_2 -3Y and (b) co-doped with 3Y-6 CeO_2 - ZrO_2 .

with high ultimate compressive strength >3.5 GPa and inelastic strain around 8% due to the transformation toughening. At higher temperatures, the high dislocation density induced by the flash sintering conditions improves the plasticity of the sintered ceramics and retards the cracks nucleation and propagation [65].

3.2. Classification of transparent materials and applications of transparent ceramics

Nowadays, materials such as glasses, polymers, or single crystals are used for applications requiring good optical properties such as laser, lenses, camera domes, and much more.

However, transparent ceramics are an interesting alternative to the aforesaid materials. Indeed, they have a greater ease of development of large complex parts, good mechanical properties (good resistance to thermal shocks and fractures), low thermal expansion, good thermal conductivity, and good tenacity. They are already used for various applications.

3.2.1. *The manufacture of transparent ceramics*

Transparent ceramics can be classified into two different forms based on their crystalline structure: the cubic structure and the noncubic structure. The cubic transparent ceramics is one of the widely reported in the literature. Manufacture of noncubic transparent ceramics is not an easy task, which can be explained as below. Depending on the type of structure, there will be the problem of birefringence occurring at the grain boundaries. For the noncubic structure, the material is said to be anisotropic. In this case, we observe two indices of refraction: the ordinary index and the extraordinary index. This extraordinary ray is going to make our material birefringent, and it will be necessary to control very closely the growth of the grains, due to the diffusion of light caused by the ceramics with birefringence.

The methods of fabrication of transparent ceramics are numerous such as hot pressing, hot isostatic pressing, vacuum sintering, microwave sintering, and spark plasma sintering.

3.2.2. *Rare earth-based zirconia-based transparent ceramics by spark plasma sintering*

Until to date, there are no reports focusing on yielding 3YSZ and 8YSZ transparent ceramics by analyzing sintering parameters and their influence in yielding transparency by SPS sintering. Here, we report on yielding 3YSZ transparent ceramics containing tetragonal phases without addition of any dopants or high-pressure technique. Tetragonal phased zirconia has interesting mechanical strength due to its large refractive index and high dielectric constants. In order to obtain transparent ceramics, it is necessary to have maximum density and minimum porosity in the orders of <0.01 vol% in the final sintered body. The aforesaid is achieved due to the interplay of various sintering parameters (SP) such as sintering temperature, dwell time, heating/cooling rate, pressure, and temperature of pressure application. We have optimized the sintering parameters and demonstrated the possibility of obtaining transparent 3YSZ through reactive sintering during spark plasma sintering favorizing cubic phase formation with Y segregation around the grain boundaries. We demonstrated for the first time the presence of tetragonal and cubic phases in transparent ceramics of 3YSZ and 8YSZ obtained by SPS. The experimental details and results are presented in the following sections.

In the present study, 3YSZ and 8YSZ nanopowders (Tosoh Corporation) with average crystallite size ~20 nm average particle diameter 0.3 μm were used for the fabrication of 3YSZ and 8YSZ transparent ceramics. Spark plasma sintering (SPS) experiments were performed with DR. SINTER LAB Spark Plasma Sintering system, Model SPS-515S-FUJI. The experiments were performed under a vacuum of 10 Pa with the pulse sequence for the SPS applied voltage of 12:2 (i.e., 12 ON/2 OFF). 1 g of powder was used for each experiment. The experiment was carried out in a graphite mold with inner diameter of 10 mm and external diameter of 25 mm. The internal of the graphite die was covered with carbon foil (Papyex). The mold was covered with carbon fiber felt to limit the loss of heat radiation. Due to the usage of pyrometer, the temperature was first increased to 600°C within 3 min without regulation and then increased to a range of temperatures from 1150–1400°C with different heating rate (R_H) ranging from 2.5 to 100°C/min and with 20 min dwell time. Uniaxial pressures ranging from 40 to 100 MPa were applied at room temperature (T_R) and sintering temperature (T_S), and their significances have been analyzed. The cooling rates (R_C) and R_H were maintained equal in all the experiments. Then, the ceramics were ground and polished to a thickness of 1 mm with optical finishing. Powder X-ray diffraction (XRD) analysis was performed with a PANalytical X'Pert MDP diffractometer with θ - θ Bragg Brentano configuration, with a backscattering graphite monochromator for K_α Cu radiation working at 40 kV and 40 mA. Temperature dependent XRD has been performed using a powder diffractometer (PANalytical X'Pert Pro) equipped with a high-temperature chamber Anton Paar HTK16 (1600°C) measuring with K_α Cu radiation. The temperatures of analyses used were from room temperature until 1400°C. The density was measured by the Archimedes method in distilled water. The microstructure was observed by a scanning electron microscope (Joel 840 SEM) on fractured surface without polishing. The optical transmittance spectrum was measured by using a double beam spectrophotometer (Varian Cary 5000) at a range of between 200 and 7000 nm for a sample thickness of 1.5 mm.

It has to be mentioned that so far the ceramics of pure monoclinic ZrO_2 did not yield transparency, whereas the samples of 3YSZ were translucent and that of 8YSZ are well transparent. In order to study the behavior of ZrO_2 with three different compositions, all the samples were treated under same conditions, i.e., sintering temperature = 1200°C, heating/cooling rate = 2.5°, 5°, and 10°C/min, dwell time = 20 min, pressure applied = 100 MPa, and point of pressure application at the start of sintering cycle and the other being only during the dwell time. Though transparency was obtained for the pure ZrO_2 , the sample was dense under the following conditions: sintering temperature = 1200°C, heating/cooling rate = 2.5°C/min, dwell time = 20 min, pressure applied = 100 MPa, and point of pressure application = only during the dwell time. The translucent sample of 3YSZ was obtained at sintering temperature = 1200°C, heating/cooling rate = 2.5°C/min, dwell time = 20 min, pressure applied = 100 MPa, and point of pressure application = only during the dwell time/beginning of sintering cycle. The transparent sample of 8YSZ was obtained at sintering temperature = 1200°C, heating/cooling rate = 2.5°C/min, dwell time = 20 min, pressure applied = 100 MPa, and point of pressure application = only during the dwell time.

The XRD analysis in **Figure 6(a)**, which shows stabilized zirconia, shows that two samples have the same chemical composition. The initial one-phase powder monoclinic (Baddeleyite) was expected, since it is at room temperature and there is no addition of stabilizer. In addition,

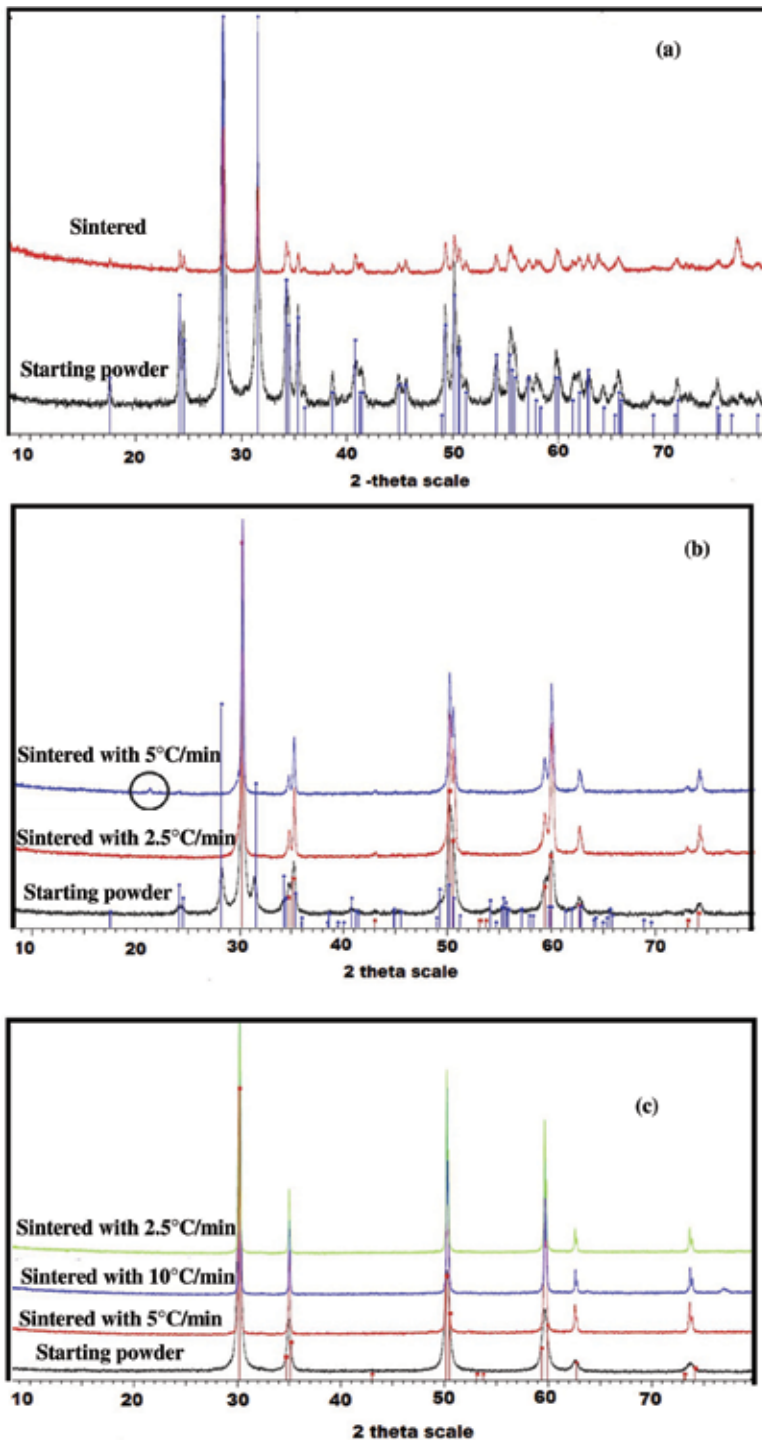


Figure 6. XRD analyses of sintered compacts of (a) pure zirconia, (b) 3YSZ, and (c) 8YSZ at 1200°C for 20 min with different heating rates.

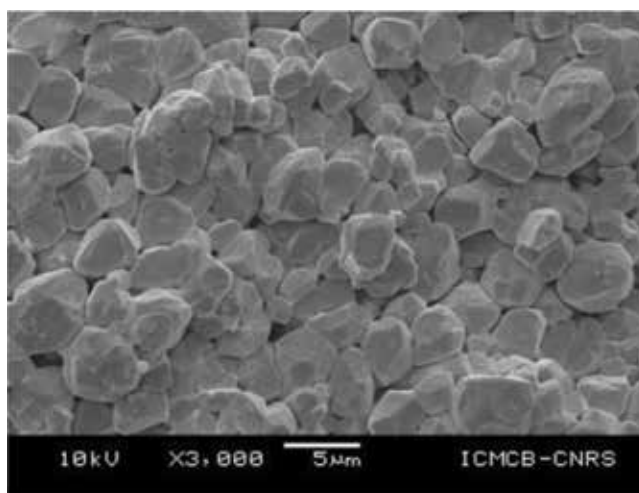


Figure 7. SEM analysis of pure zirconia at sintering temperature of 1200°C for 20 min; Heating and cooling rate: 5°C/min.

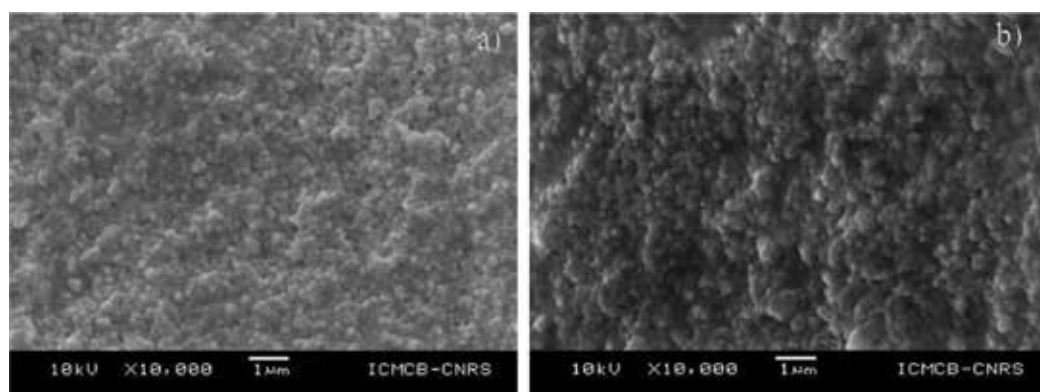


Figure 8. SEM analyses of zirconia 3YSZ at a sintering temperature of 1200°C for 20 min and at heating and cooling rates of (a) 5°C/min and (b) 10°C/min.

pure zirconia after sintering at 1200°C always has a monoclinic phase because its stabilization and sintering temperature is too low for the transition to a tetragonal phase. However, we note that the characteristic peaks of the monoclinic phase disappear more and more, which shows the beginning of a transition to a tetragonal phase. The analysis in **Figure 6(b)** shows that the three samples of 3YSZ contain the same chemical elements. The initial powder of 3YSZ has a monoclinic phase that tends to become tetragonal. For stabilized zirconia with 3% Yttria at sintering temperature of 1200°C, for heating and cooling rates 5 and 10°C/min, the tetragonal phase is obtained. However, a slight peak is observed for the 3YSZ at a heating and cooling rate of 10°C/min, which must correspond to a chemical reaction or to the fact that the corresponding heating rate is not low enough, which does not allow time for the material to change correctly of phases. The analysis in **Figure 6(c)** shows that the three samples of 8YSZ contain the same chemical elements. The initial powder of 8YSZ has a mixture of tetragonal and cubic phase that tends to become cubic. For stabilized zirconia with 8% Yttria at sintering

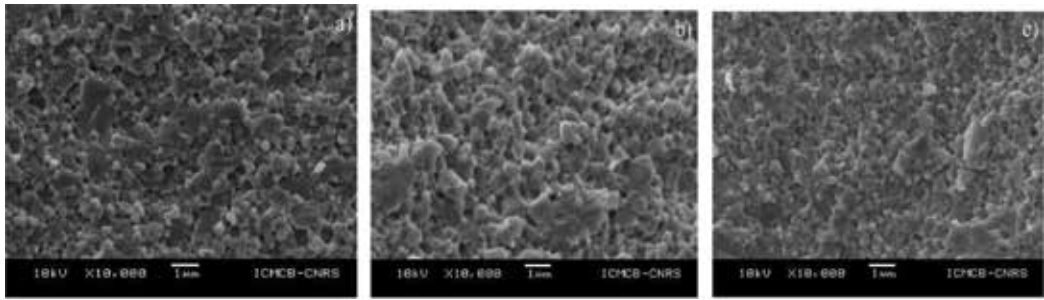


Figure 9. SEM analyzes of zirconia 8YSZ at a sintering temperature of 1200°C for 20 min and at heating and cooling rates of (a) 5°C/min; (b) 2.5°C/min; and (c) 10°C/min.

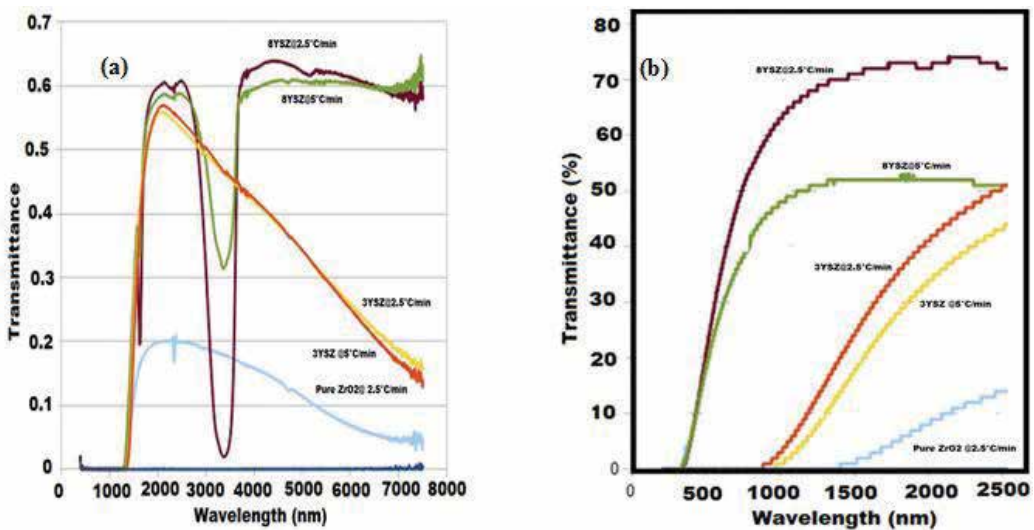


Figure 10. Transmittance spectrum of pure zirconia stabilized with yttria in (a) UV-visible range and (b) near infrared sintered at 1200°C for a dwell time of 20 min with different heating rates.

temperature of 1200°C, for heating and cooling rates of 5° and 10°C/min, the cubic phase is obtained. The conversion to the cubic phase is induced by the segregation of the Y in the grain boundaries, which were probably caused due to the slow heating rate employed during the sintering cycle (Figures 7–9).

The spectra of Figure 10 show similar results. Indeed, the samples that have a maximum transmittance in the UV-visible near IR are the same as those in the IR, and the transmittance varies just slightly between the two spectra and it depends on the samples.

Zirconia stabilized with higher % yttria and the more the ceramic has high transmittance. In addition, in the case of a zirconia partially stabilized and fully stabilized, the effect of a higher or lower heating rate has a significant impact. Indeed, the lower the heating rate, the more the material has a high maximum transmittance. It is clearly evident from Figure 10 that the transmittance corresponding to the rate of transmission is 2.5°C/min, which shows high transmittance, with transmittance of >50% in the visible and >65% in the near IR [66].

4. Conclusion

The current chapter deals with the various fabrication methodologies and synthesis of rare earth doped zirconia that can be employed for applications in areas, including catalysis, glassmaking, metallurgy, optoelectronics, batteries, and coatings for extreme environments. During recent years, it has been reported that using mixed rare earth oxides as dopant may strongly improve the functional properties of the matrix such as increasing thermal shock resistance of zirconia-based thermal barrier coatings (TBCs) and improve ionic conductivity of solid oxide fuel cells (SOFCs) by surface segregation mechanisms. Various powder synthesis methodologies with an accent on hydrothermal powder synthesis is discussed. The feasibility of obtaining the sintering compacts of rare earth oxides and co-doped rare earth oxides both from the commercial and hydrothermal synthesis by rapid sintering methods such as spark plasma sintering is demonstrated. The role of rare earth oxides on sintering and in the point of view of applications is evident from the current work for the zirconia. Further investigations are necessary to validate the role of co-doped rare earth oxides for thermal barrier coatings and in SOFCs. The aforesaid is being investigated as a part of the project "MONAMIX" and will be reported elsewhere later.

Acknowledgements

The authors duly acknowledge the following funding agencies for the present work through

1. Grant agreement 692216 SUPERMAT from European Union's Horizon 2020 research and innovation program
2. Grant agreement ERAMIN 2 COFUND-Research & Innovation program on raw materials to foster circular economy-"MONAMIX"- "ANR-17-MIN2-0003-03"
3. Part of collaboration in photonics between University of Bordeaux and Huazhong University of Science and Technology.

Author details

Mythili Prakasam^{1*}, Sorina Valsan³, Yiyang Lu^{1,2}, Felix Balima¹, Wenzhong Lu², Radu Piticescu³ and Alain Largeteau¹

*Address all correspondence to: mythili.prakasam@icmcb.cnrs.fr

1 CNRS, University of Bordeaux, ICMCB, UMR 5026, Pessac, France

2 Huazhong University of Science and Technology (HUST) School of Optical and Electronic Information, Wuhan, China

3 National R&D Institute for Nonferrous and Rare Metals, Pantelimon, Romania

References

- [1] Bangchao Y, Jiawen J, Yican Z. Spark-plasma sintering the 8-mol% yttria-stabilized zirconia electrolyte. *Journal of Materials Science*. 2004;**39**:6863-6865
- [2] Takeuchi T, Kondoh I, Tamari N, Balakrishnan N, Nomura K, Kageyama H, et al. Improvement of mechanical strength of 8 mol% yttria-stabilized zirconia ceramics by spark-plasma sintering. *Journal of the Electrochemical Society*. 2002;**149**:A455-A461
- [3] Cao XQ, Vassen R, Stoever D. Ceramic materials for thermal barrier coatings. *Journal of the European Ceramic Society*. 2004;**24**:1-10
- [4] Rambo CR, Cao J, Sieber H. Preparation, and properties of highly porous, biomorphic YSZ ceramics. *Materials Chemistry and Physics*. 2004;**87**:345-352
- [5] Balakrishnan N, Takeuchi T, Nomura K, Kageyama H, Takeda Y. Aging effect of 8 mol% YSZ ceramics with different microstructures. *Journal of the Electrochemical Society*. 2004;**151**:A1286-A1291
- [6] Li Q, Zhang YF, Ma XF, Meng J, Cao XQ. High-pressure sintered yttria stabilized zirconia ceramics. *Ceramics International*. 2009;**35**:453-456
- [7] Patil DS, Prabhakaran K, Durgaprasad C, Gokhale NM, Samui AB, Sharma SC. Synthesis of nanocrystalline 8 mol% yttria stabilized zirconia by the oleate complex route. *Ceramics International*. 2009;**35**:515-519
- [8] Rajeswari K, Padhi S, Reddy ARS, Johnson R, Das D. Studies on sintering kinetics and correlation with the sinterability of 8Y zirconia ceramics based on the dilatometric shrinkage curves. *Ceramics International*. 2013;**39**:4985-4990
- [9] Kubrin R, do Rosario JJ, Lee HS, Mohanty S, Subrahmanyam RP, Smirnova I, et al. Vertical convective coassembly of refractory YSZ inverse opals from crystalline nanoparticles. *ACS Applied Materials & Interfaces*. 2013;**5**:13146-13152
- [10] Miura N, Jin H, Wama R, Nakakubo S, Elumalai P, Plashnitsa V. Novel solid-state manganese oxide-based reference electrode for YSZ-based oxygen sensors. *Sensors and Actuators B: Chemical*. 2011;**152**:261-266
- [11] Garbayo I, Tarancón A, Santiso J, Peiró J, Alarcón-LLadó E, Cavallaro A, et al. Electrical characterization of thermomechanically stable YSZ membranes for micro solid oxide fuel cells applications. *Solid State Ionics*. 2010;**181**:322-331
- [12] Drescher I, Lehnert W, Meusinger J. Structural properties of SOFC anodes and reactivity. *Electrochimica Acta*. 1998;**43**:3059-3068
- [13] Inuzuka M, Nakamura S, Kishi S, Yoshida K, Hashimoto K, Toda Y, et al. Effect of hydroxyapatite dopant to yttria stabilized zirconia ceramics for biomedical application. *Phosphorus Research Bulletin*. 2003;**16**:75-82
- [14] Klimke J, Trunec M, Krell A. Transparent tetragonal yttria-stabilized zirconia ceramics: Influence of scattering caused by birefringence. *Journal of the American Ceramic Society*. 2011;**94**:1850-1858

- [15] Chevalier J, Gremillard L, Virkar AV, Clarke DR. The tetragonal-monoclinic transformation in zirconia: Lessons learned and future trends. *Journal of the American Ceramic Society*. 2009;**92**:1901-1920
- [16] Bokhimi X, Morales A, García-Ruiz A, Xiao TD, Chen H, Strutt PR. Transformation of yttrium-doped hydrated zirconium into tetragonal and cubic nanocrystalline zirconia. *Journal of Solid State Chemistry*. 1999;**142**:409-418
- [17] Yashima M, Hirose T, Kakihana M, Suzuki Y, Yoshimura M. Size and charge effects of dopant M on the unit-cell parameters of monoclinic zirconia solid solutions $Zr_{0.98}M_{0.02}O_{2-\delta}$ (M = Ce, La, Nd, Sm, Y, Er, Yb, Sc, Mg, Ca). *Journal of the American Ceramic Society*. 1997;**80**:171-175
- [18] Suárez G, Garrido LB, Aglietti EF. Sintering kinetics of 8Y-cubic zirconia: Cation diffusion coefficient. *Materials Chemistry and Physics*. 2008;**110**:370-375
- [19] Yamashita I, Tsukuma K. Light scattering by residual pores in transparent zirconia ceramics, Lattice diffusion kinetics in Y_2O_3 -stabilized cubic ZrO_2 single crystals: A dislocation loop annealing study. *Journal of the Ceramic Society of Japan*. 2011;**119**:133-135
- [20] Chien FR, Heuer AH. Lattice diffusion kinetics in Y_2O_3 -stabilized cubic ZrO_2 single crystals: A dislocation loop annealing study. *Philosophical Magazine A*. 1996;**73**:681-697
- [21] Lu J, Ueda K-i, Yagi H, Yanagitani T, Akiyama Y, Kaminskii AA. Neodymium doped yttrium aluminum garnet ($Y_3Al_5O_{12}$) nanocrystalline ceramics—a new generation of solid state laser and optical materials. *Journal of Alloys and Compounds*. 2002;**341**:220-225
- [22] Pampuch R, Haberko K. In: Vincezini P, editor. *Ceramic Powders*. Elsevier Publ. Co.; 1983. pp. 623-634
- [23] Gope W, Reinhardt G, Rosch M. Trends in the development of solid state amperometric and potentiometric high temperature sensors. *Solid State Ionics*. 2000;**136**:519-531
- [24] Ciachi FT, Badwal SP. The system Y_2O_3 - Sc_2O_3 - ZrO_2 : Phase stability and ionic conductivity studies. *Journal of the European Ceramic Society*. 1991;**7**:197-206
- [25] Menil F, Coillard V, Debeda H, Lucat C. A simplified model for the evaluation of the electrical resistance of a zirconia substrate with co-planar electrodes. *Sensors and Actuators*. 2001;**B77**:84-89
- [26] Piticescu RR, Monty C, Millers D. Hydrothermal synthesis of nanostructured materials: Present state and future prospects. *Sensors and Actuators B*. 2005;**109**:102-106
- [27] Kosacki I, Colomban P, Anderson HV. *Proceedings of the US-Japan Workshop on Electrically Active Ceramic Interfaces*. MIT, USA; 1998. pp. 180-188
- [28] Wepner W. Tetragonal zirconia polycrystals—a high performance solid oxygen ion conductor. *Solid State Ionics*. 1992;**52**:15-21
- [29] Mahato N, Banerjee A, Gupta A, Omar S, Balani K. Progress in material selection for solid oxide fuel cell technology: A review. *Progress in Materials Science*. 2015;**72**:141-337

- [30] Manjunatha S, Hari Krishna R, Thomas T, Panigrahi BS, Dharmaprakash MS. Moss-Burstein effect in stable, cubic $\text{ZrO}_2\text{:Eu}^{+3}$ nanophosphors derived from rapid microwave-assisted solution-combustion technique. *Materials Research Bulletin*. 2018;**98**:139-147
- [31] Lovisa LX, Araújo VD, Tranquilin RL, Longo E, Li MS, Paskocimas CA, et al. White photoluminescence emission from ZrO_2 co-doped with Eu^{3+} , Tb^{3+} and Tm^{3+} . *Journal of Alloys and Compounds*. 2016;**674**:245-251
- [32] Hui Y, Zou B, Liu S, Zhao S, Xu J, Zhao Y, et al. Effects of Eu^{3+} -doping and annealing on structure and fluorescence of zirconia phosphors. *Ceramics International*. 2015; **41**:2760-2769
- [33] Guerra AIR, Merlín IM, Falcony C. The role of the stabilizing agent on the structural and luminescent properties of hydrothermally synthesized $\text{ZrO}_2\text{:Tb}^{3+}$ phosphors. *Ceramics International*. 2018;**44**:13744-13749
- [34] Hongmin AO, Xiangsheng L, He Z, Jing Z, Xiaowei H, Zongyu F, et al. Preparation of scandia stabilized zirconia powder using microwave-hydrothermal method. *Journal of Rare Earths*. 2015;**33**:746-751
- [35] Mekala R, Deepa B, Rajendran V. Preparation, characterization and antibacterial property of rare earth (Dy and Ce) doping on ZrO_2 nanoparticles prepared by co-precipitation method. *Materials Today: Proceedings*. 2018;**5**:8837-8843
- [36] Kumar V, Balasubramanian K. Progress update on failure mechanisms of advanced thermal barrier coatings: A review. *Progress in Organic Coatings*. 2016;**90**:54-82
- [37] Quarles G. Comparison of Optical, Mechanical and Thermo-Optical Properties of Oxide Polycrystalline Laser Gain Materials with Single Crystals. USA: Optical Society of America; 2006
- [38] Hu C. Developments in hot pressing (HP) and hot isostatic pressing (HIP) of ceramic matrix composites. In: *Advances in Ceramic Matrix Composites*. 2014. pp. 164-189
- [39] Huo D, Zheng Y, Sun X, Li X, Liu S. Preparation of transparent Y_2O_3 ceramic by slip casting and vacuum sintering. *Journal of Rare Earths*. 2012;**30**:57-62
- [40] Reddy VR, Upadhyay SK, Gupta A, Awasthi AM, Hussain S. Enhanced dielectric and ferroelectric properties of BaTiO_3 ceramics prepared by microwave assisted radiant hybrid sintering. *Ceramics International*. 2014;**40**:8333-8339
- [41] Fu P, Lu W, Lei W, Xu Y, Wang X, Wu J. Transparent polycrystalline MgAl_2O_4 ceramic fabricated by spark plasma sintering: Microwave dielectric and optical properties. *Ceramics International*. 2013;**39**:2481-2487
- [42] Bangi UKH, Park C-S, Baek S, Park H-H. Sol-gel synthesis of high surface area nanostructured zirconia powder by surface chemical modification. *Powder Technology*. 2013; **239**:314-318
- [43] Díaz-Parralejo A, Macías-García A, Sánchez-González J, Ángeles Díaz-Díez M, Eduardo M. Cuerda-Correa; a novel strategy for the preparation of yttria-stabilized zirconia

- powders-deposition and scratching of thin films obtained by the sol-gel method. *Journal of Non-Crystalline Solids*. 2011;**357**:1090-1095
- [44] Yao W, Tang Z, Zhang Z, Luo S. Preparation of 8 mol% yttria-stabilized zirconia by an oil flotation-assisted chemical coprecipitation route. *Materials Letters*. 2002;**57**:502-506
- [45] Yuan FL, Chen CH, Kelder EM, Schoonman J. Preparation of zirconia and yttria stabilized zirconia (YSZ) fine powders by flame assisted ultrasonic spray pyrolysis. *Solid State Ionics*. 1998;**109**:119-123
- [46] Gaudon M, Djurado E, Menzler NH. Morphology and sintering behaviour of yttria stabilised zirconium (8-YSZ) powders synthesized by spray pyrolysis. *Ceramics International*. 2004;**30**:2295-2303
- [47] Somiya S, Akiba T. Hydrothermal zirconia powders: A Bibliography. *Journal of the European Ceramic Society*. 1999;**19**:81-87
- [48] Oliveira AP, Torem ML. The influence of precipitation variables on zirconia powder synthesis. *Powder Technology*. 2001;**119**:181-193
- [49] Byrappa K, Yoshimura M. *Handbook of Hydrothermal Technology*. 2nd ed. Elsevier Inc; 2012
- [50] Piticescu RR, Hrovath M, Belavic D, Ionascu A, Malic B, Motoc AM, et al. Zirconia pressure sensors: From nanopowders to device. In: *Solid State Phenomena*. Vol. 99. Switzerland: Transtech Publications; 2004. pp. 89-98
- [51] Wei Chen I, Wang WH. Sintering dense nanocrystalline ceramics without final-stage grain growth. *Nature*. 2000;**404**:168-171
- [52] Charles Greskovich D, William Minnear P, Milivoj Brun K, Robert Riedner J. Preparation of high uniformity polycrystalline ceramics by presintering, hot isostatic pressing and sintering and the resulting ceramic. US5013696 A; 1991
- [53] Omori M. Sintering, consolidation, reaction, and crystal growth by the spark plasma system (SPS). *Materials Science and Engineering A*. 2000;**287**:183-188
- [54] Agrawal DK. Microwave processing of ceramics. *Current Opinion in Solid State and Materials Science*. 1998;**3**:480-485
- [55] Alaniz JE, Perez-Gutierrez FG, Aguilar G, Garay JE. Optical properties of transparent nanocrystalline yttria stabilized zirconia. *Optical Materials*. 2009;**32**:62-68
- [56] Kim M-J, Ahn J-S, Kim J-H, Kim H-Y, Kim W-C. Effects of the sintering conditions of dental zirconia ceramics on the grain size and translucency. *The Journal of Advanced Prosthodontics*. 2013;**5**:161-166
- [57] Jiang L, Liao Y, Wan Q, Li W. Effects of sintering temperature and particle size on the translucency of zirconium dioxide dental ceramic. *Journal of Materials Science: Materials in Medicine*. 2011;**22**:2429-2435

- [58] Yi F, Cheng J, Roy R, Roy DM, Agrawal DK. Enhancing densification of zirconia-containing ceramic-matrix composites by microwave processing. *Journal of Materials Science*. 1997;**32**:4925-4930
- [59] Anselmi-Tamburini U, Woolman JN, Munir ZA. Transparent nanometric cubic and tetragonal zirconia obtained by high-pressure pulsed electric current sintering. *Advanced Functional Materials*. 2007;**7**:3267-3273
- [60] Casolco SR, Xu J, Garay JE. Transparent/translucent polycrystalline nanostructured yttria stabilized zirconia with varying colors. *Scripta Materialia*. 2008;**58**:516-519
- [61] Krell A, Hutzler T, Klimke J. Defect strategies for an improved optical quality of transparent ceramics. *Optical Materials*. 2014;**38**:61-74
- [62] Yamashita I, Kudo M, Tsukuma K. Development of highly transparent zirconia ceramics. *TOSOH Research & Technology Review*. 2012;**56**:11-16
- [63] Miao X, Sun D, Hoo PW, Liu J, Hu Y, Chen Y. Effect of titania addition on yttria-stabilised tetragonal zirconia ceramics sintered at high temperatures. *Ceramics International*. 2004;**30**:1041-1047
- [64] Dragut DV, Badilita V, Motoc AM, Piticescu RR, Zhao J, Hijji H, et al. Thermal stability and field assisted sintering of cerium-doped YSZ ceramic nanoparticles obtained via a hydrothermal process. *Manufacturing Review*. 2017;**4**(11):18-28
- [65] Cho J, Weng H, Fan Z, Xue S, Vikrant KSN, Wang H, et al. High temperature deformability of ductile flash-sintered ceramics via in-situ compression. *Nature Communications*. 2018;**9**:2063-2068
- [66] Prakasam M, Weill F, Lebraud E, Viraphong O, Buffière S, Largeteau A. Densification of 8Y-tetragonal-stabilized zirconia optoceramics with improved optical properties by Y segregation. *International Journal of Applied Ceramic Technology*. 2016;**2016**(13):904-911

On the Performance of Carbon Nanotubes on Sintered Alumina-Zirconia Ceramics

Miguel Humberto Bocanegra-Bernal,
Alfredo Aguilar-Elguezabal, Armando Reyes-Rojas,
Carlos Dominguez-Rios and Armando Garcia-Reyes

Additional information is available at the end of the chapter

<http://dx.doi.org/10.5772/intechopen.78542>

Abstract

The alumina (Al_2O_3) and zirconia (ZrO_2) ceramic monoliths and their combination are used in both technical and biomedical applications due to their combination of excellent chemical, physical, and mechanical properties. Pressureless sintering (PLS), reaction bonding (RB), hot pressing (HP), hot isostatic pressing (HIP), and spark plasma sintering (SPS) are the sintering methods more commonly used. The high brittleness, the low fracture toughness, and low thermal stability that possess these ceramics are its Achilles heel for numerous engineering applications. The incorporation of a second phase such as carbon nanotubes (CNTs) into the ceramic matrix has been attempted to overcome these drawbacks but the obtained results are still controversial considering that the homogeneous dispersion of CNTs and the interfacial bonding between two different ceramic materials remains as a difficult task leading to little or even no improvement in mechanical properties. Besides, the role of CNTs in the sintering of ceramic materials is not clear in the scientific literature taking into account parameters such as materials used and particularly inconsistencies in dispersion and mixing of the CNTs. We discuss how the CNTs can affect the sintering behavior and microstructural evolution of alumina and zirconia ceramics and the combination of them.

Keywords: alumina, zirconia, carbon nanotubes, sintering, fracture toughness

1. Introduction

Carbon nanotubes (commonly abridged as CNTs) are structures of nanometric dimension built up entirely by atoms of carbon and they have a high Young's modulus with good flexibility and

good thermal and chemical stability being visualized as a graphene sheet that has been rolled into a tube with hemispherical caps at one or both ends [1, 2]. It is well known that the sp^2 - sp^2 covalent carbon-carbon bonding is one of the strongest existing in nature, which in turn leads to exceptional material properties as a consequence of their symmetric structure. In the scientific literature, many researchers have reported mechanical properties of CNTs that exceed those of any previously existing materials [3] attracting an intense interest from the scientific community, as well as from industry. Nanotubes along with graphene are currently the subject of several papers per day. Undoubtedly, the discovery of CNTs [4] has aroused greatest interest as a potential reinforcing agent for different composite materials [5, 6] in order to impart stiffness, strength, and toughness considering their outstanding intrinsic physical properties and low density.

Taking into account that ceramic oxides such as aluminum oxide (Al_2O_3), zirconium oxide (ZrO_2), and a combination of them (alumina toughened zirconia (ATZ) and zirconia toughened alumina (ZTA)) are used in both structural and biomedical applications, it is of paramount importance to impart in these composites outstanding mechanical properties. In spite of combining the high strength and toughness of the tetragonal zirconia with the excellent hardness of the alumina ceramic, the low fracture toughness of brittleness of the alumina-based ceramics is still the main issue [7]. To overcome this weakness, the reinforcement in oxide ceramics can be carried out by short and long fibers. However, the CNTs due to their outstanding properties are fascinating materials as a reinforcement agent [5] and commonly two major structural forms of CNTs are known to exist as follows: single walled carbon nanotube (SWCNT) bundles and multi-walled carbon nanotubes (MWCNTs) [8]. Some experimental measurements have indicated that SWCNTs have Young's moduli ranging from 1 to 5 TPa, meanwhile MWCNTs have an average value of 1.8 TPa and a very similar relative density value [9, 10].

Nonetheless, the reduced size and dimensionality of CNTs lead to form complex networks of aggregates and bundles within ceramic composites [11]. In this context, this aggregation state plays an important role in defining the mechanical, electrical as well as thermal properties of the ceramic composites.

2. CNTs into the ceramic matrix during sintering

Although the role of CNTs in the sintering and microstructural evolution of ceramic composites is not completely clarified in the literature, these can be processed using the regular processing route and then densified mainly by pressureless sintering (PLS), hot pressing (HP) sintering, and spark plasma sintering (SPS) [12, 13]. Regardless the sintering method used, the scientific literature has reported significant improvement of mechanical properties but the results obtained with CNTs reinforced alumina- and zirconia-based ceramics remain controversial and can be observed that the wide scattered and highly debatable could be arise from different testing techniques used [3]. Unfortunately, today there is very limited experimental data on whether the final distribution of CNTs within microstructure of composites is mainly achieved during the powder phase processing or the sintering process [14]. Two main challenges in the processing of CNTs as a reinforcement agent in ceramics remain the heel of Achilles: a homogeneous dispersion of CNTs in matrix materials and the interfacial bonding

between the two different materials (CNTs and ceramic matrix) [5, 11]. In spite of this, many interesting works have been carried out to improve the mechanical properties of ceramic composites. Indeed, Zhan et al. [15] prepared 100% dense $\text{Al}_2\text{O}_3 + 10 \text{ vol}\%$ SWCNTs at 1150°C during 3 min with SPS as densification method obtaining a fracture toughness of $9.7 \text{ MPa m}^{1/2}$ being nearly three times that of nanocrystalline alumina ($3.5 \text{ MPa m}^{1/2}$); however, the results have not been reproduced up to now. In fact, these results were refuted by Wang et al. [16] who reported that CNT-alumina composites are highly contact damage-resistant and also showed that a more reliable single edge V-notched beam test could reveal no enhanced toughening, refuting therefore the claims of high toughness by Zhan et al. [16] in reference to the fracture toughness technique used. In other ceramic system prepared by HP, a mixture of MWCNTs and nano-SiC powders were reported by Ma et al. [17] being the dispersion of the MWCNTs very poor. However, an increase in both the bending strength and fracture toughness was obtained with a carbon nanotube content of around 10 vol%.

The above mentioned are few examples where both SWCNTs and MWCNTs have been used as reinforcement agents and the results have been some controversial and contradictory. To reinforce ceramic matrices, there are different kinds of CNTs available and there has been much documented research reporting the incorporation of SWCNTs and MWCNTs into the ceramic matrices in order to convert them into tough, strong, electric, and thermal conductive materials [18, 19]. Indeed, approximately 88% of the reported cases used the readily available and economically feasible MWCNTs as a reinforcement agent in comparison to SWCNTs. Regardless of this, it is noteworthy that the problems to achieve homogeneous distribution of CNTs as well as the related problems to the reproducible preparation of ceramic composites with improved mechanical properties can be considered as key obstacles. This difficulty to disperse CNTs into the ceramic matrices has led to explore and to develop efficient and economical processing methods that enable homogeneous dispersion of different types of CNTs in ceramic hosts. Those dispersion methods are referred to colloidal, sol-gel, and electrophoretic deposition processing techniques that are of paramount importance as methods to directionally emplace the CNTs while reducing the energy demands for the manufacture of the final product. Nonetheless, nowadays the main attention is paid to ultrasonic, plasma techniques, and other physical techniques in combination to the use of surfactants, functionalizing, and debundling agents of distinct nature including elemental substances, metal and organic salts, mineral and organic acids, oxides, inorganic and organic peroxides, organic sulfonates, polymers, dyes, natural products, biomolecules, and coordination compounds in order to produce ceramic nanocomposites with excellent mechanical properties [20].

Although currently there are several processes to manufacture CNTs containing alumina- and zirconia-based ceramic nanocomposites, some of them with a range of controversial results, it is evident that MWCNTs are preferably used as the reinforcement compared with SWCNTs [18, 21]. With the purpose to achieve nanostructures with outstanding mechanical properties, undoubtedly the nature of the different available CNTs and their processing conditions are of paramount importance and must therefore be considered. Commercially a great variety of CNTs are available with different conditions of preparation and subsequent treatment, which in turn and considering the sintering route adopted for the densification of the ceramic composite, could be the main reason for the controversy of results on their mechanical properties.

Under this assumption, it could be asserted that the different types of CNTs and the amount of these, added to the ceramic matrix, can lead to strong variations of the mechanical properties and affinity to the ceramic matrix as a consequence of their tubular structure, the number of the roller graphene sheets, diameter, length and their crystallinity linked to the number and nature of surface defects, and surface chemistry [23, 34]. All these aspects in turn will produce microstructural variations and fracture behavior of ceramic nanocomposites manufactured under different densification methods even with the same percentage of CNTs content within the ceramic matrix and using the same sintering technique. **Figure 1** shows fracture surfaces corresponding to an alumina ceramic with additions of 0.1 wt% of four different kinds of MWCNTs and sintered by SPS at 1500°C 3 min.

Knowing that the CNTs addition significantly retards grain growth during sintering [16, 19, 22, 25, 26] due to the pinning of matrix grains by the presence of CNTs, it is curious to observe from **Figure 1** the growth grain in alumina for low CNT contents and dispersed into the ceramic matrix under same conditions. These results reflect the unexpected effect that CNTs

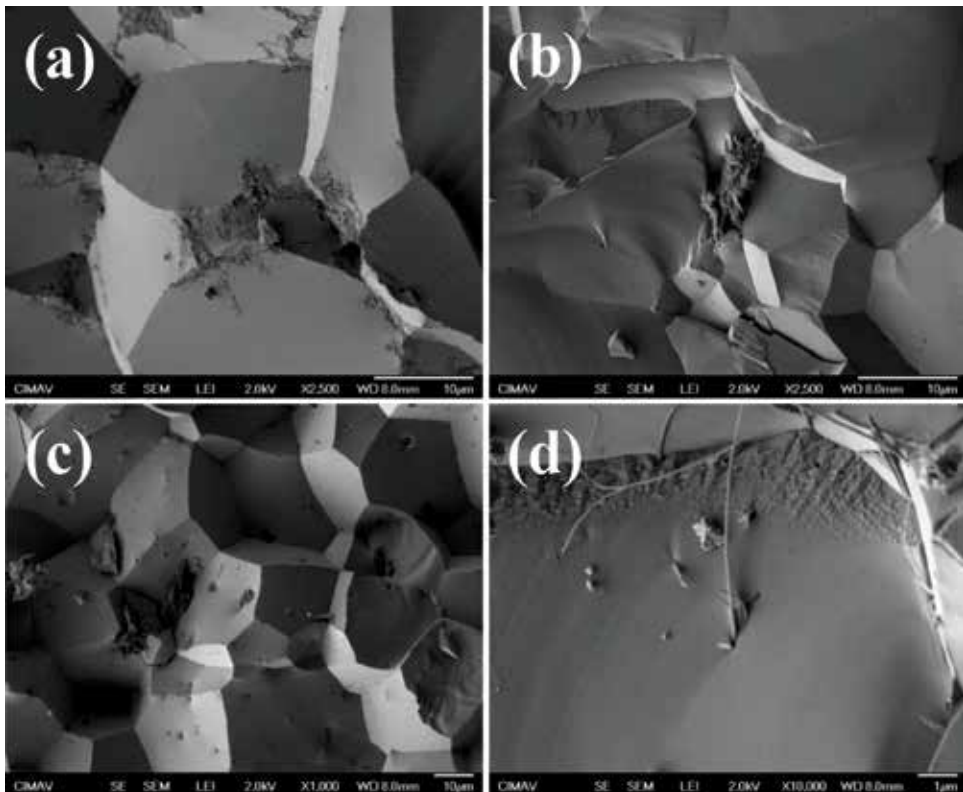


Figure 1. Scanning electron microscopy (SEM) micrographs of fracture surfaces of Al_2O_3 with additions of 0.1 wt% of four different kinds of MWCNTs. (a) MWCNT 1, outer diameter 50–80 nm, length 10–30 μm ; (b) MWCNT 2, outer diameter 10–20 nm, length 10–30 μm ; (c) MWCNT 3, outer diameter < 8 nm, length 10–30 μm ; and (d) MWCNT CIMAV, outer diameter 10–70 nm, length 120–160 μm sintered by SPS at 1500°C 3 min. Figures (b) and (c) from the paper: SWCNTs versus MWCNTs as reinforcement agents in zirconia- and alumina-based nanocomposites: which one to use, Bocanegra-Bernal et al. [24]. © 2016 Scrivener Publishing LLC. With permission.

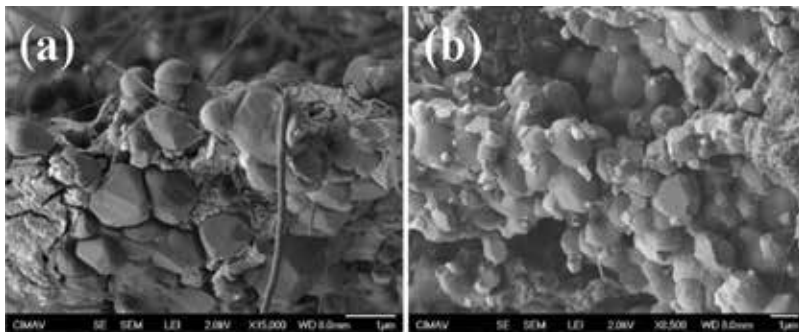


Figure 2. SEM of fracture surfaces of ZTA with additions of (a) 10 vol% MWCNT, and 10 vol% SWCNT (b), sintered at 1520°C during 1 h, showing agglomeration of SWCNT in (b).

could have on the microstructural evolution, affecting mainly the mechanical properties what contrasts with the results reported in the literature [11, 27–29]. On the other hand, it is expected that low levels of CNTs can be easier to disperse into the comparison with high levels of them. Likewise, the presence and distribution of the CNTs within the ceramic matrix induces a combination of fracture mode in each composite where the CNTs as the second phase could be responsible for altering the fracture modes [18]. Conversely, high levels of both MWCNTs and SWCNTs induce to an undesirable agglomeration state which is detrimental to achieve high densification by the formation of clusters owing to van der Waals forces [30] and the concentration of reinforcement at certain point leading to worsening of overall mechanical properties [11] such as can be illustrated in **Figure 2** for zirconia toughened alumina (ZTA) with additions of 10 vol% of CNTs.

For the same nanotubes content in **Figure 2**, generally the MWCNTs can be homogeneously dispersed (**Figure 1a**) meanwhile denser agglomerates of SWCNTs were formed (**Figure 2b**). Similar observations have been reported by Zhang et al. [31] in CNTs- Al_2O_3 with variable CNT content and Zhang et al. [32] in alumina ceramics with additions of 1, 3, and 5 vol% MWCNTs. In view of experimental evidences, such as **Figure 1** [33] and **Figure 2** [34], and other more reported in the scientific literature (for example Tables 1 and 2 in Ref. [18]) showing a broad spectrum of final densities and mechanical properties using different methods of purification and dispersion of CNTs into the several ceramic matrix systems, a too high CNT content must be avoided with the purpose to achieve a good dispersion by means of conventional and economic methods, since the use of sophisticated techniques can make the process expensive and its industrial scaling more difficult.

3. Requirements for optimum performance of CNTs as reinforcement agents in ceramics

Taking into account that intrinsic factors of CNTs such as diameter, length, nature of surface defects, orientation, mechanical strength, and affinity with the ceramic matrix have a strong influence on the microstructure and grain growth of the ceramic composites, the effective and optimum

utilization of CNTs in composite applications depends strongly on the ability to disperse CNTs homogeneously throughout the matrix to obtain a good interfacial bonding which is required to achieve an efficient load transfer across the CNT-matrix interface as a primary condition for improving the mechanical properties of ceramic composites [35]. As a consequence of high van der Waals force, surface area and high aspect ratio of CNTs (most notorious in SWCNTs), inevitably self-aggregation occurs and therefore, the improvement of dispersion has become a challenge to maximize the properties of CNTs [36, 37]. **Figure 3** shows the fracture surface of alumina with additions of 0.5 wt% of SWCNTs where bundles of CNTs located intergranularly are evident impeding the densification of the ceramic composite during the sintering at high temperatures. Nevertheless, the characterization of the dispersion of CNTs within the microstructure in the sintered composites is often based on the visual observation of micrographs obtained from scanning electron microscopy (SEM). It is of paramount importance to quantify the quality of distribution of CNTs in the microstructure of the sintered samples to understand the broad properties that the CNTs can offer as reinforcement agents in the ceramic nanocomposites [14, 30].

Regardless of dispersion method used, it is indisputable that the quantity, location, and distribution of CNTs in the ceramic matrix play an important role in the sintering of the composites producing compounds with a varied range of mechanical properties stressing that the dispersion of CNTs is not an easily controllable and reproducible process and, therefore, that the final properties can depend in first instance on the route followed for their dispersion into the ceramic matrix, as well as the sintering route chosen. **Figure 4** illustrates the fracture surface of an alumina ceramic doped with 0.5 wt% of MWCNTs that are located parallel to the fracture surface indicating a poor bonding to the ceramic matrix not contributing to the improvement of the fracture toughness by the absence of toughening mechanisms such as crack branching, pull out, and crack deflection.

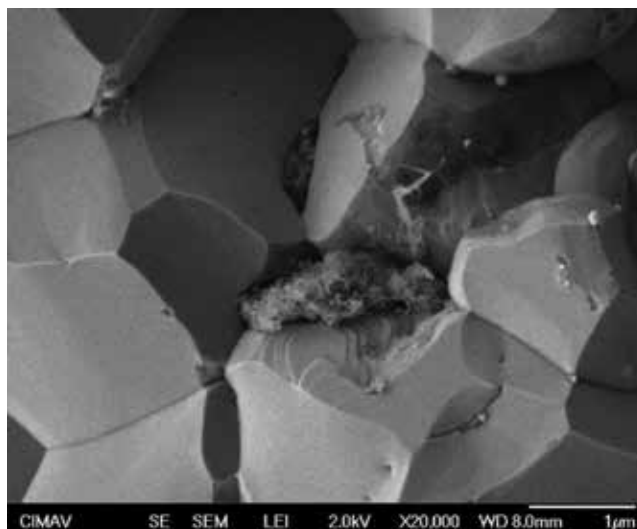


Figure 3. Scanning electron microscopy (SEM) micrograph of fracture surfaces of Al_2O_3 with additions of 0.5 wt% of SWCNTs sintered at 1520°C under atmospheric pressure with graphite powder as powder bed.

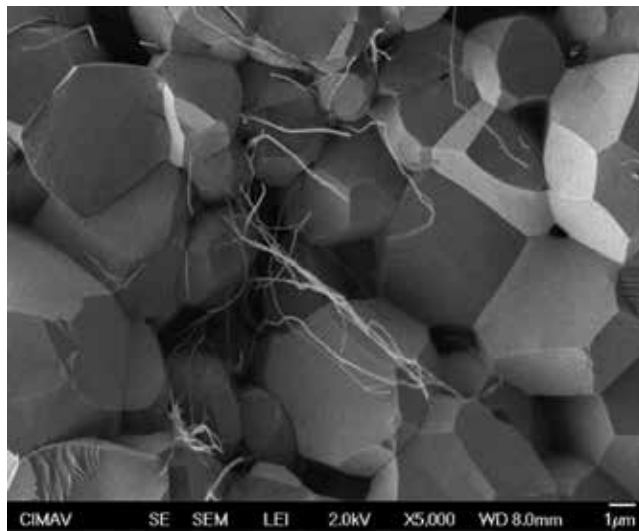


Figure 4. Scanning electron microscopy (SEM) micrograph of fracture surfaces of Al_2O_3 with additions of 0.5 wt% of MWCNTs sintered at 1520°C under atmospheric pressure with graphite powder as powder bed. Note the poor bonding of the CNTs to the ceramic matrix affecting the mechanical properties.

Recent work [38] reports for a same content of CNTs (0.1 wt%), a wide range of grain sizes and fracture toughness values, with the hardness remaining practically the same in alumina ceramic composites prepared by PLS, hot isostatic pressing (HIP), and sintering + hot isostatic pressing (sinter + HIP) routes. In all cases, the dispersion of CNTs and mixture preparation was performed under same conditions and the substantial difference observed in the final results could be explained by the different sintering kinetics of the three techniques applied in that work [38]. According to Orsolya [14], at temperatures higher than 1500°C and long sintering times, large amount of mass diffusion takes place facilitating a significant rearrangement of the nanotubes as well, while for SPS the sintering is completed in short time, where it is expected less and most likely short range rearrangements of the CNTs aggregates formed during the powder phase processing. However, it is well known that PLS and HP are the techniques that commonly require high temperatures, which could induce in some cases to the partial destruction of CNTs at these temperatures. Based on this, these sintering techniques have been replaced long ago by SPS, due to the damage of the CNTs by the higher temperatures and longer sintering times attained in those conventional methods.

Considering the pros and cons of the different sintering methods used in the manufacture of ceramic nanocomposites, undoubtedly that SPS so far only facilitates the fabrication of simple geometries such as discs, rings, and cylinders, but the manufacture of more complex geometries is still in the development stage implying that on an industrial scale, PLS remains as the main sintering method adopted when complex geometries must be manufactured, mentioning that this method has been continuously perfected to obtain the best properties in the final compounds without compromising the integrity of nanotubes at high temperatures. Thus, intimate interfacial bonding between CNTs and ceramic matrix by an optimum dispersion of CNTs to achieve toughening of ceramic nanocomposite by a specific sintering method are the main key points for preparing CNTs reinforced oxide ceramics [39].

4. Conclusions

Many attempts have been made to improve the mechanical properties of ceramics through incorporating CNTs taking advantage of its mechanical and physical properties combined with their low density and judging from the results of several researchers, where unfortunately most of them have been disappointing for toughening, since very little or no increase in toughening upon introduction of either single- or multi-walled carbon nanotubes into alumina-zirconia-based ceramics has been shown. During the last decade, the CNTs and their processing and dispersion methods have been intensively studied. However, the controversial results reported could be arise from different dispersion techniques, sintering processes, and finally testing techniques used for their characterization. On the other side, there is the controversy to choose between the different kinds of CNTs to reinforce ceramic matrices to improve the mechanical properties. Another debatable question is to define the proper amount of CNT content to obtain a ceramic composite with improved mechanical properties, considering that even using the same contents (vol% or wt%) as well as the same type of CNTs into the ceramic matrix, the expected values of fracture toughness, and/or hardness could differ from each other favorably or unfavorably, particularly for higher concentrations of CNTs. Therefore, the meticulous selection of a specific kind of CNT as a reinforcement agent for a determined ceramic must be carried out after experimental trials, since the prediction of results starting from raw material known such as ceramic powders and CNTs (even knowing its diameter, length, and agglomeration state) is not an option, considering as above mentioned that dispersion of CNTs is nowadays considered by a sector of scientific community as a process very difficult to control and to reproduce and with base of this, the final properties will be different for each specific ceramic composition.

Concluding, the development of CNT-based ceramic nanocomposites is a promissory subject but still with many difficulties and challenges and there is a lack of sufficient knowledge to systematically improve properties over traditional ceramic composites or their monoliths with notable enhancements. As can be pointed out by Curtin and Sheldon [40], *“the traditional interplay of careful processing and evaluation, coupled with mechanistic assessment of properties, remains a valid paradigm at the nanoscale and should be assiduously applied to future research in CNT-composite systems.”* In other words, the optimum dispersion of CNTs into liquids could be achieved by mechanical (physical) or chemical methods, taking into account the amount and the type of CNTs to be dispersed as well as the optimal concentrations of aqueous surfactant solution and sonication time to contribute to the efficiently dispersion of CNTs.

Acknowledgements

The authors wish to express their appreciation to Wilber Antúnez for SEM work.

Conflict of interest

The authors declare that there is no conflict of interest.

Author details

Miguel Humberto Bocanegra-Bernal^{1*}, Alfredo Aguilar-Elguezabal¹, Armando Reyes-Rojas¹, Carlos Dominguez-Rios¹ and Armando Garcia-Reyes²

*Address all correspondence to: miguel.bocanegra@cimav.edu.mx

1 Centro de Investigación en Materiales Avanzados, CIMAV S.C., Laboratorio Nacional de Nanotecnología, Chihuahua, Mexico

2 Interceramic, Department R and D, Chihuahua, Mexico

References

- [1] Sekhar Samal S, Bal S. Carbon nanotube reinforced ceramic matrix composites: A review. *Journal of Minerals and Materials Characterization and Engineering*. 2008;**7**:355-370. DOI: 10.4236/jmmce.2008.74028
- [2] Mazzuccoa D, Squizzatoa D, Mantovania S, Canonicob P. Nano-Toughened Carbon Fibers Composite Materials. SAATI Group (SEAL S.p.A.), Lombardy Region, Republic of Italy, A partner of Nanoledge; 2009
- [3] Thostenson ET, Ren Z, Chou T-W. Advances in the science and technology of carbon nanotubes and their composites: A review. *Composites Science and Technology*. 2001;**61**:1899-1912. DOI: 10.1016/S0266-3538(01)00094-X
- [4] Iijima S. Helical microtubules of graphitic carbon. *Nature*. 1991;**354**:56-58. DOI: 10.1038/354056a0
- [5] Lee K, Mo CB, Park SB, Hong SH. Mechanical and electrical properties of multiwalled CNT-alumina nanocomposites prepared by a sequential two-step processing of ultrasonic spray pyrolysis and spark plasma sintering. *Journal of the American Ceramic Society*. 2011;**94**:3774-3779. DOI: 10.1111/j.1551-2916.2011.04689.x
- [6] Harris PJF. Carbon nanotubes composites. *International Materials Review*. 2004;**49**: 31-43. DOI: 10.1179/095066004225010505
- [7] Bartolomé JF, Smirnov A, Kurland H-D, Grabow J, Müller FA. New ZrO₂/Al₂O₃ nanocomposite fabricated from hybrid nanoparticles prepared by CO₂ laser CO-vaporization. *Scientific Reports*. 2016;**6**:20589. DOI: 10.1038/srep20589
- [8] Qian D, Liu WK, Ruoff RS. Load transfer mechanism in carbon nanotube ropes. *Composites Science and Technology*. 2003;**63**:1561-1569. DOI: 10.1016/S0266-3538(03)00064-2
- [9] George R, Kashyap KT, Rahul R, Yamdagni S. Strengthening in carbon nanotube/aluminium (CNT(Al)) composites. *Scripta Materialia*. 2005;**53**:1159-1163. DOI: 10.1016/j.scriptamat.2005.07.022

- [10] Liao J-Z, Tan M-J, Sridhar I. Spark plasma sintered multi-wall carbon nanotube reinforced aluminium matrix composites. *Mater Design*. 2010;**31**:S96-S100. DOI: 10.1016/j.matdes.2009.10.022
- [11] Cho J, Boccaccini AR, Shaffer MSP. Ceramic matrix composites containing carbon nanotubes. *Journal of Materials Science*. 2009;**44**:1934-1951. DOI: 10.1007/s10853-009-3262-9
- [12] Takano Y, Ozawa T, Yoshinaka M, Hirota K, Yamaguchi O. Microstructure and mechanical properties of ZrO₂ (2Y)-toughened Al₂O₃ ceramics fabricated by spark plasma sintering. *Journal of Materials Synthesis and Processing*. 1999;**7**:107-111. DOI: 10.1023/A:1021869714265
- [13] Laurent C, Peigney A, Dumortier O, Rousset A. Carbon nanotubes-Fe-alumina nanocomposites. Part II: Microstructure and mechanical properties of the hot-pressed composites. *Journal of the European Ceramic Society*. 1998;**18**:2005-2013. DOI: 10.1016/S0955-2219(98)00142-3
- [14] Orsolya T, Hartmut L, Márton M, Katalin B, Csaba B, Levente T. The influence of sintering on the dispersion of carbon nanotubes in ceramic matrix composites. *Chemical Physics Letters*. 2014;**614**:148-150. DOI: 10.1016/j.cplett.2014.09.029
- [15] Zhan GD, Kuntz JD, Wan J, Mukherjee AK. Single-wall carbon nanotubes as attractive toughening agents in alumina-based composites. *Nature Materials*. 2003;**2**:38-42. DOI: 10.1038/nmat793
- [16] Wang X, Padture NP, Tanaka H. Contact-damage-resistant ceramic/single-wall carbon nanotubes and ceramic/graphite composites. *Nature Materials*. 2004;**3**:539-544. DOI: 10.1038/nmat1161
- [17] Ma RZ, Wu J, Wei BQ, Liang J, Wu DH. Processing and properties of carbon nanotube/nano-SiC ceramic. *Journal of Materials Science*. 1998;**33**:5243-5246. DOI: 10.1023/A:1004492106337
- [18] Ahmad I, Yazdani B, Zhu Y. Recent advances on carbon nanotubes and grapheme reinforced ceramic nanocomposites. *Nanomaterials*. 2015;**5**:90-114. DOI: 10.3390/nano5010090
- [19] Padture NP. Multifunctional composites of ceramics and single-walled carbon nanotubes. *Advanced Materials*. 2009;**21**:1767-1770. DOI: 10.1002/adma.200802270
- [20] Kharisov BI, Kharissova OV, Ortiz Méndez U. Methods for dispersion of carbon nanotubes in water and common solvents. In: *Symposium MM—Nanotubes and Related Nanostructures*. Vol. 1700. 2014. pp. 109-114. DOI: 10.1557/opl.2014.605
- [21] Sarkar S, Kr DP. Processing and properties of carbon nanotube/alumina nanocomposites: A review. *Reviews on Advanced Materials Science*. 2014;**37**:53-82. ISSN 1606-5131
- [22] Hayashi T, Endo M. Carbon nanotubes as structural material and their application in composites. *Composites Part B: Engineering*. 2011;**42**:2151-2157. DOI: 10.1016/j.compositesb.2011.05.011

- [23] Sedláček J, Galusek D, Riedel R, Hoffmann MJ. Sinter-HIP of polymer-derived Al_2O_3 -SiC composites with high SiC contents. *Materials Letters*. 2011;**65**:2462-2465. DOI: 10.1016/j.matlet.2011.04.094
- [24] Bocanegra-Bernal MH, Dominguez-Rios C, Garcia-Reyes A, Aguilar-Elguezabal A, Echeberria J. SWCNTs versus MWCNTs as Reinforcement Agents in Zirconia and Alumina-based Nanocomposites: Which One to Use. In: Ashutosh Tiwari and, Rosario A. Gerhardt, editors. *Advanced Ceramic Materials*, (261-298). © 2016 Scrivener Publishing LLC
- [25] Inam F, Peijs T, Reece MJ. The production of advanced fine-grained alumina by carbon nanotube addition. *Journal of the European Ceramic Society*. 2011;**31**:2853-2859. DOI: 10.1016/j.jeurceramsoc.2011.07.011
- [26] Bakhsh N, Ahmad Khalid F, Saeed Hakeem A. Synthesis and characterization of pressureless sintered carbon nanotube reinforced alumina nanocomposites. *Materials Science and Engineering A*. 2013;**578**:422-429. DOI: 10.1016/j.msea.2013.04.020
- [27] Inam F, Yan H, Peijs T, Reece MJ. The sintering and grain growth behaviour of ceramic-carbon-nanotube nanocomposites. *Composites Science and Technology*. 2010;**70**:947-952. DOI: 10.1016/j.compscitech.2010.02.010
- [28] Kasperski A, Weibel A, Estournès C, Laurent C, Peigney A. Preparation-microstructure-property relationships in double-walled carbon/nanotubes alumina composites. *Carbon*. 2013;**53**:62-72. DOI: 10.1016/j.carbon.2012.10.030
- [29] Zapata-Solvas E, Gomez-Garcia D, Dominguez-Rodriguez A. Towards physical properties tailoring of carbon nanotubes-reinforced ceramic matrix composites. *Journal of the European Ceramic Society*. 2012;**32**:3001-3020. DOI: 10.1016/j.jeurceramsoc.2012.04.018
- [30] Bakshi SR, Lahiri D, Agarwal A. Carbon nanotube reinforced metal matrix composites—A review. *International Materials Review*. 2010;**55**:41-64. DOI: 10.1179/095066009X12572530170543
- [31] Zhang T, Kumari L, Du GH, Li WZ, Wang QW, Balani K, Agarwal A. Mechanical properties of carbon nanotube-alumina nanocomposites synthesized by chemical vapor deposition and spark plasma sintering. *Composites: Part A*. 2009;**40**:86-93. DOI: 10.1016/j.compositesa.2008.10.003
- [32] Zhang SC, Fahrenholtz WG, Hilmas GE, Yadlowsky EJ. Pressureless sintering of carbon nanotube- Al_2O_3 composites. *Journal of the European Ceramic Society*. 2010;**30**:1373-1380. DOI: 10.1016/j.jeurceramsoc.2009.12.005
- [33] Bocanegra-Bernal MH, Dominguez-Rios C, Echeberria J, Reyes-Rojas A, Garcia-Reyes A, Aguilar-Elguezabal A. Spark plasma sintering of multi-, single/double- and single-walled carbon nanotube-reinforced alumina composites: Is it justifiable the effort to reinforce them? *Ceramics International*. 2016;**42**:2054-2062. DOI: 10.1016/j.ceramint.2015.09.060
- [34] Bocanegra-Bernal MH, Echeberria J, Ollo J, Garcia-Reyes A, Domínguez-Rios C, Reyes-Rojas A, Aguilar-Elguezabal A. A comparison of the effects of multi-wall and single-wall

- carbon nanotube additions on the properties of zirconia toughened alumina composites. *Carbon*. 2011;**49**:1599-1607. DOI: 10.1016/j.carbon.2010.12.042
- [35] Sun J, Gao L, Li W. Colloidal processing of carbon nanotube/alumina composites. *Chemistry of Materials*. 2002;**14**:5169-5172. DOI: 10.1021/cm020736q
- [36] Park C, Oundaies Z, Watson KA, Crooks RE, Smith J Jr, Lowther SE, Connell JW, Siochi EJ, Harrison JS, St Clair TL. Dispersion of single wall carbon nanotubes by in-situ polymerization under sonication. *Chemical Physics Letters*. 2002;**364**:303-308. DOI: 10.1016/S0009-2614(02)01326-X
- [37] Hilding J, Grulke EA, Zhang ZG, Lockwood F. Dispersion of carbon nanotubes in liquids. *Journal of Dispersion Science and Technology*. 2003;**1-41**:24. DOI: 10.1081/DIS-120017941
- [38] Bocanegra-Bernal MH, Dominguez-Rios C, Echeberria J, Reyes-Rojas A, Garcia-Reyes A, Aguilar-Elguezabal A. Effect of low-content of carbon nanotubes on the fracture toughness and hardness of carbon nanotube reinforced alumina prepared by sinter, HIP and sinter + HIP routes. *Materials Research Express*. 2017;**4**:085004. DOI: 10.1088/2053-1591/aa7f22
- [39] Fu Z, Huang L, Zhang J, Todd R. Ultra-fast densification of CNTs reinforced alumina based on combustion reaction and quick pressing. *Science China Technological Sciences*. 2012;**55**:484-489. DOI: 10.1007/s11431-011-4674-8
- [40] Curtin WA, Sheldon BW. CNT-reinforced ceramics and metals. *Materials Today*. 2004;**7**:44-49. DOI: 10.1016/S1369-7021(04)00508-5

Edited by Malin Liu

Sintering technology is an old and extensive technology in many areas, and it has been used especially in ceramic fabrication. This book covers many fields, for example, the development of different sintering technologies in recent years, such as spark plasma sintering, flash sintering, microwave sintering, reaction and laser sintering, and so on, and also some special ceramic material fabrication methods and applications, such as carbon nanotubes mixed with alumina and zirconia ceramics, pure and doped zirconia, ZnO ceramic varistors, and so on.

Published in London, UK

© 2018 IntechOpen
© lavendertime / iStock

IntechOpen

